UNIVERSITY OF CALIFORNIA SAN DIEGO

CTCF facilitates subset-specific chromatin interactions to limit the formation of terminally-differentiated $CD8^+$ T cells

A Dissertation submitted in partial satisfaction of the requirements
for the degree Doctor of Philosophy

in

Biology

by

Sara Quon

Committee in charge:

Professor Ananda Goldrath, Chair
Professor John Chang
Professor Christopher Glass
Professor Susan Kaech
Professor Cornelis Murre

2022

The Dissertation of Sara Quon is approved, and it is acceptable in quality and form for publication on microfilm and electronically.

University of California San Diego

2022

DEDICATION

To 5 years of graduate school.

TABLE OF CONTENTS

LIST OF FIGURES

LIST OF ABBREVIATIONS

TCR	T cell receptor
TE	terminal effector
MP	memory precursor
t-T_{EM}	terminal effector memory
T_{EM}	effector memory
T_{CM}	central memory
IEL	intraepithelial lymphocyte
T_{RM}	resident memory
TIL	tumor infiltrating lymphocytes
CTCF	CCCTC-binding factor
TAD	topologically associating domain
Lm-OVA	*Listeria monocytogenes* expressing the OVA peptide SIINFEKL
LCMV	Lymphocytic choriomeningitis virus

ACKNOWLEDGEMENTS

I would like to thank the following people for helping me throughout graduate school:

To my mentor Ananda: For training me as a scientist and helping me develop as an independent researcher. For teaching me the art of collaboration, the importance of networking, and the real details behind managing an academic lab. For providing me with opportunities to grow outside my comfort zone.

To my committee members - Chris Glass, John Chang, Kees Murre, Sue Kaech: For their advice and encouragement.

To the previous and present members of the Goldrath lab: For their support, training, and encouragement in the everyday science journey.

To all our collaborators, especially Stephen Turner, Brendan Russ, and Kirill Tsyganov: For their warm welcome, support, and advice.

To my friends and family: For their support and care.

Chapter 1, in part, has been submitted for publication of the material. Quon S, Yu B, Russ BE, Tsyganov K, Nguyen H, Toma C, Heeg M, Hocker JD, Milner JJ, Crotty S, Pipkin ME, Turner SJ, Goldrath AW. CTCF facilitates subset-specific chromatin interactions to limit the formation of terminally-differentiated $CD8^+$ T cells. The dissertation author was the primary researcher and first author of this paper.

Chapter 2, in part, has been submitted for publication of the material. Quon S, Yu B, Russ BE, Tsyganov K, Nguyen H, Toma C, Heeg M, Hocker JD, Milner JJ, Crotty S, Pipkin ME, Turner SJ, Goldrath AW. CTCF facilitates subset-specific chromatin interactions to limit the formation of

terminally-differentiated $CD8^+$ T cells. The dissertation author was the primary researcher and first author of this paper.

VITA

2017 Bachelor of Science in Biochemistry and Cell Biology, University of California San Diego

2022 Doctor of Philosophy in Biology, University of California San Diego

PUBLICATIONS

Quon, S., Yu, B., Russ, B.E., Tsyganov, K., Nguyen, H., Toma, C., Heeg, M., Hocker, J.D., Milner, J.J., Crotty, S., Pipkin, M.E., Turner, S.J., Goldrath, A.W. CTCF facilitates subset-specific chromatin interactions to limit the formation of terminally-differentiated $CD8^+$ T cells. Manuscript submitted for review.

Russ, B.E., Tsyganov, K., **Quon, S.**, Yu, B., Li, J., Lee, J.K.C, Olshansky, M., He, Z., Harrison, F.P., Barugahare, A., See, M., Nussing, S., Morey, A.E, Udupa, V.A., Bennett, T.J., Kallies, A., Murre ,C., Collas, P., Powell, D., Goldrath, A.W., Turner, S.J. Active maintenance of $CD8^+$ T cell naïvety through regulation of global genome architecture. Manuscript submitted for review.

Nguyen, Q.P., Takehara, K, Deng, T.Z. , O'Shea, S.M., Heeg, M. , Omilusik, K., Milner, J.J., **Quon, S.**, Pipkin, ME.. , Choi J., Crotty, S., Goldrath, A.W. (2022). Transcriptional programming of $CD4^+$ T_{RM} differentiation following viral infection balances TH1 effector- and memory-associated gene expression. Manuscript submitted for review.

Milner, J.J., Toma, C., **Quon, S.**, Omilusik, K., Scharping, N.E., Dey, A., Reina-Campos, M., Nguyen, H., Getzler, A.J., Diao, H., et al. (2021). Bromodomain protein BRD4 directs and sustains CD8 T cell differentiation during infection. J Exp Med 218. 10.1084/jem.20202512.

Liikanen, I., Lauhan, C., **Quon, S.**, Omilusik, K., Phan, A.T., Bartroli, L.B., Ferry, A., Goulding, J., Chen, J., Scott-Browne, J.P., et al. (2021). Hypoxia-inducible factor activity promotes antitumor effector function and tissue residency by $CD8^+$ T cells. J Clin Invest 131. 10.1172/JCI143729.

Wu, C.J., Cho, S., Huang, H.Y., Lu, C.H., Russ, J., Cruz, L.O., da Cunha, F.F., Chen, M.C., Lin, L.L., Warner, L.M., Liao, H. Utzschneider, D.T., **Quon, S.**, Berner, J., Camara, N.O.S., Zehn, D. Belmonte, J.C.I., Chen, L., Huang, S., Kuo, M., Lu, L. (2019). MiR-23~27~24-mediated control of humoral immunity reveals a TOX-driven regulatory circuit in follicular helper T cell differentiation. Sci Adv 5, eaaw1715. 10.1126/sciadv.aaw1715.

Wu, C.J., Tseng, P.H., Chan, C.C., **Quon, S.**, Chen, L.C., and Kuo, M.L. (2018). OK-432 Acts as Adjuvant to Modulate T Helper 2 Inflammatory Responses in a Murine Model of Asthma. J Immunol Res 2018, 1697276. 10.1155/2018/1697276.

Huang, T.S., Wang, K.C., **Quon, S.**, Nguyen, P., Chang, T.Y., Chen, Z., Li, Y.S., Subramaniam, S., Shyy, J., and Chien, S. (2017). LINC00341 exerts an anti-inflammatory effect on endothelial cells by repressing VCAM1. Physiol Genomics 49, 339-345. 10.1152/physiolgenomics.00132.2016.

ABSTRACT OF THE DISSERTATION

CTCF facilitates subset-specific chromatin interactions to limit the formation of terminally-differentiated $CD8^+$ T cells

by

Sara Quon

Doctor of Philosophy in Biology

University of California San Diego, 2022

Professor Ananda Goldrath, Chair

$CD8^+$ T cells play an indispensable role in the host protection from infections and malignancies. As such, many current immunotherapies target molecules that alter $CD8^+$ T cell function and differentiation. Although genome organization is known to be important for

regulating cell development and function, the changes in spatial chromatin organization accompanying effector and memory $CD8^+$ T cell differentiation remain unknown. Here, we studied how genome organization is integrated with other molecular mechanisms regulating $CD8^+$ T cell differentiation and targeted CTCF, a key factor that regulates genome organization through blocking or facilitating chromatin interactions, to determine how altering interactions affect the $CD8^+$ T cell response. We observed T cell subset-specific changes in intra-TAD interactions at sites related to transcriptional rewiring, such as genes encoding for transcription factors that regulate $CD8^+$ T cell differentiation. Further, terminally-differentiated effector cell differentiation was accompanied by enrichment of interactions among subset-specific enhancers and promoters, reflecting their terminally differentiated state. We next characterized the binding profile of CTCF, a known regulator of chromatin interactions. CTCF binding changed with $CD8^+$ T cell differentiation, and weak-affinity CTCF binding is needed to promote terminal differentiation in both an infection and tumor setting. Strikingly, disruption of a single CTCF binding site upregulated expression of corresponding memory-associated molecules, providing clear evidence that $CD8^+$ T cell differentiation is regulated through chromatin interactions. Thus, this study not only provides key insights into the remodeling of chromatin architecture during the $CD8^+$ T cell response to infection, but also provides high quality sequencing data to act as a resource to further identify novel regulators of the $CD8^+$ T cell response.

INTRODUCTION

0.1 $CD8^+$ T cell differentiation in infectious diseases

Infectious diseases have been and still are a significant problem worldwide as highlighted by the threat of Ebola and Zika, evolution of antibiotic-resistant pathogens, and more recently the outbreak of COVID-19, a new highly transmissible and pathogenic respiratory coronavirus, which crippled healthcare systems worldwide. In response to the COVID-19 pandemic, countries prioritized developing vaccines and discovering applicable therapeutics to prevent the spread of infection and the onset of serious symptoms. The new vaccines effectively decreased the severity and mortality of COVID-19 infection, and repurposed therapeutics helped ease some of the immunopathological symptoms. However, as seen from the multiple waves of new variants, invading pathogens are constantly evolving to escape the purview of the immune system, and more strategies are needed for combating infectious disease.

$CD8^+$ T cells are a key component of the adaptive immune system, which protects the host from both infectious and malignant diseases. Effector $CD8^+$ T cells kill infected or malignant cells, while memory $CD8^+$ T cells confer long-term protection against reinfection or tumor growth. Both effector and memory $CD8^+$ T cell populations are heterogenous, encompassing a spectrum of cytotoxicity and stem-like characteristics such as self-renewal, which are important for determining the functional capacity and persistence of the $CD8^+$ T cell response [1, 2]. Inappropriate activation of T cells, however, can harm the host, manifesting as autoimmune diseases such as diabetes and arthritis. Thus, advancing the understanding of $CD8^+$ T cell differentiation and maintenance will inform the development of preventative vaccines and therapeutics to combat infections, autoimmune diseases, and cancer.

In response to T cell receptor (TCR)-mediated recognition of antigen, naive $CD8^+$ T cells initiate molecular programs promoting rapid proliferation and acquisition of cytotoxic and cytokine-producing effector functions to provide protection from intracellular infections and tumor growth. While the majority of effector $CD8^+$ T cells undergo terminal differentiation and programmed cell death following antigen clearance, a small proportion of pathogen-specific cells persist and give rise to long-lived memory T cells that provide lasting protection from reinfection. Both the effector and memory T cell populations display a spectrum of functional, proliferative, trafficking, and re-differentiation potentials [1, 2]. Terminally-differentiated effectors cells (TE) are short-lived and express high levels of killer cell like receptor G1 (KLRG1) and low levels of interleukin-7-receptor-α (CD127), which mark memory precursor cells (MP) that are $KLRG1^{lo}$ and give rise to long-lived memory T cell subsets [3, 4] (**Figure 0.1**). At the memory timepoint, recirculating subsets include central memory (T_{CM}), effector memory (T_{EM}), and terminal-effector memory (t-T_{EM}) cells (phenotypically defined as $CD127^{hi}CD62L^{hi}$, $CD127^{hi}CD62L^{lo}$, and $CD127^{lo}CD62L^{lo}$, respectively), which show descending stem-like potential and ascending cytolytic capacity [5] (**Figure 0.1**). Further, a non-recirculating tissue-resident memory T cell population that is marked by expression of CD69, and in some cases CD103, is established in tissues, providing a front-line defense at sites of potential reinfection [6] (**Figure 0.1**). The heterogeneity of the memory $CD8^+$ T cell response is the basis of effective protection from repetitive infection due to the specializations of each subset. Hence, a thorough understanding of how different $CD8^+$ T cell subsets are formed can be harnessed for development of therapeutics and vaccines.

0.2 $CD8^+$ T cell exhaustion

In cases of persistent antigen exposure, such as chronic infection and tumors, $CD8^+$ T cells display an alternate form of terminal differentiation with blunted effector functions, which can mediate immunopathology and allow persistence of pathogens or malignant cells [7]. The major subsets of tumor infiltrating lymphocytes (TIL) include progenitor and terminally-exhausted TILs (defined by PD-1^+Tim-3^-Tcf1^+CD101^- and PD-1^+Tim-3^+Tcf1^-CD101^+, respectively), among which there is a spectrum of descending cytotoxicity and stem-like characteristics with an intermediate transitory population marked by effector molecules such as T-bet [8-10] (**Figure 0.2**). Progenitor-exhausted TIL are marked by their polyfunctionality, long-term survival, and ability to respond to checkpoint blockade, while terminally-exhausted TILs are short-lived with higher cytotoxicity [8]. The balance of terminal differentiation, effector function, and retention of stem-like characteristics is key for determining the functional capacity and persistence of $CD8^+$ T cell populations, and promoting the effector-like state without the dampening effects of exhaustion is important for immune protection [1, 8].

0.3 Transcriptional regulation of $CD8^+$ T cell differentiation

The cell-fate of naive $CD8^+$ T cells undergoing activation is influenced by many factors. Cell-extrinsic factors include precursor frequency, TCR signaling strength, antigen affinity, and cytokine exposure, while cell-intrinsic factors include transcription factors, epigenetic modifications, and chromatin architecture [2, 11-14]. Many studies illustrate transcription-factor-mediated regulation of heterogenous differentiation of T cells in both infections and tumors [14]. Altering the transcription factor landscape affects the composition of the responding T cell populations by activating subset-specific enhancers to drive transcriptional programs [14-16]. Extensive research has revealed many transcription factors that are crucial for regulating $CD8^+$ T

cell differentiation. Transcription factors such as T-bet, B lymphocyte-induced maturation protein 1 (Blimp1), Id2, Stat4, and Zeb2 support the effector program whereas transcription factors such as Eomesodermin (Eomes), Bcl6, Id3, Stat3, Foxo1, Foxo3, and Tcf1 support the memory program [3, 16-23]. In the context of chronic antigen, transcription factors such as Tox, Batf, and Irf4 promote the development of terminal exhausted cells, while Tcf1 and Bach2 promote the development of progenitor exhausted cells [24-27]. Transcription factors can work cooperatively and hierarchically to enforce cell-fate. However, transcription factors both regulate and are regulated by chromatin organization and epigenetic mechanisms [28-30].

0.4 Epigenetic regulation of $CD8^+$ T cell differentiation

Several studies have characterized the role of epigenetic modifications and changes in genome accessibility for regulating *in vivo* $CD8^+$ T cell differentiation [29-31]. Epigenetic modifications include histone modification, chromatin accessibility, DNA methylation, and chromatin architecture. These modifications can promote or repress gene expression through both direct and indirect mechanisms. DNA methylation, which occurs at cytosine residues, alters transcription factor binding affinity that affects the expression of target genes and also contributes to heterochromatin formation [32]. In a $CD8^+$ T cell response to acute LCMV, DNA is demethylated at effector-associated genes and regulatory regions and methylated at naive-associated genes and regulatory regions upon effector differentiation [33]. Upon memory T cell differentiation, the naive-associated genes and regulatory regions are then demethylated [33]. Deletion of a methyltransferase, Dnmt3, reduced DNA methylation, accelerated the re-expression of naive genes, and hastened memory T cell development, highlighting the role of DNA

methylation in regulating differentiation programs and suggesting that memory T cells are formed from effector T cells that were partially dedifferentiated [33].

Active histone modifications such as histone acetylation allow chromatin to become less compact by decreasing the binding affinity between DNA and histones [34, 35]. They are also recognized by reader proteins that promote gene transcription [34, 35]. In contrast, repressive histone modifications prevent DNA accessibility and gene expression [35]. Previous studies used changes in histone modifications and chromatin accessibility across $CD8^+$ T cell differentiation in response to infection to show that subsets have distinct enhancer repertoires that foreshadow subset-specific transcriptional programs [15, 30]. Further, a subset of chromatin regions displays bivalent chromatin signatures with both active and repressive histone modifications [36]. These regions, while transcriptionally silent, are poised to promote gene expression once the cell has received appropriate signals [36]. Strikingly, poised enhancers in $CD8^+$ T cells, in contrast to other cell types, acquire a non-canonical chromatin signature by gaining H3K4me3, a modification traditionally linked to active promoters [37, 38]. This epigenetic state marks transcriptionally poised genes that are prepared for upregulation upon infection [37]. Interestingly, a previous study linked the bifurcation of H3K4me1 and H3K4me3 to different levels of DNA methylation [39], which raises the idea of a regulatory network among epigenetic modifications to regulate transcriptional programs in conjunction with transcription factor activity. Despite many studies exploring the epigenetic mechanisms regulating $CD8^+$ T cell differentiation, the role of chromatin organization in $CD8^+$ T cell differentiation in response to antigen has not been comprehensively addressed.

0.5 Genome organization

Every somatic cell in the body contains the same DNA sequence with around 1.8 meters of DNA folded and compacted to fit into nuclei that are only 6 micrometers wide. DNA is tightly wound around histone protein complexes to form nucleosomes, which are the subunits of chromatin. Chromatin is separated into different chromosomes which are positioned into discrete chromosome territories. These territories are further separated into active and inactive compartments; active regions have a permissive transcriptional environment and inactive regions have a repressive transcriptional environment, as indicated by chromatin accessibility, histone marks, and positioning within the nucleus [40, 41]. Chromatin in these compartments are organized into topologically associated domains (TADs), which have high interactions within the domain whose borders are marked by CTCF and cohesin binding [40, 41]. TADs are composed of smaller DNA loops that can facilitate enhancer-promoter interactions, which regulate gene expression [40, 41]. The many layers of chromatin organization in the nuclei contribute to the regulation of cell function by positioning regions into transcriptionally repressive or active areas of the nucleus or facilitating or blocking chromatin interactions that are necessary for transcriptional programs. Although chromatin architecture is known to regulate cell differentiation and function, the genomic organization of $CD8^+$ T cells *in vivo* is not well-characterized.

The majority of studies investigating chromatin interactions in T cells were conducted in developing thymocytes and $CD4^+$ T cells. Early T-cell development in the thymus is accompanied by compartment switching and alterations in intra-TAD interactions [42]. Specifically, differentiation signals move the loci encoding for lymphocyte-commitment transcription factors into the active compartment to promote expression, and these factors then go on to rewire the transcriptome to promote differentiation [43]. One specific example of this phenomenon is CTCF and cohesin facilitation of an enhancer-promoter interaction to promote the transcription of

ThymoD, a non-coding RNA, which mediates the repositioning of the *Bcl11b* locus from the inactive compartment to the active compartment during early DN T-cell differentiation [44]. Additionally, chromatin organization is key for VDJ recombination during receptor rearrangement [45]. As T cells mature and enter the circulation, $CD4^+$ T cells can further differentiate into different T helper subtypes with different abilities to produce specific cytokines. The 3D chromatin architecture is known to establish long-range enhancer-promoter interactions that shape T helper subtype cytokine production. For example, Ifnγ production by Th1 cells rely on interactions between the *Ifng* promoter and enhancer elements that are mediated by Th1-specific binding of CTCF, cohesins, and T-bet, while Th2-associated genes are repositioned towards centromeric heterochromatin [46-48]. Thus, in developing thymocytes and $CD4^+$ T cells, chromatin architecture is key for regulating cell-fate decisions and function.

In contrast, the genome organization in $CD8^+$ T cells, especially for *in vivo* $CD8^+$ T cells, is not well understood. A recent study of *in vitro* activated human $CD8^+$ T cells found that T cell activation altered long-range chromatin interactions that correlated with changes in gene expression and remodeled the boundaries of a subset of TADs to form smaller domains, while active/inactive compartments were largely unchanged [49]. Studies focusing on the role of Tcf in regulating chromatin looping found that naive cells required Tcf1/Lef1-mediated chromatin interactions to enforce $CD8^+$ T cell identity and function, while T_{CM} cells needed Tcf1-mediated interactions for an appropriate recall response [50, 51]. A separate study performed in developing T cells revealed that Tcf1 cobinds with CTCF to alter TADs that supervised long-range chromatin interactions between regulatory elements and target genes that were gained during the late stages of T cell development [52]. These gained interactions were linked to active enhancers, as denoted by deposition of H3K27ac and recruitment of Nipbl, a cohesin-loading factor important for the

formation of chromatin looping [52, 53]. Altogether, these studies demonstrate that chromatin architecture is important for the progression of T cell development, T cell activation, and the enforcement of T cell identity and function, suggesting that genome organization may also be important for *in vivo* $CD8^+$ T cell differentiation in response to antigen.

0.6 CTCF

Studies in multiple cell types have utilized CTCF, a well characterized architectural protein, to study the impact of chromatin organization [54-57]. CTCF is a highly conserved protein, and expression is vital for cell survival [58, 59]. First identified as an insulator protein that prevents gene expression by blocking enhancer-promoter interactions, subsequent studies revealed the ability of CTCF to facilitate the formation of TADs and intra-TAD loops that facilitate interactions between distant enhancers and promoters [56, 60]. Thus, CTCF can act as both a transcriptional activator and transcriptional repressor. CTCF functions are also determined by its protein partners [61]. Previous research has identified cooperation with various protein partners such as Yy1, Cohesins, and RNAP II that contribute to CTCF-mediated regulation of transcription and genome organization [62-64]. Due to the many mechanisms and protein partners of CTCF, the cellular function of CTCF is highly dependent on the biological context.

CTCF has been shown to repress genes associated with "stemness" in hematopoietic stem cells and the liver cancer cell line HepG2 [65-67]. In a B leukemia cell line, CTCF was not necessary for transdifferentiation into macrophages, but was required for the upregulation of inflammatory genes in macrophages [68]. For developing T cells and B cells, CTCF-dependent, long-distance chromatin interactions are key for the rearrangement of antigen receptor loci where CTCF deficiency impairs differentiation and proliferation [45, 59, 69, 70]. Further, in mature B

cells, CTCF is necessary for the promotion of the germinal cell transcriptional program and repression of plasma cell differentiation [71]. In $CD4^+$ T cells, CTCF regulates the production of cytokines such as IFNγ and IL-21 [46, 72, 73]. Moreover, CTCF interacts with BATF, and ETS1 to regulate chromatin organization, which is key for the transcriptional programming of effector $CD4^+$ T cells (Pham et al., 2019). For both $CD4^+$ and $CD8^+$ T cells, CTCF binding is regulated by IL-2 and α-ketoglutarate signals necessary for the effector T cell phenotype [74]. Despite these studies highlighting the role of CTCF in regulating immune responses, the role of CTCF and genome organization in $CD8^+$ T cell differentiation in infection or tumor settings has yet to be addressed.

0.7 Outline

In this dissertation I address the following two questions, aiming to further the understanding of molecular mechanisms that regulate $CD8^+$ T cell differentiation:

How does genome organization change with $CD8^+$ T cell differentiation in response to infection?

In Chapter 1, we reported genome-wide mapping of chromatin interactions in antigen-specific naive, TE, and MP cells generated in response to an acute bacterial infection. We found that intra-TAD chromatin interactions with altered upon effector differentiation, and subset-specific interactions occurred near genes that drive differentiation programs.

What is the role of CTCF, a regulator of chromatin architecture, in $CD8^+$ T cell differentiation?

In Chapter 2, we described the CTCF binding profile in naive and effector $CD8^+$ T cells. We determined that CTCF is necessary for terminal differentiation in both infection and tumor

settings by regulating transcriptional programs, chromatin accessibility, and the transcription factor landscape.

0.8 Figures

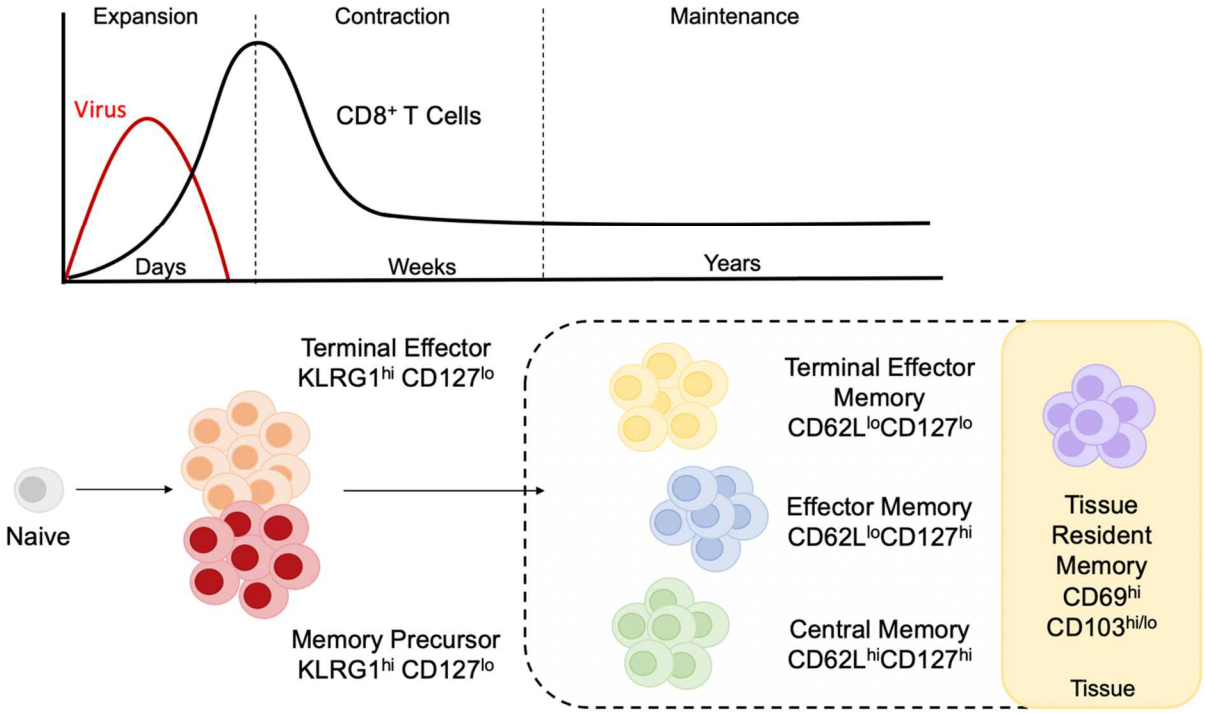

Figure 0.1: Schematic of CD8$^+$ T cell differentiation in response to infection

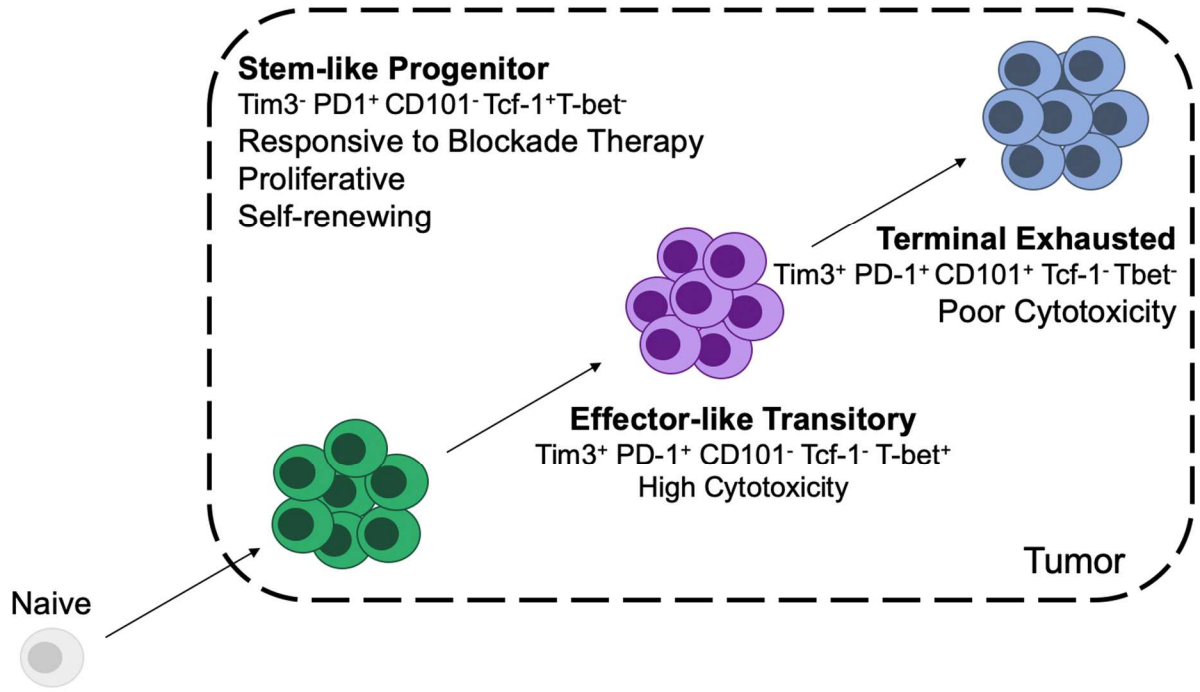

Figure 0.2: Schematic of CD8$^+$ T cell differentiation in response to a tumor.

CHAPTER 1: THE 3D GENOME ORGANIZATION OF $CD8^+$ T CELLS

1.1 Results

$CD8^+$ T cell subsets have similar genome organization

To capture differences in chromatin interactions as T cells responded to infection, we characterized the 3D genome organization of effector $CD8^+$ T cell subsets. CD45 congenically distinct naive OT-I $CD8^+$ T cells that recognize a peptide fragment of ovalbumin ($OVA_{257-264}$) bound to $H\text{-}2K^b$ were adoptively transferred into host mice, followed by intravenous (i.v.) infection with *Listeria monocytogenes* expressing ovalbumin (Lm-OVA). OT-I $CD8^+$ T cell subsets were identified by phenotypic criteria, naive ($CD44^{lo}CD62L^{hi}$), TE ($KLRG1^{hi}CD127^{lo}$, day 8), and MP ($KLRG1^{lo}CD127^{hi}$, day 8), and were sort purified for in situ Hi-C [75] (**Figure 1.1A**). All Hi-C experiments were performed in biological replicates with >1 billion chimeric sequences mapped per T cell subset. In total, we mapped 3.5 billion contacts across the 3 cell states for a total of 26,313 unique chromatin loops. The Hi-C sequencing files were normalized using multiHiCcompare [76] and processed with HiCExplorer [77-79] and HOMER [80].

Collaborating research found that $CD8^+$ T cell differentiation in response to infection did not alter chromatin organization at a gross-scale, but instead altered interactions occurring within TADs. Similarly, we found that overall chromatin structure did not have large-scale changes among the different T cell subsets (**Figure 1.1B**). Further, although previous research in human T cells found that in vitro activation led to a decrease in TAD size [49], we did not see a change in TAD size upon effector differentiation (**Figure 1.2A**). A similar picture was obtained analyzing the data using HiCExplorer [77-79] to characterize differentiation-induced changes in chromatin compartmentalization with H3K27ac marking active chromatin [30] (**Figure 1.2B**). The analysis

detected a substantial number of regions undergoing compartment switching in the transition from naive T cells to the TE or MP cells, while few changes were detected upon comparison of the two effector populations (**Figure 1.2B**). Although previous research has linked compartmentalization with transcriptional activity [40], there was no noticeable pattern between changes in gene expression and compartment switching with effector differentiation (**Figures 1.2C, 1.2D**). Thus, although genes move compartments during effector cell differentiation, compartment switching is not a significant mechanism regulating $CD8^+$ T cell differentiation. These data suggest that T cell activation and differentiation does not grossly remodel TADs, and the subset-specific transcriptional programs are not regulated through compartment switching.

$CD8^+$ T cell differentiation alters intra-TAD interactions

Terminal differentiation of TE cells involved substantial changes in the interaction landscape at a finer resolution. This was reflected in a gradual loss of correlation in overall interactions (**Figure 1.1C**) as well as differential interactions (**Figure 1.1D**) as defined by multiHiCcompare [76]. To investigate changes in the interactions between promoters and stage-specific enhancers [30], we determined the interaction scores from each T cell subset normalized to the number of expected interactions based on the distance between regions. As expected, TE-unique enhancers and promoters had the highest enrichment of interactions in the terminally-differentiated cells (**Figure 1.1E**). However, we also detected enrichment in interactions of elements assigned to the other differentiation stages in TE cells (**Figures 1.2E-G**) in line with the idea that terminal differentiation is associated with gains in chromatin looping [81]. Therefore, effector differentiation alters intra-TAD interactions specifically among subset-specific promoter and enhancers in TE cells.

Intra-TAD looping dynamics reflects CD8$^+$ T cell differentiation state

We next calculated the Jaccard similarity index to quantify the overlap between differential interactions and the chromosomal locations of genes associated with naive, TE, and MP gene-expression signatures defined previously by RNA-Seq [82] (**Figures 1.1F, 1G**). As shown by the higher Jaccard index score, chromosome interactions that were lost upon TE differentiation overlapped the most with genes in the naive T cell gene expression signature (**Figure 1.1F**). Related, interactions that were specific to TE cells compared to MP cells overlapped the most with genes that were upregulated in TE cells compared to genes specifically expressed by naive or MP T cells (**Figure 1.1G**). Further, gene-set enrichment analysis (GSEA) comparing the expression of genes in regions of subset-specific interactions confirmed the link between altered chromatin interactions and gene expression (**Figure 1.1H**). Genes located in regions with higher chromatin interactions in naive T cells displayed elevated gene expression in the naive population, while genes located in regions with higher interactions in the effector T cell subsets displayed expression enriched in the effector T cell populations (**Figure 1.1H**). These data demonstrate that changes in chromosomal interactions correlate with the transcriptional programs that distinguish T cell subsets.

For additional insight into the relationship between chromosomal organization and transcriptional programs that direct effector CD8$^+$ T cell differentiation, we examined the *Tbx21* and *Prdm1* gene loci, which encode for transcription factors that drive effector T cell differentiation [17]. Both transcription factors are upregulated upon effector CD8$^+$ T cell differentiation with the greatest induction in TE cells (**Figures 1.1I, 1.1J**). Inversely, *Tcf7*, which is downregulated in TE cells and maintained in MP cells, encodes for Tcf1, which drives the

memory T cell response by maintaining high differentiation potential [83] (**Figure 1.1K**). As reflected by the changes in interaction scores and number of uniquely interacting regions denoted by connecting arcs, effector T cell differentiation was accompanied by increased chromatin interactions around *Tbx21* and *Prdm1,* mirroring the pattern of gene expression, with the greatest increase in the TE subset (**Figures 1.1I, 1.1J, 1.1L**). Further, MP cell differentiation was accompanied by MP-specific gains in chromatin interactions at the *Tcf7* locus, reflecting the pattern of expression in the effector subsets (**Figures 1.1K, 1.1L**). Our data found a similar enrichment of naive-specific interactions at gene loci important for the maintenance of stemness and quiescence as described in the accompanying paper, despite using a different infection model and effector samples, suggesting that the type of infection does not change the pattern of chromatin reorganization during T cell effector differentiation (**Figures 1.2H-J**). Altogether, these data are specific examples of the general observations shown in Figures 1F and 1G, demonstrating that effector $CD8^+$ T cell differentiation remodels DNA looping to increase interactions at gene loci that show expression in effector T cells and diminish interactions at gene loci associated with expression in naive T cells.

Regions with altered DNA methylation upon effector differentiation are enriched for naive-specific interactions

DNA methylation is known to alter chromatin organization by polarizing DNA structure to favor the heterochromatic state [84]. Therefore, we reanalyzed published DNA methylation profiles for naive, TE, and MP cells (**Figure 1.3**) [33]. Quantification of the overlap among DNA methylation profiles and differentially methylated DNA regions revealed a similar pattern to the original publication with more similarity between the effector populations (TE and MP) than

between the naive and effector subsets (Naive and TE, Naive and MP) (**Figure 1.3A-B**). We then looked at the averaged chromatin interactions around the differentially methylated regions and found that there was a strong bias towards naive-specific chromatin interactions for all comparisons with the most striking difference in regions demethylated upon TE differentiation (**Figure 1.3C**). These data suggest that both regions that are demethylation and methylated upon effector differentiation occur at sites that lose chromatin interactions with effector differentiation.

1.2 Discussion

Immune cell function and differentiation are regulated through transcriptional changes that are controlled at multiple levels, including transcription factor binding and epigenetic modifications [16, 30]. While genome organization is known to regulate transcription and differentiation in many cell types and has been shown to change during T cell activation *in vitro* [49], the genome architecture for T cells *in vivo* has not been comprehensively characterized. Here, we profiled the 3D genome organization of $CD8^+$ T cell subsets responding *in vivo* to infection. We found that effector $CD8^+$ T cell differentiation was accompanied by changes in genome compartmentalization and intra-TAD chromatin interactions with magnitudes proportional to the lineage proximity of the subsets. These altered chromatin interactions occurred around genes expressed in a subset-specific manner, and enhancer-promoter interactions were specifically enriched in TE cells compared to other T cell subsets. Further, gene loci that encode key transcription factors known to regulate $CD8^+$ T cell differentiation underwent subset-specific chromatin remodeling that reflected the pattern of gene expression. These genome-scale changes correlated with transcriptional rewiring, highlighting that alterations in chromatin looping contribute to the regulation of $CD8^+$ T cell fate.

Our observations of discrete changes in intra-TAD looping accompanying effector $CD8^+$ T cell differentiation correspond to previous research where B cell activation and differentiation were associated with subtle changes at the level of chromatin looping instead of higher order chromatin architecture [85]. In contrast, a recent study which profiled the genome organization of *in vitro* activated human T cells found that activation remodeled TAD boundaries to form smaller domains [49]. We, however, do not see an alteration in TAD sizes, which raises the question if the observed smaller domains are alterations in intra-TAD interactions instead of TAD remodeling.

Studying the genome architecture in T cells is important for furthering the understanding of diseases and genetic disorders. Genome-wide association studies have identified regions that are associated with diseases such as cancer and autoimmune disease [86, 87]. Regions of interest, however, may be distal from the targeted element, hence chromatin interaction data is of great value for annotating genomic regions. For example, genetic variations associated with type I diabetes, a disease caused by T-cell-mediated killing of insulin-producing islet beta cells, altered enhancer-promoter interactions linked with aberrant gene expression [88]. This study highlights how studying genome organization in T cells is needed to further understand genetic susceptibility to disease and genetic disorders mediated by the T cell response.

Our study used Hi-C sequencing to measure chromatin interactions, however cell numbers and sequencing depth limit the resolution of the generated 3D genomic maps and prevent measuring chromatin architecture in rare cell populations. Recent developments in molecular methods to capture chromatin interactions have lowered the required amount of cells and increased resolution of measured chromatin folding [89, 90]. This advancement in technology opens the door to survey rarer T cell populations such as T_{RM} cells and TILs. In combination with Cut&Run, a technique to measure histone modifications and transcription actor binding with low cell numbers

[91, 92], future studies will be able to survey the interplay of chromatin architecture, the enhancer-promoter landscape, and transcription factor activity on regulating transcriptional programs to alter T cell differentiation in tissues and tumors.

1.3 Acknowledgements

Chapter 1, in part, has been submitted for publication of the material. Quon S, Yu B, Russ BE, Tsyganov K, Nguyen H, Toma C, Heeg M, Hocker JD, Milner JJ, Crotty S, Pipkin ME, Turner SJ, Goldrath AW. CTCF facilitates subset-specific chromatin interactions to limit the formation of terminally-differentiated $CD8^+$ T cells. The dissertation author was the primary researcher and first author of this paper.

1.4 Figures

Figure 1.1: Genome organization changes upon effector cell differentiation and occurs at subset-specific gene loci. (A) Schematic of experimental set-up. CD45 congenically distinct OT-I $CD8^+$ T cells were transferred into hosts and then infected with Lm-OVA. Eight days after infection, TE (CD127loKLRG1hi) and MP (CD127hiKLRG1lo) cells were sort purified. Naive (CD44loCD62Lhi) OT-I $CD8^+$ splenocytes were also sort purified from spleens. Hi-C, ChIP-Seq, and Cut&Run were performed on nuclei extracted from these populations. (B) Heatmaps portraying the log10 transformed normalized chromatin interaction scores for chromosome 1. (C) To determine the linear association for interaction scores between two samples, Pearson correlation analysis was performed on multiHiCcompare normalized Hi-C samples using HiCExplorer and visualized as a heatmap with rows and columns hierarchically clustered. (D) Quantification of differential chromatin interactions between $CD8^+$ T cell subsets. P.adj cutoff of 0.05, logfc cutoff of .667, and logcpm cutoff of 1 was used. (E) Interaction score enrichment for TE-specific enhancer and promoters normalized to expected interactions based on distance between regions using HOMER annotateInteractions. (F) Quantification of the overlap between regions with higher interactions in naive compared to TE cells and lists of chromosomal coordinates of subset gene signatures. (G) Quantification of the overlap between regions with higher interactions in TE cells compared to MP cells and lists of chromosomal coordinates of subset gene signatures. (H) GSEA of genes in areas of differential interactions for indicated comparisons. (I) RNA expression of Tbx21 from RNA-Seq data. (J) RNA expression of Prdm1 from RNA-Seq data. (K) RNA expression of Tcf7 from RNA-Seq data. (L) Heatmaps portraying chromosomal interactions in naive, MP, and TE cells around the Tbx21, Prdm1, and Tcf7 loci. Arcs represent enriched interactions in that relevant subset with a p.adj cutoff of 0.05, logfc cutoff of .667, and logcpm cutoff of 1.

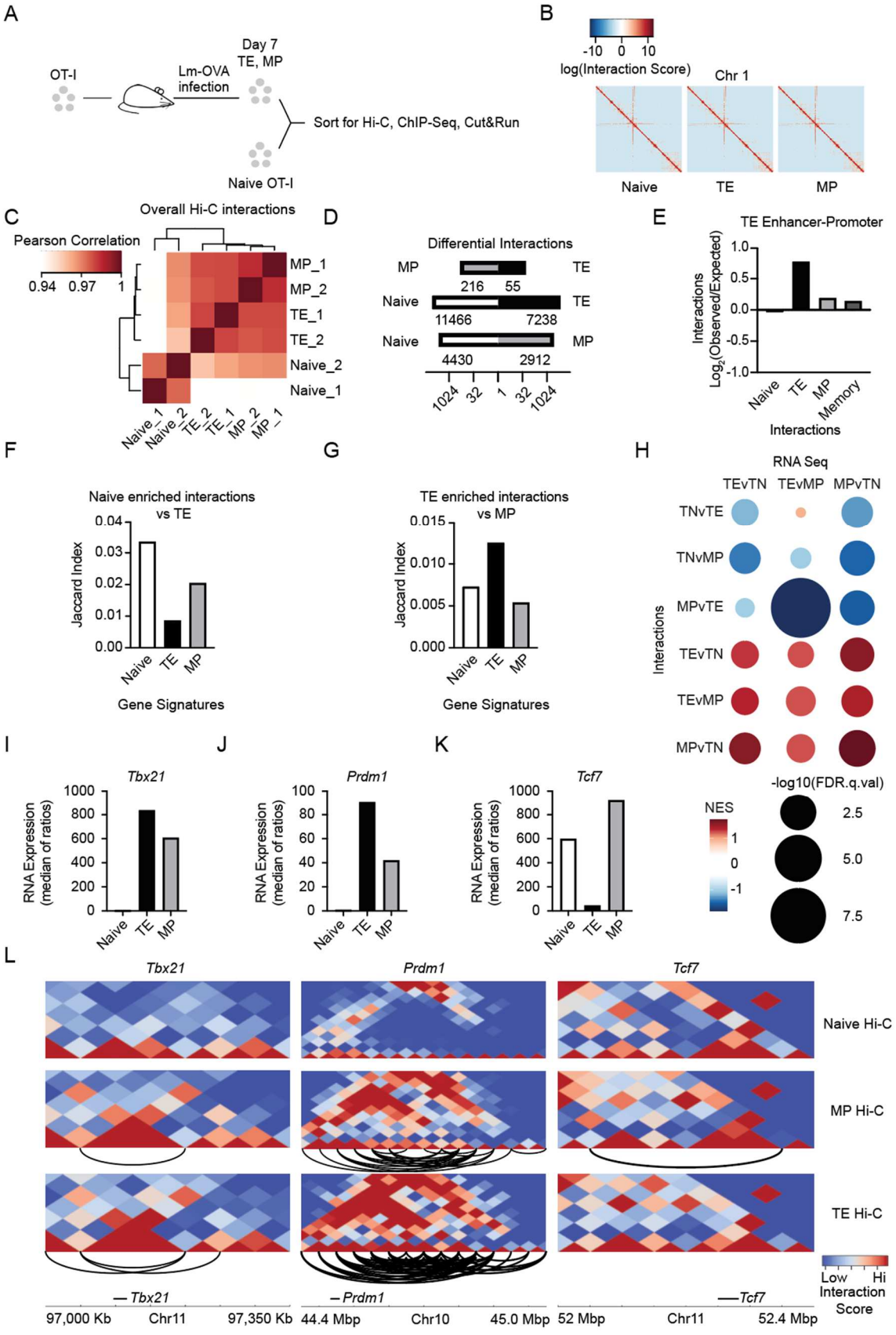
A
OT-I
Lm-OVA infection
Day 7 TE, MP
Sort for Hi-C, ChIP-Seq, Cut&Run
Naive OT-I
B
-10 0 10
log(Interaction Score)
Chr 1
Naive
TE
MP
C
Overall Hi-C interactions
Pearson Correlation
0.94 0.97 1
MP_1
MP_2
TE_1
TE_2
Naive_2
Naive_1
D
Differential Interactions
MP
TE
216 55
Naive
TE
11466 7238
Naive
MP
4430 2912
1024 32 1 32 1024
E
TE Enhancer-Promoter
Interactions
Log2(Observed/Expected)
1.0 0.5 0.0 -0.5 -1.0
Naive TE MP Memory
Interactions
F
Naive enriched interactions vs TE
Jaccard Index
0.04 0.03 0.02 0.01 0.00
Naive TE MP
Gene Signatures
G
TE enriched interactions vs MP
Jaccard Index
0.015 0.010 0.005 0.000
Naive TE MP
Gene Signatures
H
RNA Seq
TEvTN TEvMP MPvTN
TNvTE
TNvMP
MPvTE
TEvTN
TEvMP
MPvTN
Interactions
NES
1 0 -1
-log10(FDR.q.val)
2.5 5.0 7.5
I
Tbx21
RNA Expression (median of ratios)
1000 800 600 400 200 0
Naive TE MP
J
Prdm1
RNA Expression (median of ratios)
100 80 60 40 20 0
Naive TE MP
K
Tcf7
RNA Expression (median of ratios)
1000 800 600 400 200 0
Naive TE MP
L
Tbx21
Prdm1
Tcf7
Naive Hi-C
MP Hi-C
TE Hi-C
Low Hi
Interaction Score
— Tbx21
97,000 Kb Chr11 97,350 Kb
— Prdm1
44.4 Mbp Chr10 45.0 Mbp
— Tcf7
52 Mbp Chr11 52.4 Mbp

Figure 1.2: Characterization of chromatin interactions in CD8$^+$ T cell subsets. (A) Distribution of TAD sizes. (B) Quantification of A/B compartments that change in sign between CD8$^+$ T cell subsets. (C-D) Distribution of changes in gene expression for genes that switch compartments. (E-G) Enrichment of subset-specific enhancer-promoter interactions in (E) naive, (F) MP, and (G) memory cells measured by HOMER annotateInteractions. (H-J) Circos plots showing interactions enriched in naive (gray), TE and MP (red), or memory precursors and naive cells (blue) at the Satb1 (H), Sox4 (F), or Prickle1 (I) locus. (J) Quantification of overlap between subset-specific differential interactions and Bach2-deletion-induced changes in chromatin interactions.

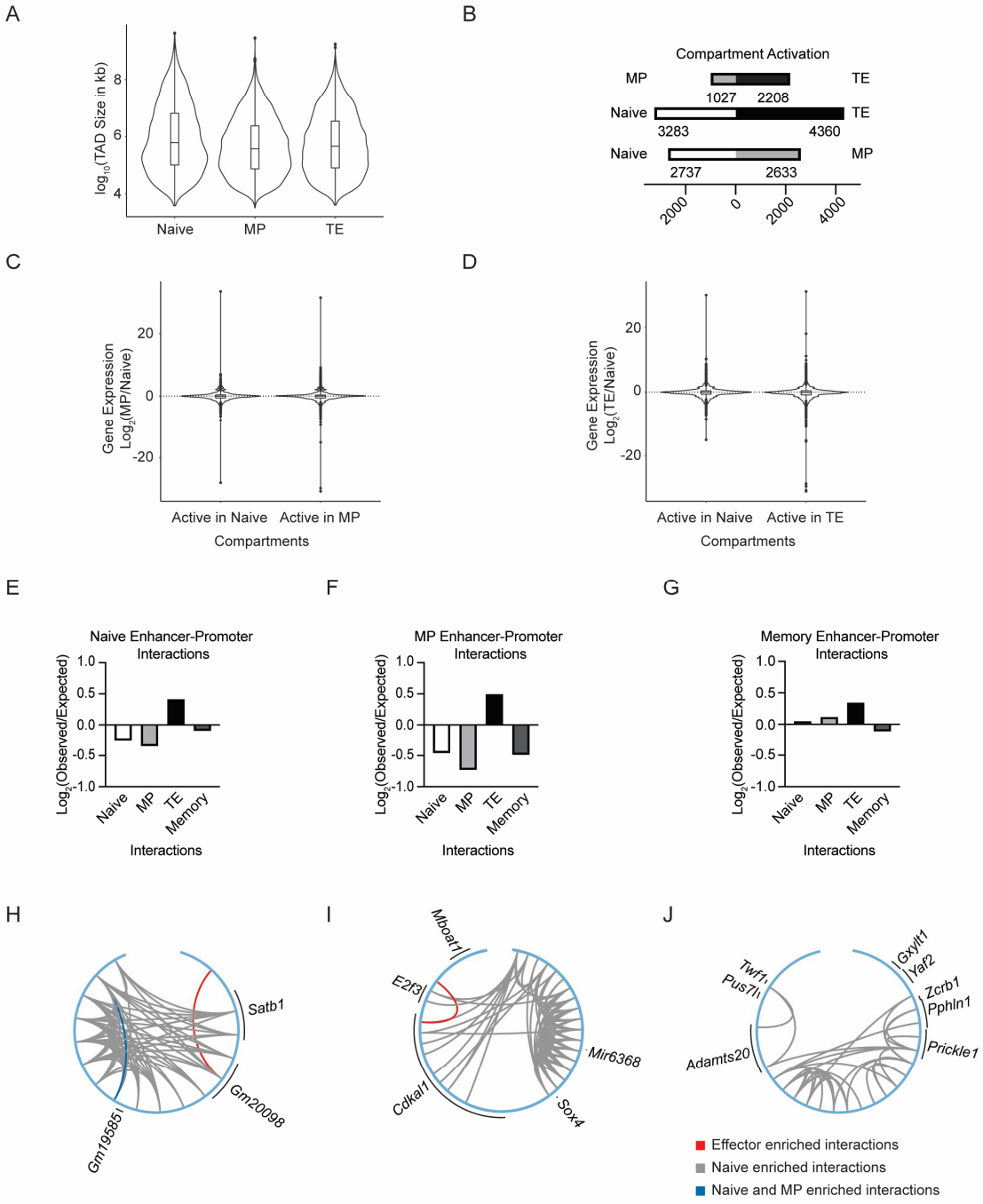
A
log10(TAD Size in kb)
8
6
4
Naive
MP
TE
B
Compartment Activation
MP
TE
1027
2208
Naive
TE
3283
4360
Naive
MP
2737
2633
2000
0
2000
4000
C
Gene Expression
Log2(MP/Naive)
20
0
-20
Active in Naive
Active in MP
Compartments
D
Gene Expression
Log2(TE/Naive)
20
0
-20
Active in Naive
Active in TE
Compartments
E
Naive Enhancer-Promoter Interactions
Log2(Observed/Expected)
1.0
0.5
0.0
-0.5
-1.0
Naive
MP
TE
Memory
Interactions
F
MP Enhancer-Promoter Interactions
Log2(Observed/Expected)
1.0
0.5
0.0
-0.5
-1.0
Naive
MP
TE
Memory
Interactions
G
Memory Enhancer-Promoter Interactions
Log2(Observed/Expected)
1.0
0.5
0.0
-0.5
-1.0
Naive
MP
TE
Memory
Interactions
H
Satb1
Gm20098
Gm19585
I
Mboat1
E2f3
Mir6368
Cdkal1
Sox4
J
Gxylt1
Yaf2
Twf1
Pus7l
Zcrb1
Pphln1
Adamts20
Prickle1
Effector enriched interactions
Naive enriched interactions
Naive and MP enriched interactions

Figure 1.3: Changes in DNA methylation accompanying effector differentiation occur at naive-specific interactions. (A) Overlap of differentially methylated regions between $CD8^+$ T cell subsets. (B) Quantification differentially methylated regions between $CD8^+$ T cell subsets. (C) Averaged chromatin interactions around the indicated differentially methylated regions.

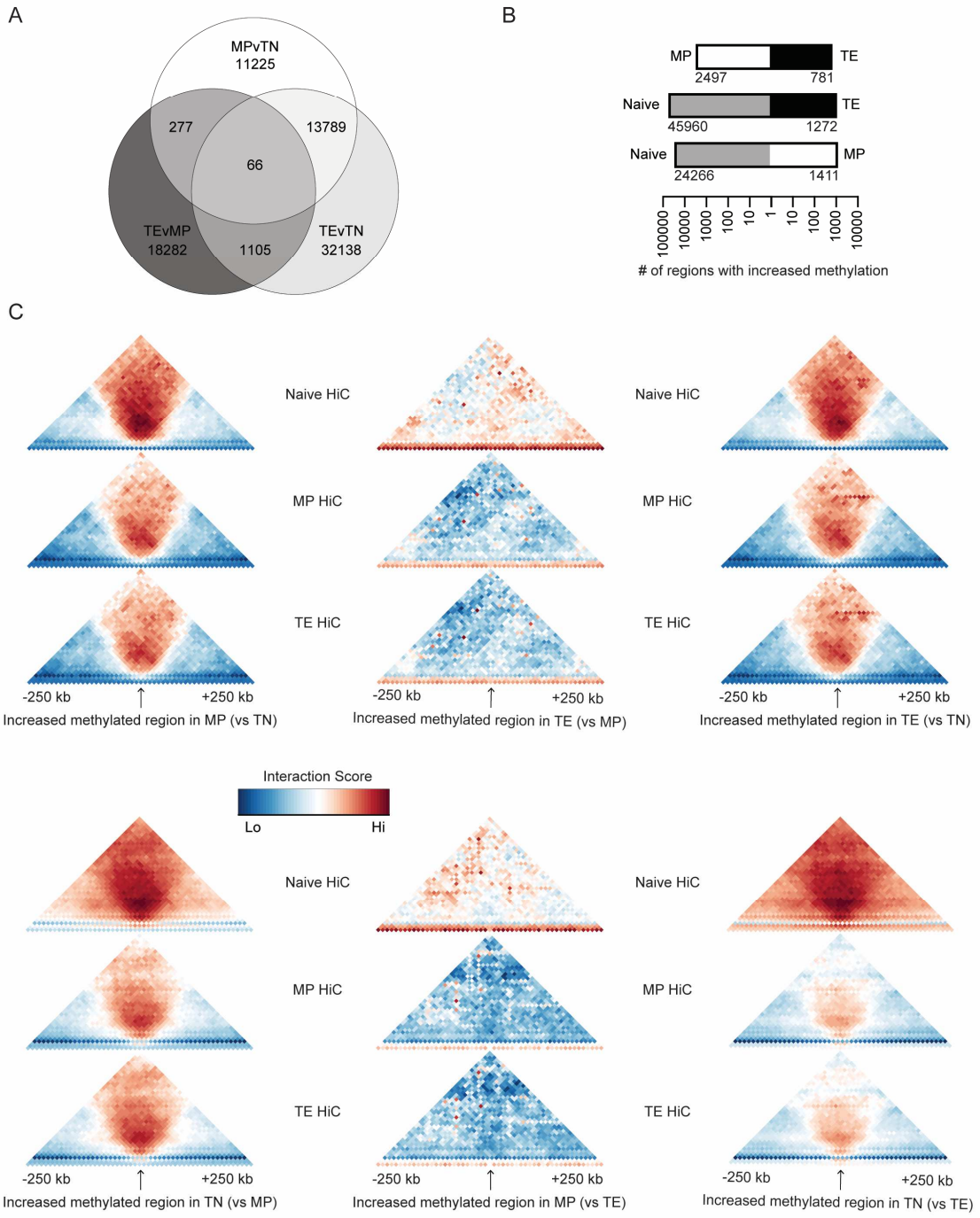
A
MPvTN
11225
277
13789
66
TEvMP
18282
1105
TEvTN
32138
B
MP
TE
2497
781
Naive
TE
45960
1272
Naive
MP
24266
1411
100000
10000
1000
100
10
1
10
100
1000
10000
# of regions with increased methylation
C
Naive HiC
MP HiC
TE HiC
-250 kb
+250 kb
Increased methylated region in MP (vs TN)
Increased methylated region in TE (vs MP)
Increased methylated region in TE (vs TN)
Interaction Score
Lo
Hi
Increased methylated region in TN (vs MP)
Increased methylated region in MP (vs TE)
Increased methylated region in TN (vs TE)

CHAPTER 2: CHARACTERIZATION OF CTCF IN CD8$^+$ T CELL SUBSETS

2.1 Results

Subset-specific CTCF binding corelates with increased interactions

As we observed changes in chromatin interactions that accompanied CD8$^+$ T cell differentiation, we hypothesized that CTCF, a regulator of chromatin looping [56], may regulate CD8$^+$ T cell genome organization associated with subset-specific gene expression. Consistent with this hypothesis, CTCF expression was upregulated with effector T cell differentiation, with significantly greater induction in the *Klrg1*^{hi} population at day 7 in previously published scRNA-Seq data [93] (**Figure 2.1A**). To compare CTCF binding among CD8$^+$ T cell subsets, we performed CTCF ChIP-Seq and Cut&Run on sort purified naive, TE, and MP OT-I CD8$^+$ T cell populations. The ENCODE ChIP-Seq pipeline was used to process the ChIP-Seq samples and obtain reproducible peak sets. Similar to the genome organization profiles, CTCF binding patterns were related to the lineage proximity of the subsets as shown by the higher overlap of CTCF peaks for the MP and TE subsets versus naive cells (**Figure 2.1B**). Naive-cell-associated CTCF binding was diminished upon effector cell differentiation (**Figure 2.1C**).

As CTCF is a key regulator of genome organization for both TAD borders and intra-TAD interactions, we characterized the averaged interaction scores +/- 50 kb around sites with subset-specific CTCF binding (**Figures 2.1D-F**). CTCF binding enriched in TE cells compared to MP or naive cells occurred at locations that had the highest interaction scores in TE cells at and around the CTCF binding sites (**Figure 2.1D**). In contrast, as denoted by the decreased interaction scores in the effector subsets, CTCF binding profiles that were enriched in MP cells compared to TE cells were strongest in the naive and then the MP subsets, suggesting that these sites may be important

for the retained ability to further differentiate into other subsets (**Figure 2.1E**). CTCF binding that was lost in TE or MP cells compared to naive cells occurred on average at TAD borders as denoted by low interaction scores (blue) at the binding site surrounded by high interaction scores (red) (**Figure 2.1F**). However, as indicated by the decrease in interactions at and surrounding the naive-specific CTCF binding sites in the effector cells (MP and TE subsets), the strength of interactions overall was weakened in MP and TE cells, indicating that the loss of CTCF binding was accompanied by a decrease in interactions (**Figure 2.1F**).

To measure the overlap of CTCF binding enriched in TE cells with the chromosomal locations of T cell subset gene-expression signatures, we used the Jaccard similarity index to quantify the relationship between CTCF binding and transcriptional regulation of $CD8^+$ T cell differentiation (**Figures 2.1G, 2.1H**). CTCF binding gained with TE differentiation from naive cells had the greatest overlap with the naive gene signature, suggesting that the majority of CTCF binding sites were insulating naive gene expression within the TE subset (**Figure 2.1G**). Interestingly, the opposite trend was observed when focusing on TE-enriched CTCF binding versus MP cells (**Figure 2.1H**). These TE-specific CTCF binding events had the greatest overlap with genes upregulated in TE cells, suggesting that more of these CTCF sites may facilitate interactions that accompany increased gene expression (**Figure 2.1H**). CTCF and T-bet have been shown to cooperate to regulate *Ifng* expression by $CD4^+$ Th1 cells [46]; thus, we examined CTCF and T-bet binding at effector gene loci using previously published T-bet ChIP-Seq in $CD8^+$ effector T cells [19] (**Figures 2.1I-K**). The loci encoding the effector marker Klrg1, the effector molecules Gzma and Gzmk, and the effector cytokine Ifnγ showed effector-specific interactions around altered T-bet and CTCF binding in effector T cells (**Figures 2.1I-K**). Russ et al. used the *Klrg1* locus, which contains effector-specific interactions and active regulatory elements, as an example

of the idea that differentiation-state-specific chromatin loops were enriched for active and poised regulatory elements (accompanying manuscript). In combination with our observation of altered CTCF and T-bet binding at the same locus and TE-specific binding occurring at TE-specific chromatin interactions, these data indicate that subset-specific CTCF binding may correspond with altered regulatory elements. Taken together, these data emphasize the diversity of CTCF function, reveal subset-specific differences in CTCF function, and suggest CTCF cooperation with T-bet and other chromatin remodeling transcription factors. Thus, effector cell differentiation appears to lead to a loss of CTCF binding at TAD borders and a gain in CTCF binding associated with increased intra-TAD interactions that accompany changes in gene expression.

Graded loss of CTCF expression reveals differential impact on CD8$^+$ T cell differentiation

Altering CTCF expression has been used to study the role of genome organization in various cellular settings, however CTCF acts in a dose-dependent manner, and complete ablation of CTCF expression is lethal [54, 55, 69]. Further, CTCF can regulate the expression of cell-cycle and cell-death genes, leading to developmental arrest with deletion [69, 70]. Therefore, we diminished CTCF levels with shRNAs to knockdown, but not eliminate, expression, retaining T cell proliferation and differentiation. As previously described, we utilized retrovirus encoding shRNAs to target the expression of CTCF in CD8$^+$ T cells [82]. We compared two shRNAs, and the first shRNA (shCTCF1) diminished CTCF mRNA and protein expression to approximately 50% while the second CTCF shRNA (shCTCF2) reduced CTCF mRNA and protein expression to approximately 25% of levels observed for shCD19 transduced control cells (shCtrl) (**Figures 2.2A-B**). To measure the impact of shRNA knockdown on cell death and cell proliferation, a 1:1 mixed transfer of OT-I cells transduced with shCtrl or shCTCF1/2 was co-transferred into mice

that were subsequently infected with Lm-OVA (**Figure 2.2C**). On day 5 of infection, neither of the two CTCF targeting shRNA constructs affected Annexin V staining (**Figure S2.2D**), while shCTCF2 significantly impaired proliferation as measured by the loss of $BrdU^+$ cells, but shCTCF1 did not (**Figure 2.2E**). Hence, we chose shCTCF1 for subsequent studies of CTCF-mediated regulation of genome organization in $CD8^+$ T cell subset differentiation.

Loss of CTCF impairs terminal differentiation and favors MP, T_{EM}, and T_{RM} cell subsets

To investigate the role of CTCF in regulating the $CD8^+$ T cell response to pathogen infection, we transduced OT-I cells with shCTCF or shCtrl and co-transferred into recipients that were then infected with Lm-OVA (**Figure 2.3A**). At the peak of infection, CTCF knockdown led to a significant loss of the TE subset of effector T cells, with a small impact on overall accumulation compared to control cells (**Figures 2.3B-C**). A corresponding gain in frequency of MP cells and $CD127^+KLRG1^+$ (DP) $CD8^+$ T cells was observed due to CTCF knockdown compared to shCtrl control cells (**Figures 2.3B-C**). Notably, after re-stimulation with OVA peptide for 4 hours, CTCF knockdown cells produced more IFNγ and TNFα than the control transduced cells (**Figure 2.4B**). At a memory timepoint, CTCF knockdown led to a reduction in the frequency of t-T_{EM} and an increase in frequency of T_{EM} without affecting the overall accumulation of circulating memory cells or T_{CM} (**Figures 2.3D-E**). Thus, at both the effector and memory timepoints, loss of CTCF expression represses the formation of the more terminally-differentiated cell populations (TE and t-T_{EM}), while favoring the differentiation of MP and T_{EM} populations.

In parallel, an unbiased *in vivo* shRNA screen to identify regulatory transcription factors of memory $CD8^+$ T cell differentiation after infection using the lymphocytic choriomeningitis virus (LCMV) acute infection model at a memory timepoint further confirmed the role of CTCF

in $CD8^+$ T cell differentiation (**Figures 2.4C-D**). The results of the screen were reported as the average Z-score of relative enrichment of shRNAs, and the accuracy of the screen was reaffirmed by identification of known regulators of memory $CD8^+$ T cell differentiation, such as *Bcl6* and *Tbx21* (**Figures 2.4C-D**). shRNA constructs targeting CTCF were enriched in the T_{EM} and T_{CM} populations when compared to t-T_{EM} cells, corresponding to a loss of t-T_{EM} cells (**Figures 2.4C-D**). Together, these data further demonstrate that CTCF expression was necessary for the development of the more terminally-differentiated $CD8^+$ effector and memory T cell subsets while repressing the formation of the more memory-like subsets in response to infection.

As a key characteristic of memory $CD8^+$ T cells is the ability to respond to a secondary infection, we next measured the impact of CTCF knockdown on antigen recall responses. OT-I cells transduced with shCtrl or shCTCF were co-transferred to wild-type hosts that were infected with Lm-OVA and re-infected with recombinant vesicular stomatitis virus expressing ovalbumin (VSV-OVA) (**Figure 2.4E**). Importantly, prior to reinfection, mice had a similar number of co-transferred OT-I cells that were transduced with shCtrl and shCTCF constructs (**Figure 2.4F**). CTCF knockdown led to a defect in accumulation of secondary effector $CD8^+$ T cells, of which there were fewer $KLRG1^{hi}$ cells, while the $KLRG1^{lo}$ cells were unaffected (**Figure 2.4G**). Thus, at effector, memory, and recall timepoints, CTCF expression was necessary to develop terminally-differentiated subsets, while the less differentiated subsets were unaffected.

We next characterized the role of CTCF expression in the differentiation of tissue-resident memory T cells (T_{RM}). Using the LCMV acute infection model P14 TCR transgenic $CD8^+$ T cells that recognize the LCMV glycoprotein peptide fragment 33–41 presented by H-$2D^b$, we monitored T_{RM} formation. CD45 congenically distinct P14 cells were transduced with shCtrl or CTCF shRNA-encoding retroviruses and co-transferred into recipient hosts that were subsequently

infected via intraperitoneal (i.p.) injection with LCMV-Armstrong. T cells were isolated from the small intestine epithelium to analyze intraepithelial lymphocytes (IEL) and spleen on day 14 of infection. In comparison to shCtrl cells, loss of CTCF increased the proportion of resident IEL $CD8^+$ T cells and the expression of the tissue-residency markers CD69 and CD103 in the gut, which is consistent with the observed increase in $KLRG1^{lo}$ effector T cells in the spleen that preferentially form T_{RM} at the day-7 time point [94] (**Figures 2.3F-G**). These data show that loss of CTCF expression promotes the formation of resident IEL $CD8^+$ T cells.

CTCF knockdown impairs terminal differentiation and accumulation of $CD8^+$ TIL

To investigate if CTCF depletion similarly impacts differentiation of $CD8^+$ TIL, we co-transferred P14 cells transduced with control or CTCF shRNA (**Figure 2.5A**) to B16-GP_{33-41} melanoma-bearing mice. Eleven days post transfer, we isolated T cells from tumors and spleens and found CTCF knockdown preferentially decreased the frequency of TIL and decreased expression of the exhaustion markers PD-1, Tim-3, CD38, CD39, and TOX (**Figures 2.5A-2.5E**). Since both tumor infiltration and exhaustion influence $CD8^+$-T-cell-mediated tumor control, we next measured how CTCF knockdown affects survival and tumor growth by transferring P14 cell transduced with control or CTCF shRNA into separate mice (**Figure 2.5F**). Survival decreased and tumor growth quickened with CTCF knockdown compared to the control cells, reflecting the decreased TIL accumulation (**Figures 2.5G-H**). In conjunction with the infection data, these data emphasize the necessity of CTCF expression for terminal differentiation of $CD8^+$ T cells in multiple setting, but also reveal a new role of CTCF for influencing accumulation of TILs.

De novo CTCF mutations reduce expression of the TE gene signature in human PBL

To investigate the impact of impaired CTCF in human peripheral blood lymphocytes (PBL), we analyzed two published RNA-Seq data sets from patients with de novo mutations of CTCF and from healthy controls [95, 96]. These patients have mutations that either reduce CTCF expression or affect its binding, leading to developmental disorders [95, 96]. GSEA revealed that the healthy control cells were enriched in the TE and exhausted T cell gene-expression signatures, while the patients with CTCF mutations had enriched T_{EM} and MP gene-expression signatures, mirroring the phenotype observed in our mouse studies (**Figures 2.6A-D**). Relative expression of specific transcription factors, cytokines, and chemokines provided a similar pattern to that seen in mice, with the expression of memory-associated molecules enriched in the PBL of patients with CTCF mutations and effector-associated molecules enriched in the PBL of the healthy controls (**Figures 2.6E-J**). This finding may result from altered frequencies of terminally-differentiated $CD8^+$ T cell populations or changes in gene expression by $CD8^+$ T cell subsets in PBL. This analysis is consistent with the idea that diminished CTCF expression impairs effector and terminal phenotypes in human lymphocytes as we observed for mouse T cells.

Loss of CTCF perturbs weak binding sites near TE-specific chromatin interactions

To identify which CTCF binding sites were affected by shRNA knockdown, we performed Cut&Run on the TE subset of OT-I $CD8^+$ T cells transduced with shCtrl or shCTCF (**Figure 2.7A**). Reproducible peaks were obtained using the irreproducible discovery rate (IDR) method [97] on peaks called by MACS2 [98]. HOMER (getDifferentialPeaks) [80] was used to identify differential peaks between the two samples using a fold change cutoff of 2 and a p-value cutoff of 0.05; 2,250 peaks were enriched in the transferred control TE cells, while 69 peaks were enriched in the cells with CTCF knockdown (**Figure 2.7B**). As expected, reduction of CTCF expression

resulted in loss of CTCF binding (**Figure 2.7B**); the tag score for each peak in the shCtrl and shCTCF samples were compared and the differential peaks highlighted (**Figure 2.7C**). Peaks sensitive to CTCF knockdown favored lower tag scores, suggesting that lower occupancy CTCF sites were more likely to be affected by shRNA knockdown (**Figure 2.7C**). Furthermore, we next calculated the motif scores of each CTCF binding site for TE cells that were transduced with shCtrl (black line) or shCTCF (blue line) using the Find Individual Motif Occurrences (FIMO) software tool [99]. When the subset of binding sites that lost CTCF occupancy upon CTCF knockdown were graphed (red line), these sites displayed lower motif scores with more sites with a motif score between 16 and 19 and fewer sites with a motif score above 19 (**Figure 2.7D**). The lower motif score corresponds to weaker affinity CTCF binding sites that tend to associate with active histone marks and higher gene expression [100].

To identify the effect of CTCF knockdown on transcriptional programs, pathway analysis was performed using Metascape [101] for genes located near CTCF sites that had reduced occupancy upon knockdown (**Figure 2.7E**). These nearby genes were important for T cell activation and signaling pathways consistent with the impact of the loss of CTCF expression on $CD8^+$ T cell differentiation (**Figure 2.7E**). As CTCF is important for regulating chromatin interactions, we then used HOMER [80] to determine the average chromatin interactions around sites that lost CTCF binding with knockdown (**Figure 2.7F**). When the averaged chromatin interactions were visualized as a heatmap using gplots (heatmap.2), the increased interaction scores at sites with reduced CTCF binding for the TE subset revealed that the knockdown of CTCF expression targets binding sites with TE-specific interactions (**Figure 2.7F**). The analysis of specific CTCF binding sites whose occupancies were impacted by knockdown showed that maximum levels of CTCF expression preferentially allow for binding at weak CTCF binding sites

that are enriched at TE-specific chromatin interactions near genes important for T cell activation and signaling. Thus, the 50% loss of CTCF expression with shCTCF knockdown impairs lower affinity CTCF binding at TE-specific chromatin interactions that alter $CD8^+$ T cell differentiation in favor of the more memory populations.

CTCF supports expression of the terminal-effector T cell transcriptional program

To examine how CTCF depletion affects the effector T cell transcriptional program, we performed RNA-Seq on sorted TE OT-I cells transduced with either control or CTCF shRNA on day 8 of infection with Lm-OVA (**Figure 2.7A**). Despite CTCF knockdown only affecting the expression of a subset of genes, GSEA showed that loss of CTCF expression by the TE subset resulted in an enrichment of MP-signature genes and loss of the TE gene-expression signature (**Figures 2.8A-B**). Thus, although some TE cells still differentiated with CTCF knockdown as defined by the expression of KLRG1 and lack of expression of CD127, the transcriptome more closely resembled the MP-associated transcriptional program when compared to the control TE cells (**Figure 2.8B**). No significant enrichment for the naive gene signatures was observed (**Figure 2.8B**). Meanwhile, the MP cells that differentiated with decreased CTCF expression also had only a small subset of genes with disrupted expression and loss the TE gene-expression signature (**Figures 2.9A-B**). Further analysis of transcription factors that are known to regulate $CD8^+$ T cell differentiation showed that CTCF knockdown in both TE and MP cells led to an upregulation of *Tcf7* and *Zfp683*, encoding the proteins Tcf1 and Hobit, which promote MP and T_{RM} differentiation, respectively [102, 103], consistent with the *in vivo* phenotypes (**Figures 2.8C, 2.9C**).

A previous study showed that memory T cells were enriched for a transcriptional program of self-renewal by comparing gene expression of memory populations with long-term hematopoietic stem cells [67]. In agreement with the *in vivo* phenotype where CTCF depletion repressed terminal differentiation and promoted the differentiation of the more "stem-like" subsets, CTCF knockdown let to an upregulation of genes associated with long-term hematopoietic stem cells and diminished expression of genes downregulated with hematopoietic stem cell differentiation (**Figures 2.8D, 2.9D**). Furthermore, Metascape pathway analysis [101] of genes downregulated with CTCF knockdown revealed that diminished CTCF expression led to a loss in expression of cell cycle genes, consistent with previous studies of CTCF-deficient thymocytes [69, 70], and a role for CTCF in promoting the expression of these genes (**Figure 2.8E**). On the other hand, pathway analysis revealed that genes upregulated upon CTCF knockdown were important for immunity (**Figure 2.8F**). Together, these analyses suggest that the role of CTCF in promoting or insulating gene expression targets different cell functions. Furthermore, the reduction of CTCF expression shifts the transcriptional program towards a more MP phenotype at the expense of the TE phenotype by promoting the memory T cell-associated transcriptional program.

As CTCF can regulate gene expression through facilitation of enhancer-promoter interactions, we examined whether binding was perturbed at previously published subset-specific genes, enhancers, or promoters [30, 82] by looking at the overlap of chromosomal locations as quantified by the Jaccard index. CTCF binding sites that were lost with knockdown overlapped the most with genes that were upregulated in the TE cell subset as indicated by a higher Jaccard index score (**Figure 2.8G**). Furthermore, the loss of CTCF binding with knockdown occurred at active $CD8^+$ T cell enhancers and promoters marked by active histone modifications with a slight enrichment for effector-specific enhancers (**Figures 2.8H-I**). Loss of CTCF binding with

knockdown occurred more at subset-specific enhancers than promoters and was enriched for effector-specific enhancers (**Figures 2.8H-I**). These data suggest that knockdown of CTCF may regulate gene expression by disrupting CTCF binding at enhancers active in the TE and MP subsets but not the naive subset.

CTCF knockdown reduces chromatin accessibility and alters transcription factor activity

CTCF has been shown to decrease chromatin accessibility in a human B cell lymphoblastic leukemia cell line [57]. To measure the effect of CTCF knockdown on chromatin accessibility in $CD8^+$ T cells, we performed ATAC-Seq on sort purified TE cells transduced with shCtrl or shCTCF shRNA (**Figure 2.7A**). The ENCODE ATAC-Seq pipeline [104] was used to process the samples and identify reproducible peak sets, and differential peaks were identified using HOMER [80]. CTCF knockdown led to an overall loss in chromatin accessibility, as shown by the enrichment of ATAC peaks in the control cells (**Figures 2.10A**). To link chromatin accessibility with changes in CTCF binding, we measured the ATAC-Seq tag enrichment at sites that lose CTCF binding upon knockdown (**Figure 2.10B).** Loss of CTCF binding (blue) reduced chromatin accessibility compared to the control (black) suggesting that CTCF binding may be necessary to maintain chromatin accessibility (**Figure 2.10B**).

To identify the impact of the loss of chromatin accessibility on transcription factor activity, we performed motif enrichment in the ATAC peaks lost upon knockdown of CTCF (**Figure 2.10C**). Conversely, we interrogated motif enrichment in the CTCF peaks that were lost upon knockdown of CTCF to identify potential protein partners that may be impacted by disrupted CTCF binding (**Figure 2.10D**). Both analyses identified Hic1, Bach2, and T-bet (**Figures 2.10C-D**). Hic1 is a transcriptional repressor that supports T cell accumulation in the IEL, and we found

that it supports T_{RM} residency in the small intestine [105, 106]. Therefore, loss of CTCF expression may promote Hic1 binding to regulate its target genes, perhaps explaining the increase in T_{RM} formation *in vivo* that we observed (**Figures 2.3F-G**). Meanwhile, the identification of Bach2 combined with the previous observations of CTCF binding upstream of Bach2 regulated looping architecture in Figure S1I suggests a collaboration between CTCF and Bach2 (**Figures 2.10C-D**). T-bet is a key regulator of $CD8^+$ effector and T_{RM} differentiation, promoting TE differentiation and inhibiting T_{RM} differentiation [3, 107, 108]. Therefore, the enrichment of the T-bet motif may explain why there were fewer terminally-differentiated effector cells and more T_{RM} cells with CTCF knockdown (**Figures 2.10C-D**).

To predict transcription factors with CTCF-knockdown-sensitive activity before the response to infection, we performed PageRank analysis [30] using *in vitro* ATAC-Seq and RNA-Seq data that mirrored the phenotype of the *in vivo* samples (**Figures 2.8A, 2.9A, 2.10A, 2.10E-G**). PageRank integrates RNA-Seq and ATAC-Seq data to construct a genetic network to capture the global impact of transcription factors on the network [30]. PageRank analysis ranks transcription factors based on the number and importance of genes that may be regulated, where a PageRank score with a higher number suggests a more important role for impacting gene expression in a network [30]. PageRank predicted that transcription factors, including Blimp1, Eomes, and T-bet, are more likely to mediate the transcriptional program for the control cells, suggesting that CTCF knockdown may disrupt access to binding sites to alter nearby gene expression (**Figure 2.10G**). Blimp1, Eomes, and T-bet are known to be important for $CD8^+$ T cell differentiation in effector, memory, and tumor settings [3, 94, 103, 108-110]. This suggests that loss of CTCF expression may prevent Blimp1, Eomes, and T-bet from binding to regulate their target genes, which may contribute to the loss of terminal differentiation seen *in vivo* (**Figures 2.3,**

2.4). On the other hand, PageRank predicted that transcription factors, including Bach2, Tcf1, and Lef1, are important mediators of the transcription program for cells with CTCF knockdown (**Figure 2.10G**). As Bach2, Tcf1, and Lef1 are important for memory T cell differentiation [23, 51, 111], loss of CTCF expression may promote their activity to facilitate the memory cell differentiation seen *in vivo* (**Figure 2.3**).

Previous studies showed that CTCF and T-bet cooperate to promote the expression of the effector cytokine IFNγ in $CD4^+$ T cells [46]. Our previous analysis identified T-bet as a potential target of CTCF knockdown (**Figures 2.10C-D, 2.10G**). In the RNA-Seq data, there was a lower trend in the expression of *Tbx21*, which encodes for T-bet in TE cells with CTCF knockdown, and T-bet expression was reduced with CTCF knockdown by day 14 of infection with Lm-OVA (**Figures 2.11A-B**). T-bet deficiency results in fewer TE cells and more T_{RM} cells [3, 108], so we explored if elevated T-bet expression could overcome the loss of TE cells from CTCF knockdown. We co-transduced P14 cells with shCtrl and the overexpression construct for T-bet (T-bet-GFP), shCtrl and the control construct (pMIG-GFP), shCTCF and T-bet-GFP, or shCTCF and pMIG-GFP (**Figure 2.11C**). We then co-transferred the shCtrl and shCTCF with pMIG-GFP or the shCtrl and shCTCF with T-bet-GFP into recipient mice that were subsequently infected with LCMV Armstrong (**Figure 2.11C**). T cells from the spleen were isolated at the peak of infection for phenotyping (**Figure 2.11C**). T-bet overexpression rescued the differences in subset frequency between shCtrl and shCTCF in $KLRG1^{hi}$ cells (**Figures 2.11D-E**). These data suggest that T-bet may be downstream of CTCF-mediated regulation of $CD8^+$ T cell terminal differentiation.

Our motif enrichment and Pagerank analyses also identified Bach2 as a transcription factor whose function may be altered with CTCF knockdown. Russ et al. measured chromatin interactions in T cells with *Bach2* deletion. Comparing CTCF binding with altered chromatin

interactions induced by *Bach2* deletion revealed a distinct enrichment of CTCF binding upstream of the regions with altered interactions suggesting that CTCF may be important for chromatin interactions regulated by other transcription factors (**Figure 2.12A**). Additionally, the accompanying paper found that deleting *Bach2* shifted the chromatin architecture to more closely resemble the effector subset. When *Bach2*$^{-/-}$-induced gains in chromatin interactions were compared with subset-specific chromatin interactions, they overlapped the most with chromatin interactions gained with effector and memory-cell differentiation, with a distinct overlap with MP-specific chromatin interactions and secondarily memory-specific chromatin interactions (**Figure 2.12B**). This suggests that deletion of *Bach2* specifically re-organizes chromatin architecture to more closely resemble the activated T cell subsets with greater differentiation potential. As CTCF knockdown also shares the same phenotype, these analyses suggest that CTCF and Bach2 may be working together. Together, the data suggest that CTCF knockdown may alter the transcription factor landscape to regulate CD8^{+} T cell differentiation.

Perturbation of specific CTCF binding sites enhances expression of target genes

We next examined the impact of CTCF binding on the expression of specific genes. The *Il7r, Bcl6,* and *Ccl3* loci each have nearby CTCF binding sites that were sensitive to shRNA knockdown (**Figure 2.13A**). Analysis of Hi-C interactions for the regions around the gene loci showed noticeable gains in DNA interactions upon effector differentiation at the *Il7r* and *Ccl3* loci but not the *Bcl6* locus, as indicated by the increased interaction scores and number of arcs for the TE and MP tracks (**Figure 2.13A**). Characterization of histone marks from previous studies [30] showed that the knockdown-sensitive CTCF site near *Il7r* was at an active enhancer in MP cells, as indicated by the H3K4me1 and H3K27ac peaks present in the MP subset, but not in the TE

subset (**Figure 2.14A**). The knockdown-sensitive CTCF site near *Ccl3,* however, was at an enhancer that was active in effector cells, as indicated by the H3k4me1 and H3K27ac marks present in both the MP and TE subsets (**Figure 2.14B**). In contrast, the *Bcl6* locus did not have any clear changes in chromatin interactions, and the knockdown-sensitive CTCF site near *Bcl6* did not overlap with any promoters or enhancers (**Figures 2.13A, 2.14C**). Expression of *Il7r* and *Bcl6* is important for the formation of memory $CD8^+$ T cells [112], and both displayed higher expression in the MP subset, whereas *Ccl3* is expressed by effector cells and has been shown to be important for effector function of memory T cells [113] (**Figures 2.15A-C**). mRNA expression of all three of these genes, however, increased upon CTCF knockdown (**Figures 2.15D-F**), suggesting that CTCF binding actually acts to restrain expression of these genes.

To directly link the change in CTCF binding with regulation of gene expression, we used CRISPR/Cas9 to target insertions or deletions at CTCF binding sites through mutagenic nonhomologous end joining [114]. We designed crRNAs, which anneal to tracrRNA to form gRNAs that target CD4, Thy, or specific CTCF binding sites [115] (**Figures 2.13B, 2.13C, 2.13E, 2.13G**). P14 cells were electroporated with a control guide (CD4 or Thy) or guides specific for the indicated CTCF binding sites, mixed 1:1, and co-transferred into congenically distinct wild-type recipients that were subsequently infected with LCMV-Armstrong (**Figure 2.13B**). The targeting of the CTCF binding motif largely resulted in single nucleotide deletions or additions as determined by DNA sequencing of targeted cells (**Figures 2.13C, 2.13E, 2.13G, 2.15G, 2.15H, 2.15I**). Perturbation of CTCF binding at the MP-specific enhancer upstream of *Il7r* significantly increased CD127 protein expression by P14 T cells isolated from the spleen at the effector time point (**Figure 2.13D**). Disruption of CTCF binding near the *Bcl6* locus significantly increased Bcl6 expression at the memory time point by P14 T cells isolated from the spleen (**Figure 2.13F**). Ccl3

protein levels were measured after splenocytes isolated at an effector time point were re-stimulated with GP_{33-41} for 4 hours, and disruption of CTCF binding at the enhancer active in effector cells increased Ccl3 production by approximately three-fold (**Figure 2.13H**). Together, these data show that these specific CTCF binding sites are important for restraining the expression of their neighboring genes whose functions are key for memory T cell differentiation or function.

2.2 Discussion

Here, we found that $CD8^+$ T cell differentiation was accompanied by changes in CTCF binding, and knockdown of CTCF expression prevented terminal differentiation and promoted memory differentiation by altering transcriptional programs and transcription factor activity. Strikingly, perturbation of a single CTCF binding site upregulated expression of corresponding memory molecules.

As CTCF is known to mediate chromatin interactions, studies often disrupt CTCF binding to study the role of genome organization. CTCF depletion can also prevent the upregulation of inflammatory genes in cells such as *in vitro* macrophages and $CD4^+$ T cells [46, 68]. Therefore, we characterized CTCF-binding profiles in $CD8^+$ T cells and studied how CTCF depletion impacted $CD8^+$ T cell differentiation and function during infection and malignancy. Consistent with the known role of CTCF in regulating chromatin interactions [63] and our characterization of genome organization in $CD8^+$ T cells, the pattern of CTCF binding reflected the lineage proximity of the subsets. Interestingly, CTCF binding in TE cells was particularly enriched in intra-TAD chromatin interactions compared to those sites uniquely bound in naive T cells, which were at TAD borders. CTCF levels impacted the differentiation of effector $CD8^+$ T cells, with diminished CTCF leading to loss of binding at low affinity CTCF sites and TE-specific enhancers, culminating in impaired numbers of TE, t-T_{EM}, and terminally-exhausted cells from tumors, but unaffected memory T cell differentiation. Thus, CTCF was key for promoting terminal differentiation in both infection and tumor contexts by preventing the expression of genes important for memory T cell differentiation. Coupled with our observation that TE cells have unique enrichment of enhancer-promoter interactions, we hypothesized that terminal differentiation of $CD8^+$ T cells requires the

establishment of CTCF-mediated intra-TAD chromatin interactions, with weaker affinity CTCF binding insulating the memory program.

CTCF can act as both a promoter and repressor of gene expression by facilitating or blocking enhancer-promoter interactions [116]. We surprisingly found a delineation in CTCF regulation of expression between cell-cycle genes and immune cell function genes, where loss of CTCF binding at weak-affinity sites upregulated immune genes and downregulated cell-cycle genes. Specifically, increased expression of MP genes upon CTCF knockdown suggests that CTCF acts as an insulator at genes important for memory $CD8^+$ T cells. Furthermore, mutating a single CTCF binding site motif using CRISPR-Cas9 near *Il7r, Bcl6, and Ccl3* loci resulted in upregulation of these memory-associated markers. Disruption of CTCF binding at those sites may enable interactions with alternative enhancers that drive higher gene expression. Further, investigation into CTCF-regulated enhancer-promoter interactions may provide biological insights into how chromatin interactions fine-tune gene expression to promote $CD8^+$ T cell subset differentiation.

A key feature of memory cells is their ability to proliferate and differentiate to secondary effector T cells upon antigen re-exposure. The maintenance of differentiation potential is not well understood. However, CTCF has been shown to repress genes associated with "stemness" in hematopoietic stem cells and the liver cancer cell line HepG2 [65-67]. We concordantly observed a loss of terminally-differentiated subsets and a gain in subsets with greater differentiation potential in both infection and tumor settings upon CTCF knockdown. Studies have shown that "stemness" is reinforced through epigenetic modifications and that disruptions in regulators lead to the accumulation of more-memory-like cells at the expense of more-effector-like cells [117-120]. Furthermore, genome organization has been linked to the maintenance of the "stemness"

program through changes in the nuclear positioning, chromatin compaction, and enhancer-promoter interactions [121]. Thus, our data can be a resource for further investigation to characterize the spatial organization requirements that regulate T cell differentiation potential.

Transcription factors important for $CD8^+$ T cell differentiation are known to regulate chromatin interactions. Recent studies in naive and T_{CM} $CD8^+$ T cells have shown that deletion of Tcf1/Lef1 in naive cells or Tcf1 alone in T_{CM} cells altered genome organization to respectively reduce expression of T cell lineage-enriched genes and prevent expression of genes associated with glycolysis, which is necessary for secondary effector function [50, 51]. Further, the accompanying paper found that deletion of *Bach2* or disruption of Satb1 binding in naive $CD8^+$ T cells disrupted chromatin looping to more closely resemble effector cells. While Tcf1, Bach2, and Satb1 reinforced the chromatin architecture for naive cells, we found that CTCF was needed for $CD8^+$ T cell terminal differentiation at the expense of memory formation. Our previous research showed that depletion of Yy1, a chromatin remodeler known to directly interact with CTCF and also facilitate chromatin interactions within CTCF-mediated loops [62, 122], led to a loss of TE cells [30]. Yy1 depletion and CTCF depletion both led to a loss of TE cells, which further suggests that the formation or reinforcement of genome organization may be key for the terminal-effector phenotype. Thus, numerous transcription factors are needed at different stages of $CD8^+$ T cell differentiation to regulate genome organization important for T cell fate, and linking the roles of chromatin remodelers may provide further insight into the genome-organization-mediated regulation of $CD8^+$ T cell differentiation.

Multiple possible mechanisms underly CTCF regulation of gene expression and may be affected by the number of proximal CTCF sites, the location of the binding site, and the protein partners [56, 61, 123]. In our study, motif enrichment and PageRank analyses identified potential

CTCF-regulated transcription factors, such as Hic1, T-bet, and Bach2. Hic1 regulates T_{RM} formation [105, 106], and its binding motif was enriched at sites that lose CTCF binding upon shRNA knockdown. Thus, knockdown of CTCF may impact Hic1 binding to promote T_{RM} formation as seen in our *in vivo* studies. On the other hand, T-bet is known to inhibit $CD8^+$ T_{RM} formation and promote terminal-effector differentiation [3, 108]. We identified T-bet as a potential transcription factor with binding and activity regulated by CTCF knockdown, and T-bet overexpression rescued the CTCF knockdown phenotype. Therefore, in conjunction with previous studies in $CD4^+$ T cells, where T-bet collaborates with CTCF to regulate chromatin interactions needed for IFNγ expression [46], the data suggest that T-bet may be important for chromatin interactions that drive $CD8^+$ T cell terminal differentiation.

Our data has also revealed several instances where CTCF was linked to Bach2. CTCF binding was enriched upstream of Bach2-mediated interactions, Bach2 binding motifs were identified in CTCF sites and accessible chromatin regions lost with CTCF knockdown, and Bach2 was predicted to regulate expression of genes that increased with CTCF knockdown. Altogether, these observations suggest the potential cooperation between Bach2 and CTCF in mediating chromatin interactions in $CD8^+$ T cells. Further, knockout of *Bach2* in naive cells led to remodeling of chromatin interactions to more closely resemble interactions gained upon MP cell differentiation, consistent with the increased MP cell differentiation with CTCF knockdown (accompanying manuscript). Therefore, Bach2 and CTCF may cooperate to mediate interactions needed to restrain memory $CD8^+$ T cell differentiation. Altogether, these data highlight the importance of specific transcription factors to regulate genome organization that affect T cell fate and can be used to inform the identification of additional transcription factors that regulate chromatin architecture important for $CD8^+$ T cell differentiation.

IL-2 signaling is known to be key to the formation of both effector and memory populations [124]. Prolonged expression of IL-2Rα favors more terminally-differentiated T cell subsets and increasing doses of IL-2 pushes $CD8^+$ T cells to a more terminally-differentiated fate [125]. CTCF binding has been shown to translate IL-2 signaling and αKG-sensitive metabolic changes [74]. Further, αKG is a metabolite in the glycolysis pathway, which is an important metabolic program for effector $CD8^+$ T cells in an infection and tumor setting. Based on our research showing that CTCF depletion prevents terminal differentiation, we speculate that CTCF knockdown may interfere with metabolic signaling required for IL-2-mediated promotion of terminal differentiation in $CD8^+$ T cells. These observations imply that metabolism may be linked to genomic organization in $CD8^+$ T cells, but the exact mechanisms remain unclear.

Here, we provided evidence that $CD8^+$ T cell genome organization is linked to the lineage proximity of T cell differentiation and that CTCF insulates the expression of key memory genes that reside in areas of high chromatin interaction; our future studies will aim to further refine the link between genome organization, transcriptional networks, and $CD8^+$ T cell differentiation.

2.3 Acknowledgements

Chapter 2 in part, has been submitted for publication of the material. Quon S, Yu B, Russ BE, Tsyganov K, Nguyen H, Toma C, Heeg M, Hocker JD, Milner JJ, Crotty S, Pipkin ME, Turner SJ, Goldrath AW. CTCF facilitates subset-specific chromatin interactions to limit the formation of terminally-differentiated CD8+ T cells. The dissertation author was the primary researcher and first author of this paper.

2.4 Figures

Figure 2.1: CTCF binding changes with effector cell differentiation and is linked to changes in chromatin interaction and subset-specific genes. (A) CTCF expression from scRNA-Seq data in *Klrg1*^{hi} (black) and *Klrg1*^{lo} (gray) cells at days 0, 5, 6, and 7 post infection with LCMV. Statistical significance was determined using Wilcoxon rank sum test. (B) Quantification of the overlap between CTCF binding in different T cell subsets using MSPC filtered peak sets from ChIP-Seq and Cut&Run against CTCF for the indicated samples. (C) Quantification of differential CTCF peaks (p-value < 0.0001; FC > 4) between subsets on a logarithmic scale. (D-F) Heatmaps portraying averaged chromosomal interactions around differential CTCF peaks as measured by HOMER analyzeHiC. (G) Quantification of overlap between CTCF peaks enriched in TE cells compared to naive cells and lists of chromosomal coordinates of the indicated subset gene signatures. (H) Quantification of overlap between CTCF peaks enriched in TE cells compared to MP cells and lists of chromosomal coordinates of the indicated subset gene signatures. (I) Circos plot showing interactions enriched in effector cells at the *Klrg1* locus with tracks showing T-bet and CTCF binding. Red links represent interactions that are enriched in both TE and MP cells compared to naive cells. (J) Circos plot showing interactions enriched in effector cells at the *Gzma* and *Gzmk* loci with tracks showing T-bet and CTCF binding. Red links represent interactions that are enriched in both TE and MP cells compared to naive cells. (K) Circos plot showing interactions enriched in effector cells at the *Ifng* locus with tracks showing T-bet and CTCF binding. Red links represent interactions that are enriched in both TE and MP cells compared to naive cells.

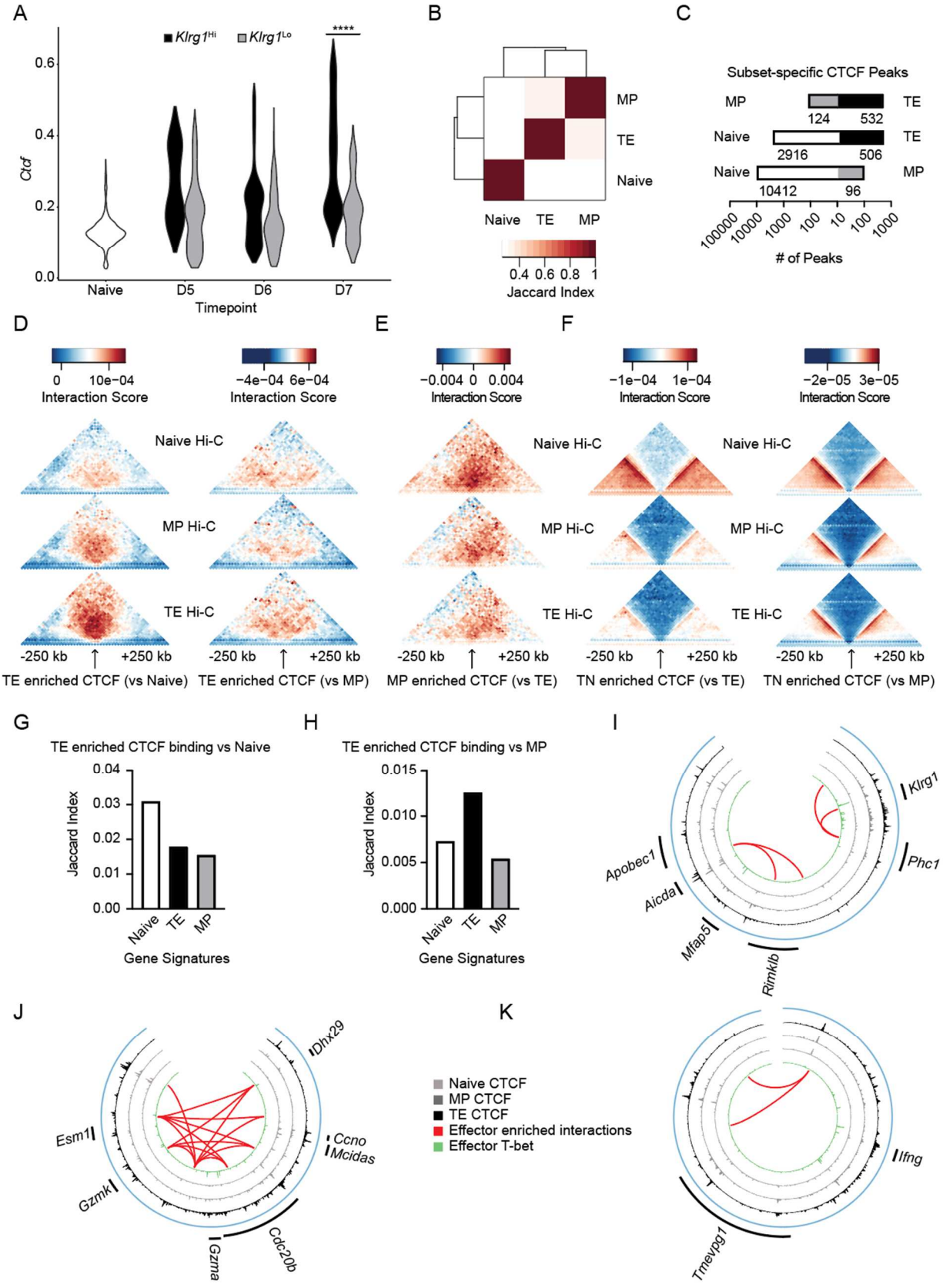
A
Klrg1Hi
Klrg1Lo
****
Ctcf
0.6
0.4
0.2
0.0
Naive
D5
D6
D7
Timepoint
B
MP
TE
Naive
Naive TE MP
0.4 0.6 0.8 1
Jaccard Index
C
Subset-specific CTCF Peaks
MP
TE
124
532
Naive
TE
2916
506
Naive
MP
10412
96
100000 10000 1000 100 10 100 1000
# of Peaks
D
0 10e−04
Interaction Score
−4e−04 6e−04
Interaction Score
Naive Hi-C
MP Hi-C
TE Hi-C
-250 kb
+250 kb
TE enriched CTCF (vs Naive)
TE enriched CTCF (vs MP)
E
−0.004 0 0.004
Interaction Score
−1e−04 1e−04
Interaction Score
−2e−05 3e−05
Interaction Score
MP enriched CTCF (vs TE)
TN enriched CTCF (vs TE)
TN enriched CTCF (vs MP)
G
TE enriched CTCF binding vs Naive
Jaccard Index
0.04
0.03
0.02
0.01
0.00
Naive TE MP
Gene Signatures
H
TE enriched CTCF binding vs MP
Jaccard Index
0.015
0.010
0.005
0.000
Naive TE MP
Gene Signatures
I
Klrg1
Phc1
Apobec1
Aicda
Mfap5
Rimklb
J
Dhx29
Esm1
Ccno
Mcidas
Gzmk
Gzma
Cdc20b
K
Naive CTCF
MP CTCF
TE CTCF
Effector enriched interactions
Effector T-bet
Ifng
Tmevpg1

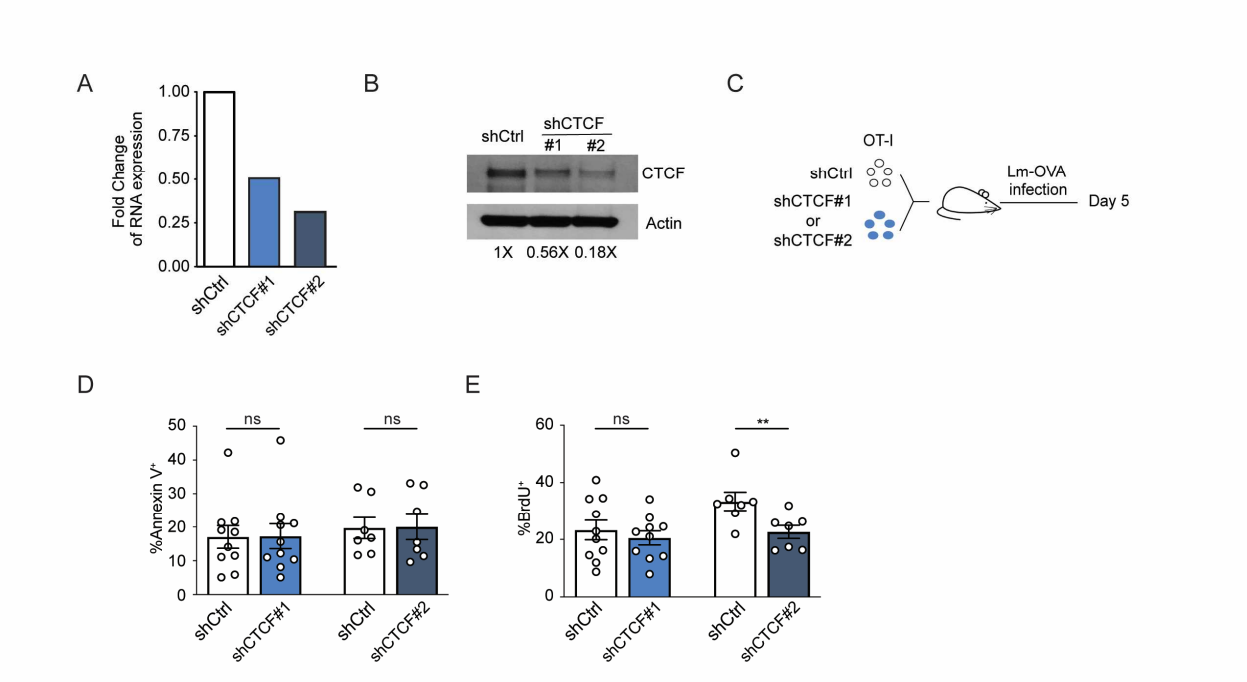

Figure 2.2: CTCF regulates proliferation in a dose-dependent manner. (A) Real-time PCR analysis of CTCF RNA expression in $CD8^+$ T cells that were activated with anti-CD3 and anti-CD28 for 24 hours, transduced with retrovirus expressing shCtrl, shCTCF#1, or shCTCF#2, and further cultured for 48 hours in IL-2. (B) Western blots of CTCF protein levels with ß-actin as a loading control in *in vitro* activated transduced T cells. Ratios were quantified with Image J. (C) Schematic of experimental setup. Recipients were given a co-transfer of OT-I $CD8^+$ T cells that were transduced with shCtrl or shCTCF. They were then subsequently infected with Lm-OVA. Spleens were collected at day 5. (D) Quantification of Annexin V expression. (n=7) (E) Quantification of BrdU expression. (n=7) (D and E) Bars and error bars represent mean ± SEM. Statistical significance was calculated using the 2-tailed paired Student's t test. Representative of two independent experiments.

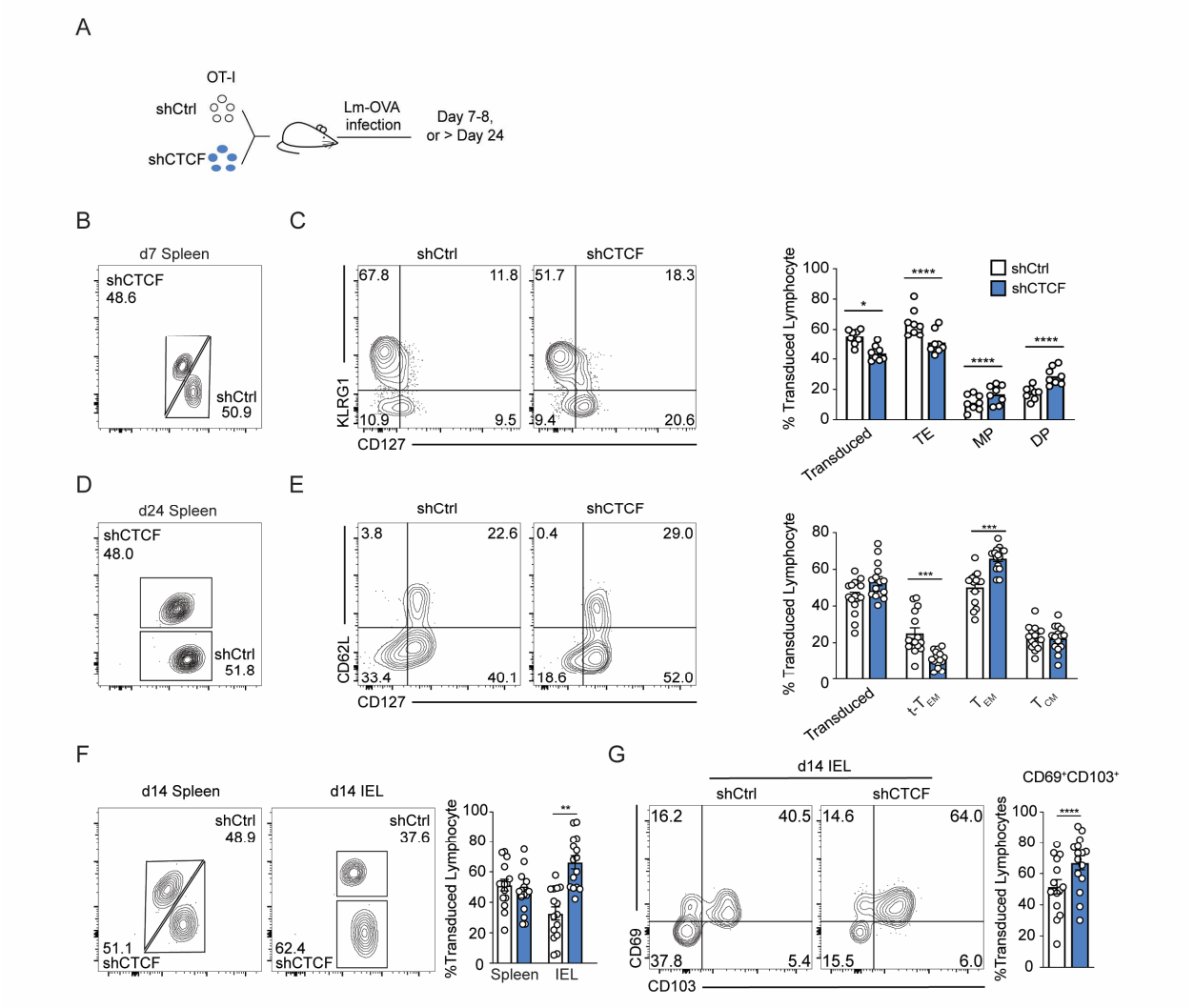

Figure 2.3: CTCF deficiency represses terminal differentiation and promotes the formation of the memory subsets in infection. (A) Schematic of experimental set-up. Recipients were given a co-transfer of OT-I CD8$^+$ T cells that were transduced with shCtrl or shCTCF. They were subsequently infected with Lm-OVA. Spleens were collected at day 7/8 or after day 24. (B) Flow cytometry of transduced OT-I cells between shCtrl and shCTCF isolated from spleens 7 days after transfer and infection with Lm-OVA. (C) Flow cytometry of cells from B for KLRG1 and CD127 expression with quantification (right). (n=8) (D) Representative FACs plots show the frequency of transduced OT-I cells between shCtrl and shCTCF isolated from spleens 24 days after transfer and infection with Lm-OVA. (E) Flow cytometry of cells from D for the expression of CD62L and CD127 with quantification (right). (n=15) (F) Flow cytometry of transduced P14 cells between shCtrl and shCTCF isolated from spleens and IEL 14 days after transfer and infection with LCMV-Armstrong. (n=15) (G) Flow cytometry of cells from F for the expression of CD69 and CD103 with quantification (right). (n=15) (C-G) Bars and error bars represent mean ± SEM. Statistical significance was calculated using the 2-tailed paired Student's t test.

Figure 2.4: CTCF knockdown, cytokine production, and rechallenge. (A) Gating scheme for transduced $CD8^+$ T cells. (B) Flow cytometry of transduced OT-I cells for IFNγ and TNFα expression with quantification (right). (n=8) (C-D) Plots showing Z scores of shRNA guides from an *in vivo* shRNA screen. (E) Schematic of experimental set-up. Recipients were given a co-transfer of OT-I $CD8^+$ T cells that were transduced with shCtrl or shCTCF. They were then subsequently infected with Lm-OVA and after 29 days, infected with VSV-OVA. (F) Frequency of transferred lymphocytes at time of reinfection in the blood. (n=5) (G) Kinetics of total (left), $KLRG1^{hi}$ (left), or $KLRG1^{lo}$ (right) transduced cells in the blood following reinfection with VSV-OVA. (n=5) (B, F, and G) Bars, lines, and error bars represent mean ± SEM. Statistical significance was calculated using the 2-tailed paired Student's t test.

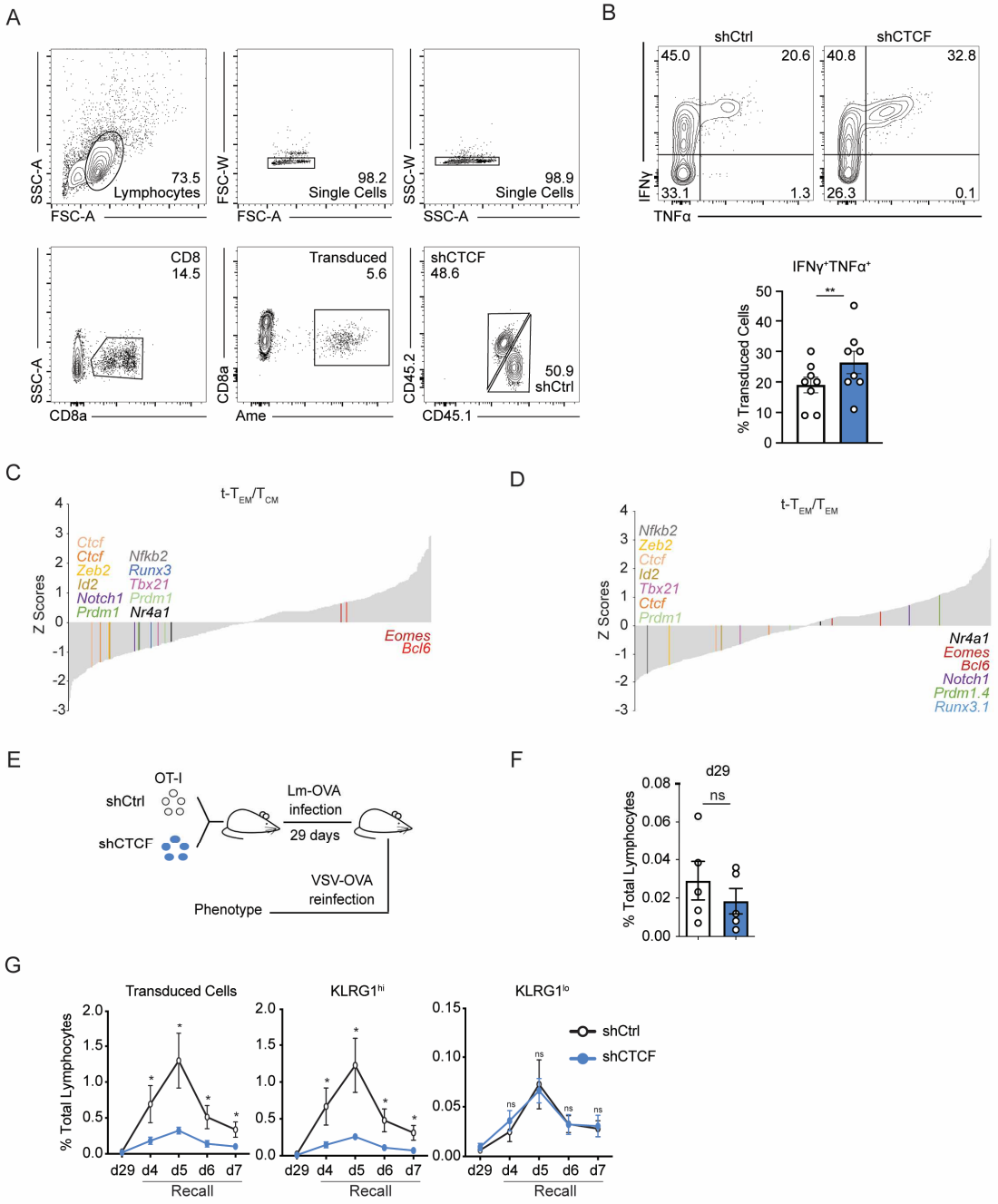
A
SSC-A
FSC-A
73.5
Lymphocytes
FSC-W
FSC-A
98.2
Single Cells
SSC-W
SSC-A
98.9
Single Cells
CD8
14.5
SSC-A
CD8a
Transduced
5.6
CD8a
Ame
shCTCF
48.6
50.9
shCtrl
CD45.2
CD45.1
B
shCtrl
shCTCF
45.0
20.6
33.1
1.3
40.8
32.8
26.3
0.1
IFNγ
TNFα
IFNγ+TNFα+
% Transduced Cells
**
C
t-TEM/TCM
Z Scores
Ctcf
Ctcf
Zeb2
Id2
Notch1
Prdm1
Nfkb2
Runx3
Tbx21
Prdm1
Nr4a1
Eomes
Bcl6
D
t-TEM/TEM
Z Scores
Nfkb2
Zeb2
Ctcf
Id2
Tbx21
Ctcf
Prdm1
Nr4a1
Eomes
Bcl6
Notch1
Prdm1.4
Runx3.1
E
OT-I
shCtrl
shCTCF
Lm-OVA
infection
29 days
VSV-OVA
reinfection
Phenotype
F
d29
ns
% Total Lymphocytes
G
Transduced Cells
KLRG1hi
KLRG1lo
shCtrl
shCTCF
% Total Lymphocytes
d29 d4 d5 d6 d7
Recall
ns

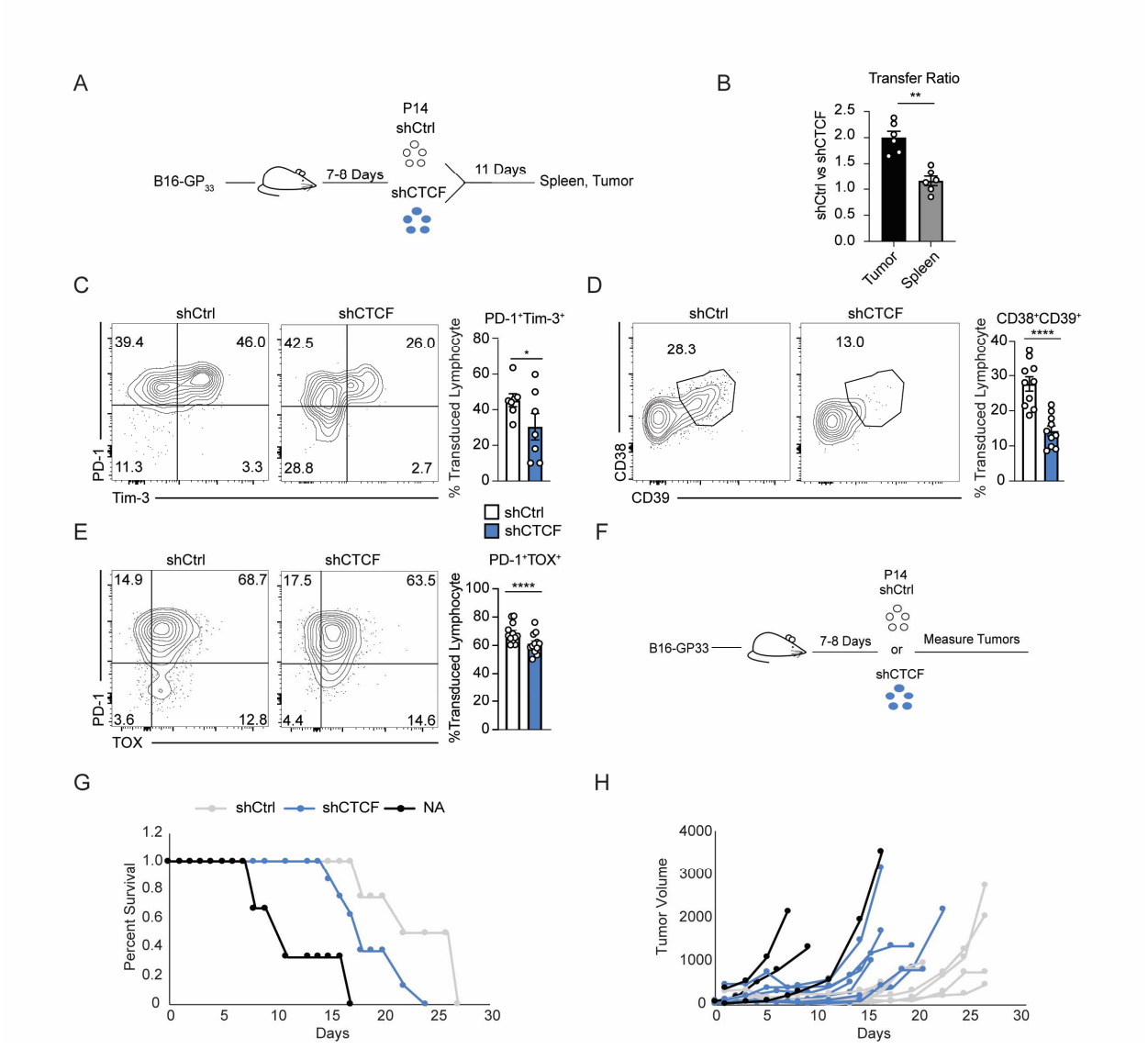

Figure 2.5: CTCF deficiency represses terminal differentiation in tumors. (A) Schematic of experimental setup. Mice were subcutaneously injected with B16-GP$_{33-41}$ and once the tumors were palpable 7-8 days later, P14 CD8^{+} T cells transduced with either shCtrl or shCTCF were co-transferred. Eleven days later, the tumors and spleens were collected for phenotyping. (B) Quantification of the ratio of shCtrl transduced P14 cells to shCTCF transduced P14 cells in the tumor and spleen. (n=6) (C) Flow cytometry of transduced P14 cells in the tumor for expression of PD-1 and Tim-3 with quantification (right). (n=7) (D) Flow cytometry of transduced cells in the tumor for expression of CD38 and CD39 with quantification (right). (n=10) (E) Flow cytometry of transduced P14 cells in the tumor for PD-1 and TOX expression with quantification (right). (n=10) (C-E) Bars and error bars represent mean ± SEM. Statistical significance was calculated using the 2-tailed paired Student's t test.

Figure 2.6: Heterozygotic de novo CTCF mutations lead to enrichment of memory-cell and loss of effector-cell associated molecules. (A) Volcano plots comparing gene expression between healthy control individuals and patients harboring *de novo* mutations of CTCF overlaid with genes that are >1.5 fold upregulated in TE cells compared to MP cells (B) or in MP cells compared to TE cells. Statistical significance was calculated using Fisher's exact tests. (C&D) GSEA analysis for subset gene signatures. (E&H) Relative expression of cytokines, (F&I) key transcription factors, and (G&J) chemokines between healthy control and patients. Bars colored in black are genes associated with TE cells, and bars colored in grey are genes associated with MP cells.

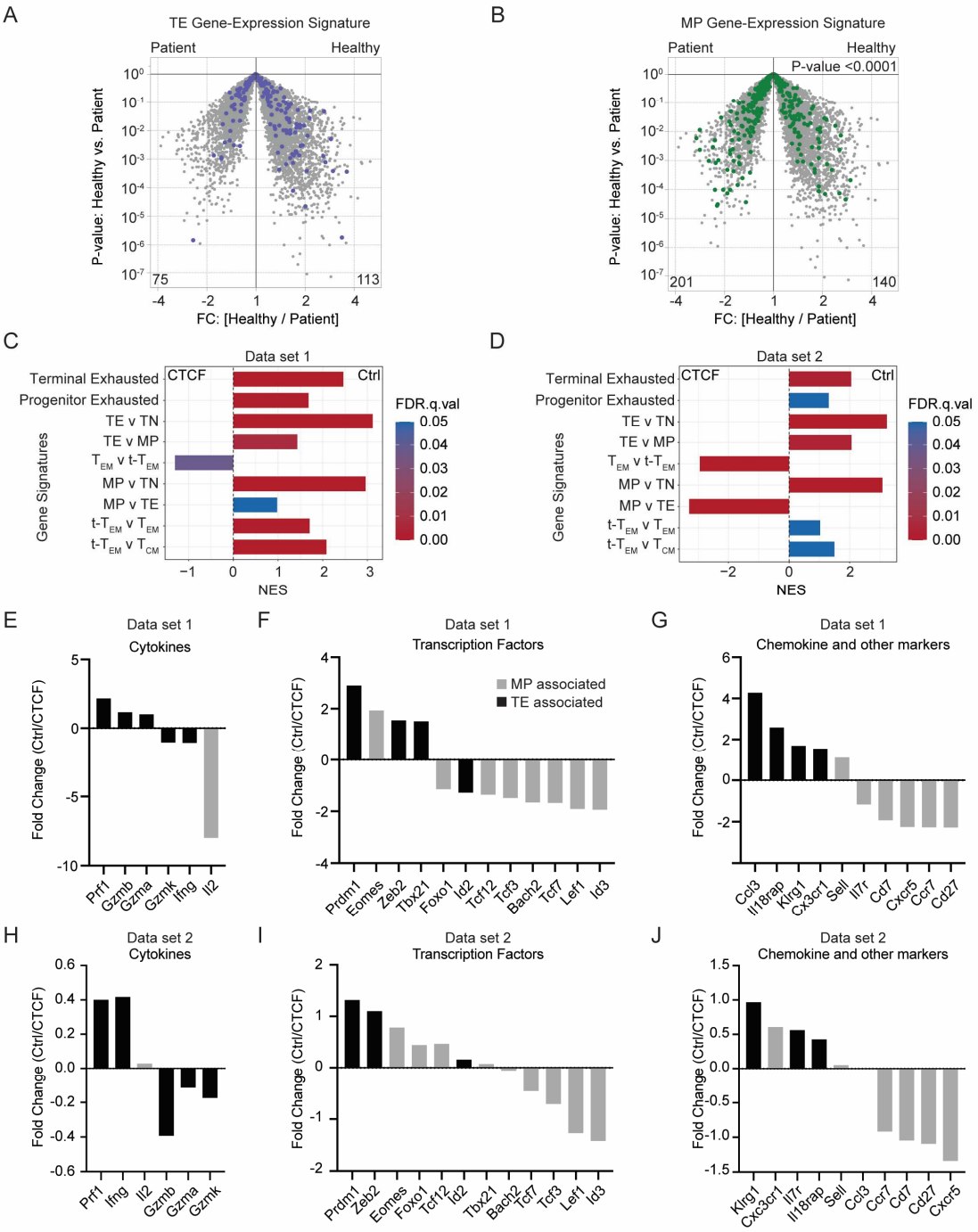
A
TE Gene-Expression Signature
Patient
Healthy
P-value: Healthy vs. Patient
75
113
FC: [Healthy / Patient]
B
MP Gene-Expression Signature
Patient
Healthy
P-value <0.0001
201
140
FC: [Healthy / Patient]
C
Data set 1
CTCF
Ctrl
Terminal Exhausted
Progenitor Exhausted
TE v TN
TE v MP
MP v TN
MP v TE
Gene Signatures
FDR.q.val
NES
D
Data set 2
E
Data set 1
Cytokines
Fold Change (Ctrl/CTCF)
Prf1
Gzmb
Gzma
Gzmk
Ifng
Il2
F
Data set 1
Transcription Factors
MP associated
TE associated
Prdm1
Eomes
Zeb2
Tbx21
Foxo1
Id2
Tcf12
Tcf3
Bach2
Tcf7
Lef1
Id3
G
Data set 1
Chemokine and other markers
Ccl3
Il18rap
Klrg1
Cx3cr1
Sell
Il7r
Cd7
Cxcr5
Ccr7
Cd27
H
Data set 2
Cytokines
I
Data set 2
Transcription Factors
J
Data set 2
Chemokine and other markers

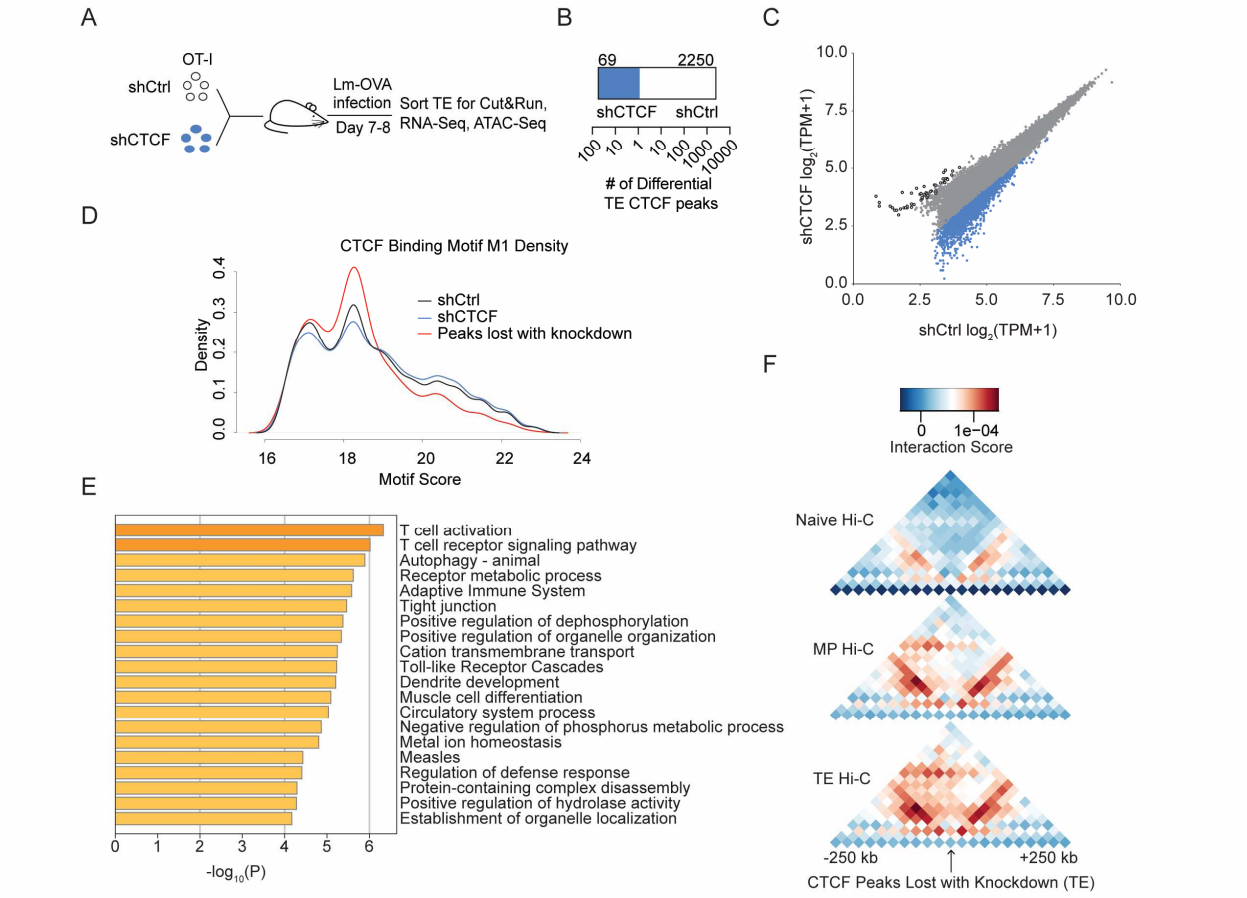

Figure 2.7: Loss of CTCF perturbs weak affinity binding sites at areas of TE-specific interactions. (A) Schematic of experimental setup. OT-I CD8$^+$ T cells were transduced with shCtrl or shCTCF shRNA, mixed 1:1, and transferred into recipient mice who were subsequently infected with Lm-OVA. Eight days post infection, shCtrl and shCTCF transduced TE cells were sort purified and used for Cut&Run, RNA-Seq, and ATAC-Seq. (B) Quantification of number of differential CTCF peaks between TE cells transduced with shCtrl or shCTCF. (C) Scatterplot showing log transformed tags per million of CTCF peaks for Cut&Run data in TE cells for shCtrl and shCTCF. Differential peaks are labelled in blue and black for shCtrl and shCTCF enriched peaks respectively. (D) Density plot of CTCF M1 motif scores for shCtrl, shCTCF, and CTCF peaks lost with knockdown. (E) Metascape analysis showing the pathways enriched in the list of genes that had a loss of CTCF binding upon shRNA knockdown. (F) Heatmaps showing average chromosome interactions around CTCF peaks that were lost with knockdown in TE OT-I cells.

Figure 2.8: CTCF knockdown in TE cells alters the effector and long-term hematopoietic stem cell transcriptional programs. (A) Quantification of differentially expressed genes between TE cells transduced with shCtrl or shCTCF. DESeq2 [126] was used to measure differential gene expression with a fold change cutoff of 1.5 and a p-value cutoff of 0.05. (B) GSEA of gene signatures obtained from published dataset in shCtrl or shCTCF transduced TE cells. (C) Heatmap showing changes in RNA expression upon CTCF knockdown for key transcription factors. (D) Heatmap showing changes in RNA expression upon CTCF knockdown of genes that are upregulated (left) or downregulated (right) in long-term hematopoietic stem cells. (E) Metascape analysis showing the pathways enriched in the list of genes that decrease in expression with CTCF knockdown. (F) Metascape analysis showing the pathways enriched in the list of genes that increase in expression with CTCF knockdown. (G) Quantification of the overlap between CTCF peaks that were lost upon shRNA knockdown and lists of chromosomal coordinates of subset gene signatures. (H) Quantification of the overlap between CTCF peaks that were lost upon shRNA knockdown and active enhancers in naive, TE, or MP cells. (I) Quantification of the overlap between CTCF peaks that were lost upon shRNA knockdown and active promoters in naive, TE, or MP cells.

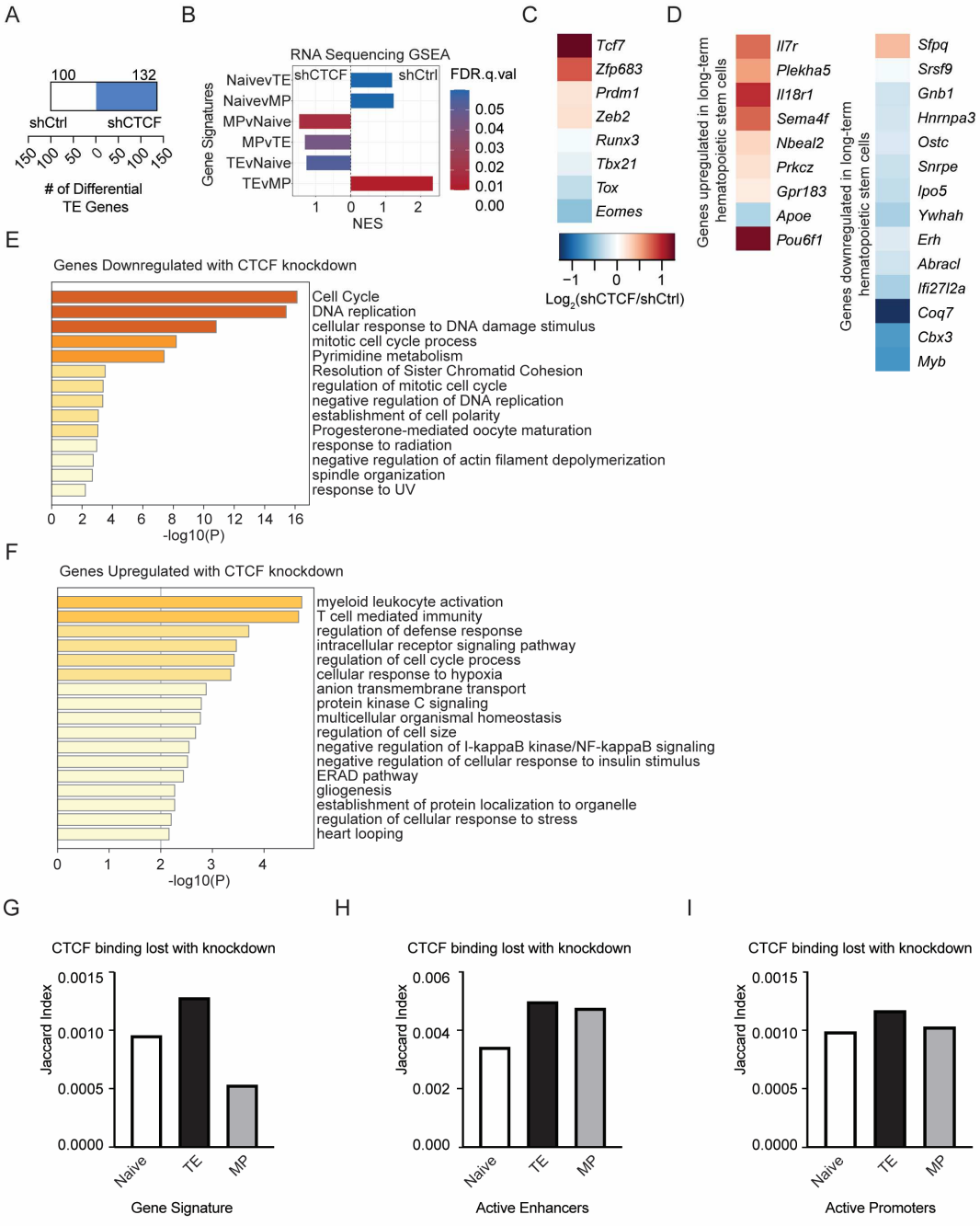
A
100
132
shCtrl
shCTCF
150
100
50
0
50
100
150
# of Differential TE Genes
B
RNA Sequencing GSEA
Gene Signatures
NaivevTE
NaivevMP
MPvNaive
MPvTE
TEvNaive
TEvMP
shCTCF
shCtrl
FDR.q.val
0.05
0.04
0.03
0.02
0.01
0.00
1
0
1
2
NES
C
Tcf7
Zfp683
Prdm1
Zeb2
Runx3
Tbx21
Tox
Eomes
−1
0
1
Log2(shCTCF/shCtrl)
D
Genes upregulated in long-term hematopoietic stem cells
Il7r
Plekha5
Il18r1
Sema4f
Nbeal2
Prkcz
Gpr183
Apoe
Pou6f1
Genes downregulated in long-term hematopoietic stem cells
Sfpq
Srsf9
Gnb1
Hnrnpa3
Ostc
Snrpe
Ipo5
Ywhah
Erh
Abracl
Ifi27l2a
Coq7
Cbx3
Myb
E
Genes Downregulated with CTCF knockdown
Cell Cycle
DNA replication
cellular response to DNA damage stimulus
mitotic cell cycle process
Pyrimidine metabolism
Resolution of Sister Chromatid Cohesion
regulation of mitotic cell cycle
negative regulation of DNA replication
establishment of cell polarity
Progesterone-mediated oocyte maturation
response to radiation
negative regulation of actin filament depolymerization
spindle organization
response to UV
0
2
4
6
8
10
12
14
16
-log10(P)
F
Genes Upregulated with CTCF knockdown
myeloid leukocyte activation
T cell mediated immunity
regulation of defense response
intracellular receptor signaling pathway
regulation of cell cycle process
cellular response to hypoxia
anion transmembrane transport
protein kinase C signaling
multicellular organismal homeostasis
regulation of cell size
negative regulation of I-kappaB kinase/NF-kappaB signaling
negative regulation of cellular response to insulin stimulus
ERAD pathway
gliogenesis
establishment of protein localization to organelle
regulation of cellular response to stress
heart looping
0
1
2
3
4
-log10(P)
G
CTCF binding lost with knockdown
Jaccard Index
0.0015
0.0010
0.0005
0.0000
Naive
TE
MP
Gene Signature
H
CTCF binding lost with knockdown
Jaccard Index
0.006
0.004
0.002
0.000
Naive
TE
MP
Active Enhancers
I
CTCF binding lost with knockdown
Jaccard Index
0.0015
0.0010
0.0005
0.0000
Naive
TE
MP
Active Promoters

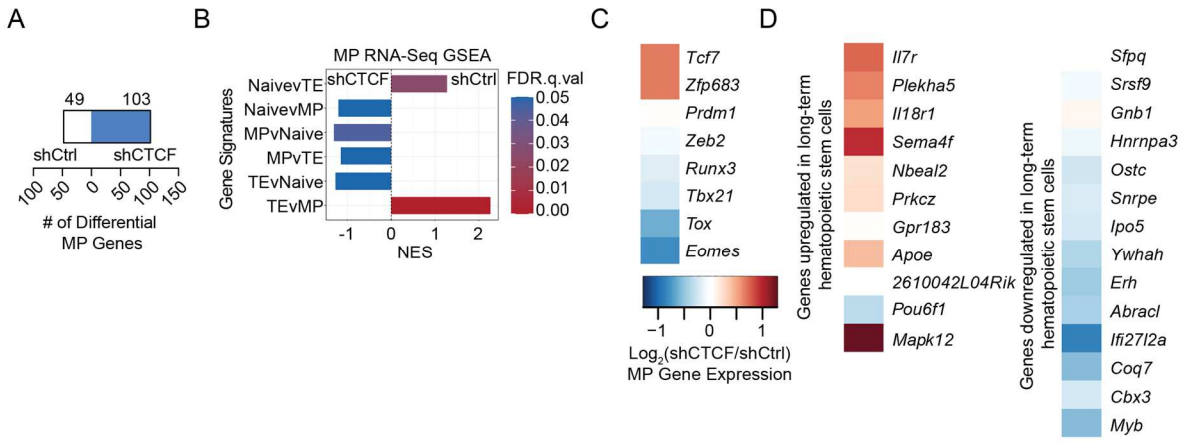

Figure 2.9: CTCF knockdown in MP cells alters the effector and long-term hematopoietic stem cell transcriptional programs. (A) Quantification of differentially expressed genes between MP cells transduced with shCtrl or shCTCF. DESeq2 [126] was used to measure differential gene expression with a fold change cutoff of 1.5 and a p-value cutoff of 0.05. (B) GSEA of gene signatures obtained from published dataset in shCtrl or shCTCF transduced MP cells. (C) Heatmap showing changes in RNA expression upon CTCF knockdown for key transcription factors. (D) Heatmap showing changes in RNA expression upon CTCF knockdown of genes that are upregulated (left) or downregulated (right) in long-term hematopoietic stem cells.

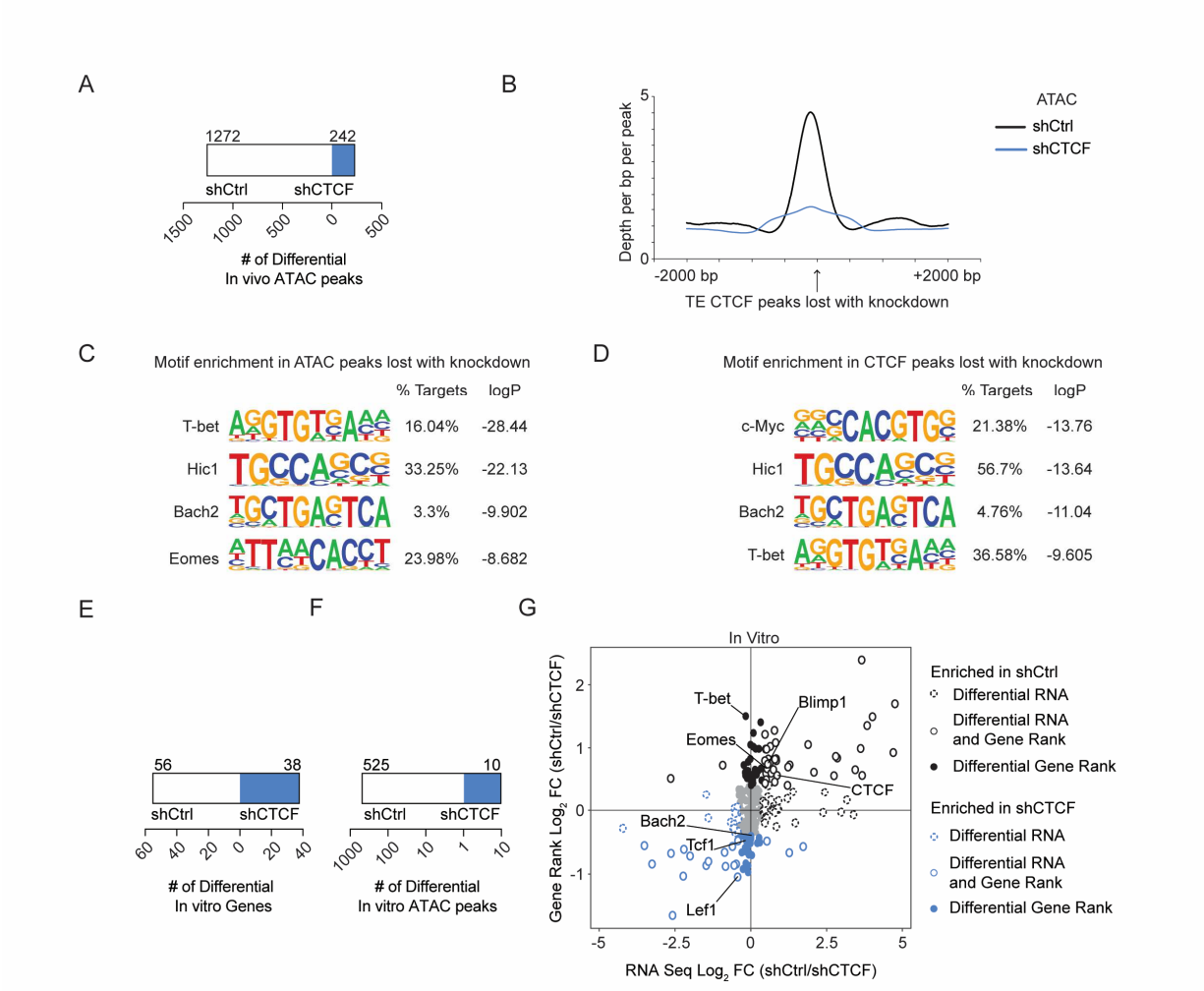

Figure 2.10: CTCF knockdown alters the chromatin accessibility landscape. (A) Quantification of differential ATAC-Seq peaks between TE cells transduced with shCtrl or shCTCF. (B) ATAC-Seq tag enrichment around CTCF peaks lost with knockdown in TE cells. (C) Table showing transcription factor motifs that are enriched in ATAC peaks lost with knockdown in TE cells. (D) Table showing transcription factor motifs that are enriched in CTCF peaks lost with knockdown in TE cells. (E) Quantification of differentially expressed genes between *in vitro* cultured $CD8^+$ T cells transduced with shCtrl or shCTCF. (F) Quantification of differential ATAC-Seq peaks between *in vitro* cultured $CD8^+$ T cells transduced with shCtrl or shCTCF. (G) Scatterplot showing log_2 transformed changes in gene rank scores from Taiji and changes in RNA expression between shCtrl and shCTCF. A log_2 fold change cutoff of 0.4 was used.

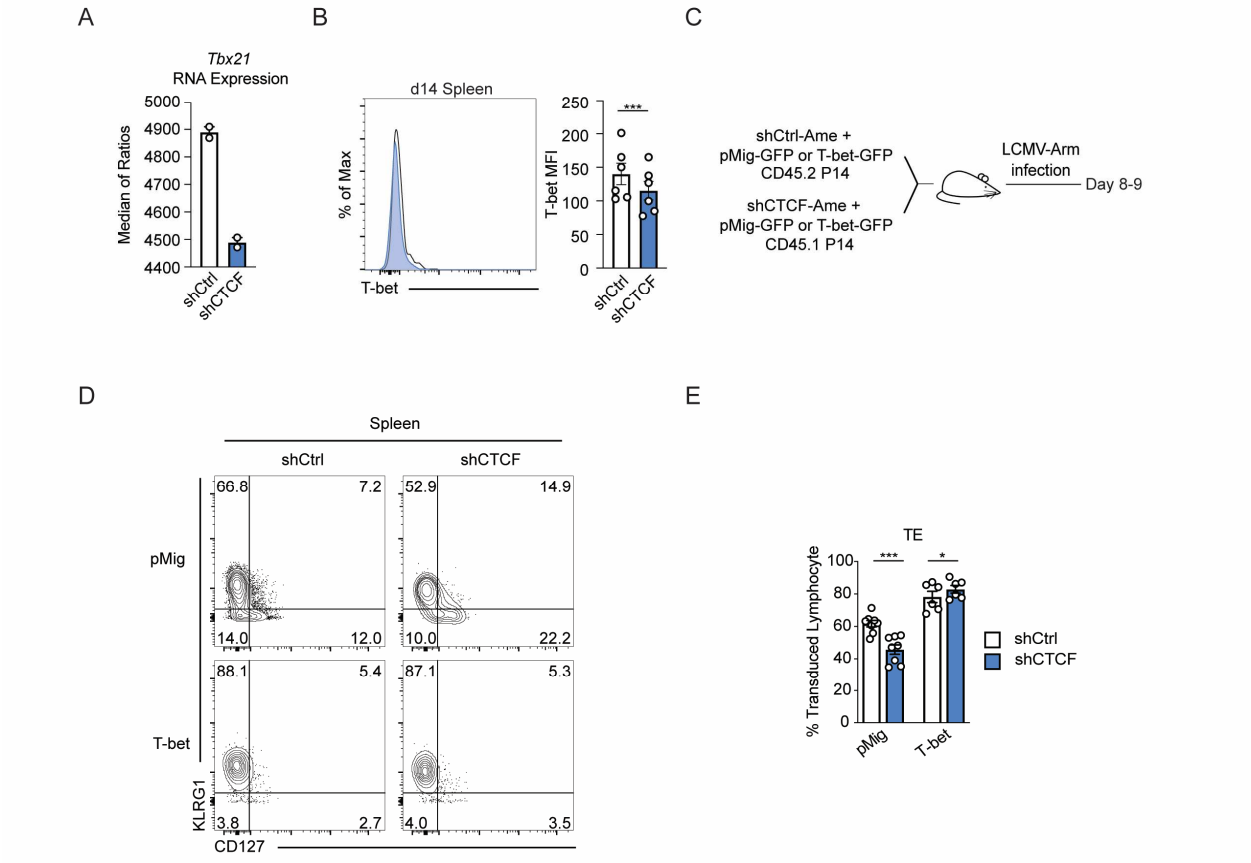

Figure 2.11: T-bet overexpression rescues TE accumulation defect from CTCF knockdown. (A) *Tbx21* gene expression for RNA-Seq on TE cells with and without CTCF knockdown. (B) T-bet expression of day 14 OT-I cells isolated from the spleen with quantification (right). (n=6) (C) Schematic of experimental setup. Recipients were given a co-transfer of P14 $CD8^+$ T cells that were transduced with shCtrl or shCTCF in addition to pMig-GFP or T-bet-GFP overexpression constructs. They were subsequently infected with LCMV Armstrong, and the spleen was collected day 8-9 post infection. (D) Flow cytometry of double transduced P14 cells for KLRG1 and CD127 expression with quantification (E). (n=6) (A, B, and E) Bars and error bars represent mean ± SEM. Statistical significance was calculated using the 2-tailed paired Student's t test.

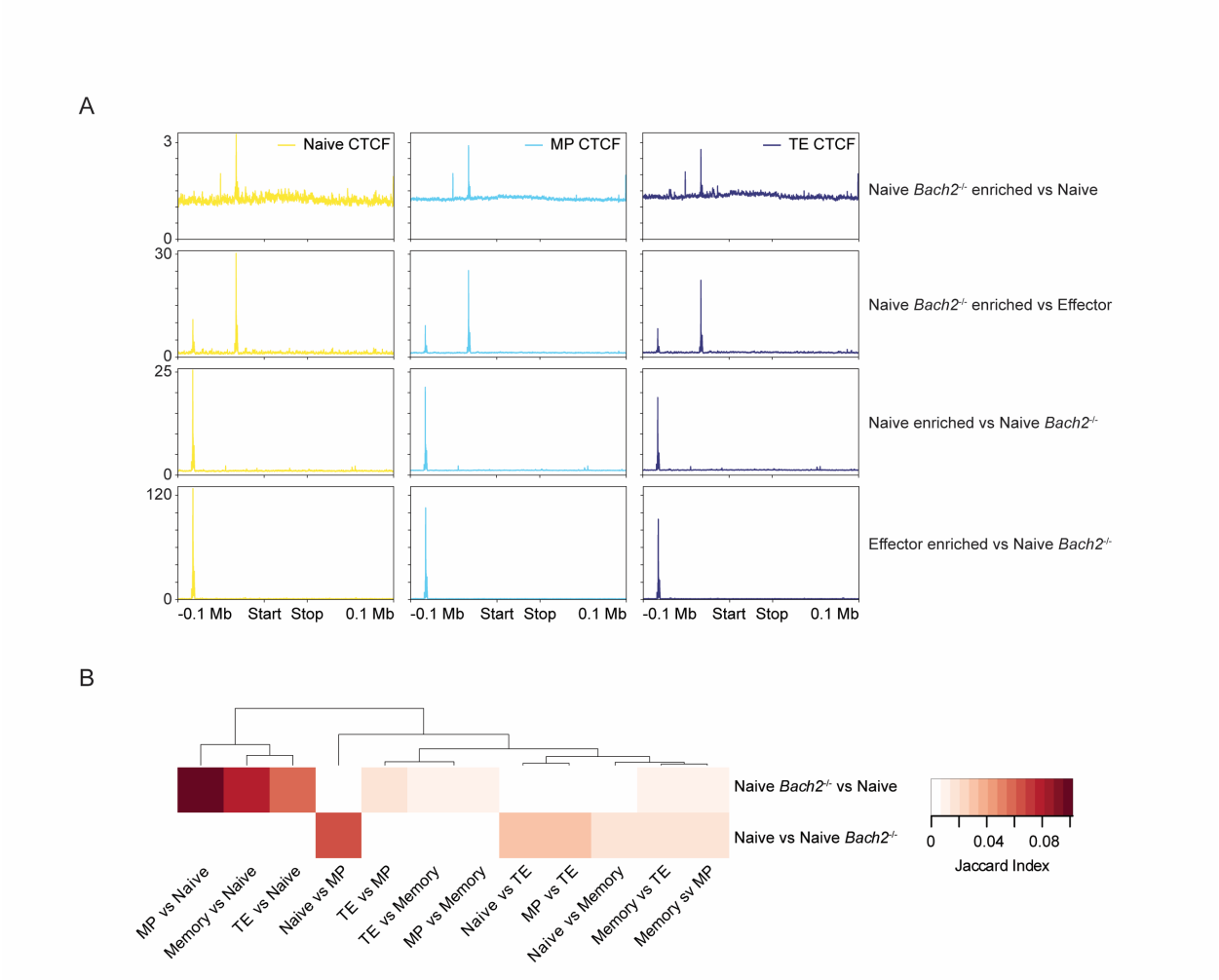

Figure 2.12: Bach2$^{-/-}$ alters chromatin interactions near CTCF binding to more closely resemble MP-specific interactions. (A) Averaged CTCF binding profiles around regions with altered chromatin interactions upon Bach2 knockout. (B) Quantification of overlap among regions with differential chromatin interactions.

Figure 2.13: Specific perturbation of CTCF binding sites promotes gene expression. (A) Heatmaps showing chromosomal interactions in naive, MP, and TE cells around the *Il7r*, *Bcl6*, and *Ccl3* loci. Arcs represent differential interactions in that relevant subset with a p.adj cutoff of 0.05, logfc cutoff of .667, and logcpm cutoff of 1. Tracks show CTCF binding signal from Cut&Run samples for TE cells transduced with shCtrl or shCTCF. (B) Schematic of experimental setup for CRISPR experiments. P14 cells were activated with anti-CD3 and anti-CD28 for 24 hours and then electroporated with crRNA, tracrRNA, and Cas9. The electroporated cells were expanded with IL-2 for 24 hours, mixed 1:1, and transferred into recipient mice who were then infected with LCMV-Armstrong. The spleens were collected at day 8 or 30. (C) Genome browser tracks showing signal tracks for CTCF binding in TE cells transduced with shCtrl or shCTCF and the targeted CTCF binding site upstream of *Il7r*. The CTCF binding peak that is lost with knockdown is highlighted in red. (D) Expression of CD127 on electroporated cells with MFI (right). (n=4) (E) Genome browser showing signal tracks for CTCF binding in TE cells transduced with shCD19 (shCtrl) or shCTCF and the targeted CTCF binding site downstream of *Bcl6*. The CTCF binding peak that is lost with knockdown is highlighted in red. (F) Expression of *Bcl6* on electroporated cells with MFI (right). (n=3) (G) Genome browser showing signal tracks for CTCF binding in TE cells transduced with shCD19 (shCtrl) or shCTCF and the targeted CTCF binding site downstream of *Ccl3*. The CTCF binding peak that is lost with knockdown is highlighted in red. (H) Expression of Ccl3 after restimulation with GP_{33-41} peptide with MFI (right). (n=4) (D, F, and H) Bars and error bars represent mean ± SEM. Statistical significance was calculated using the 2-tailed paired Student's t test. Representative of three independent experiments.

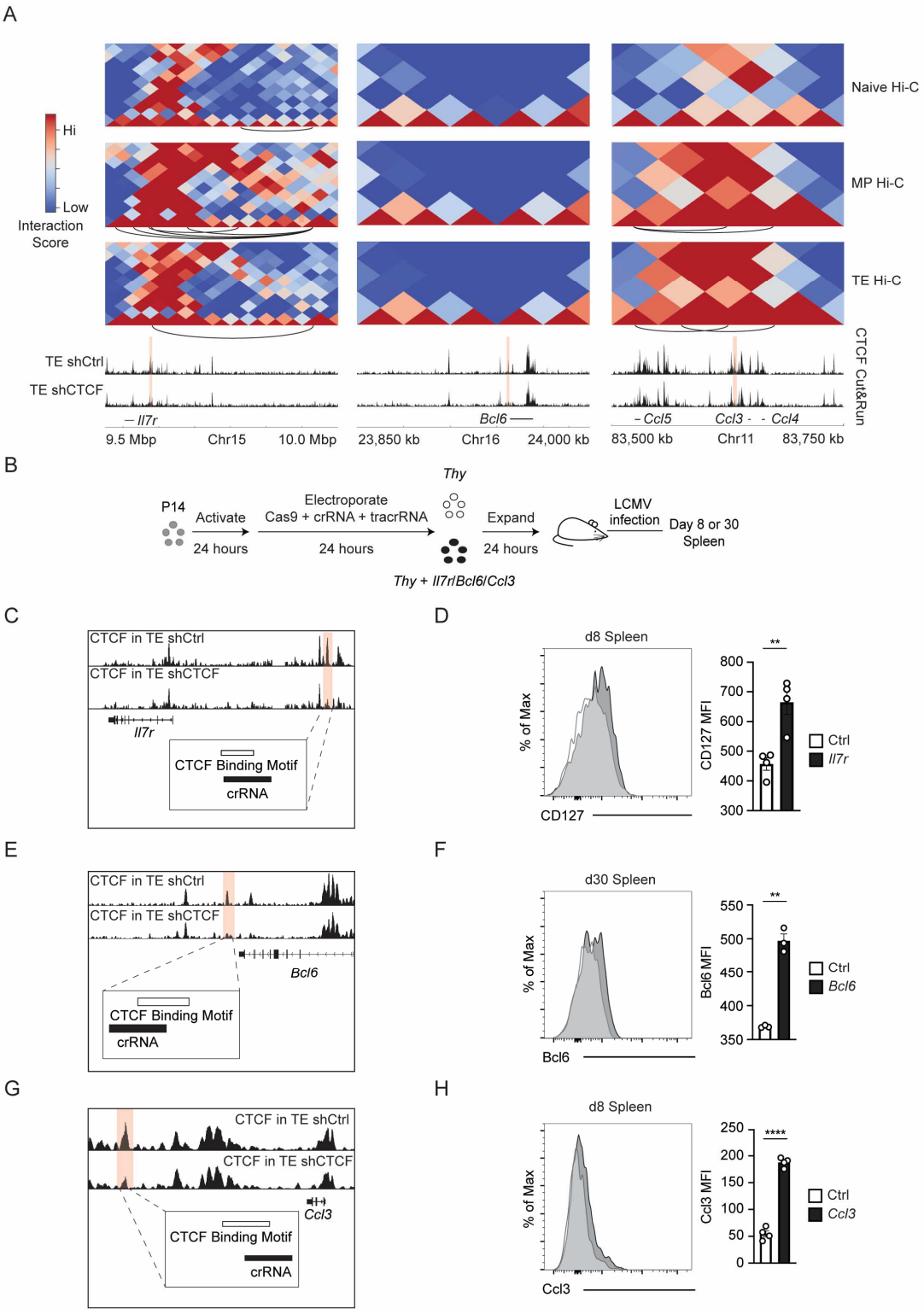
A
Hi
Low
Interaction Score
Naive Hi-C
MP Hi-C
TE Hi-C
CTCF Cut&Run
TE shCtrl
TE shCTCF
Il7r
Bcl6
Ccl5
Ccl3
Ccl4
9.5 Mbp
Chr15
10.0 Mbp
23,850 kb
Chr16
24,000 kb
83,500 kb
Chr11
83,750 kb
B
P14
Activate
24 hours
Electroporate
Cas9 + crRNA + tracrRNA
24 hours
Thy
Expand
24 hours
LCMV infection
Day 8 or 30
Spleen
Thy + Il7r/Bcl6/Ccl3
C
CTCF in TE shCtrl
CTCF in TE shCTCF
Il7r
CTCF Binding Motif
crRNA
D
d8 Spleen
% of Max
CD127
CD127 MFI
Ctrl
Il7r
E
CTCF in TE shCtrl
CTCF in TE shCTCF
Bcl6
CTCF Binding Motif
crRNA
F
d30 Spleen
% of Max
Bcl6
Bcl6 MFI
Ctrl
Bcl6
G
CTCF in TE shCtrl
CTCF in TE shCTCF
Ccl3
CTCF Binding Motif
crRNA
H
d8 Spleen
% of Max
Ccl3
Ccl3 MFI
Ctrl
Ccl3

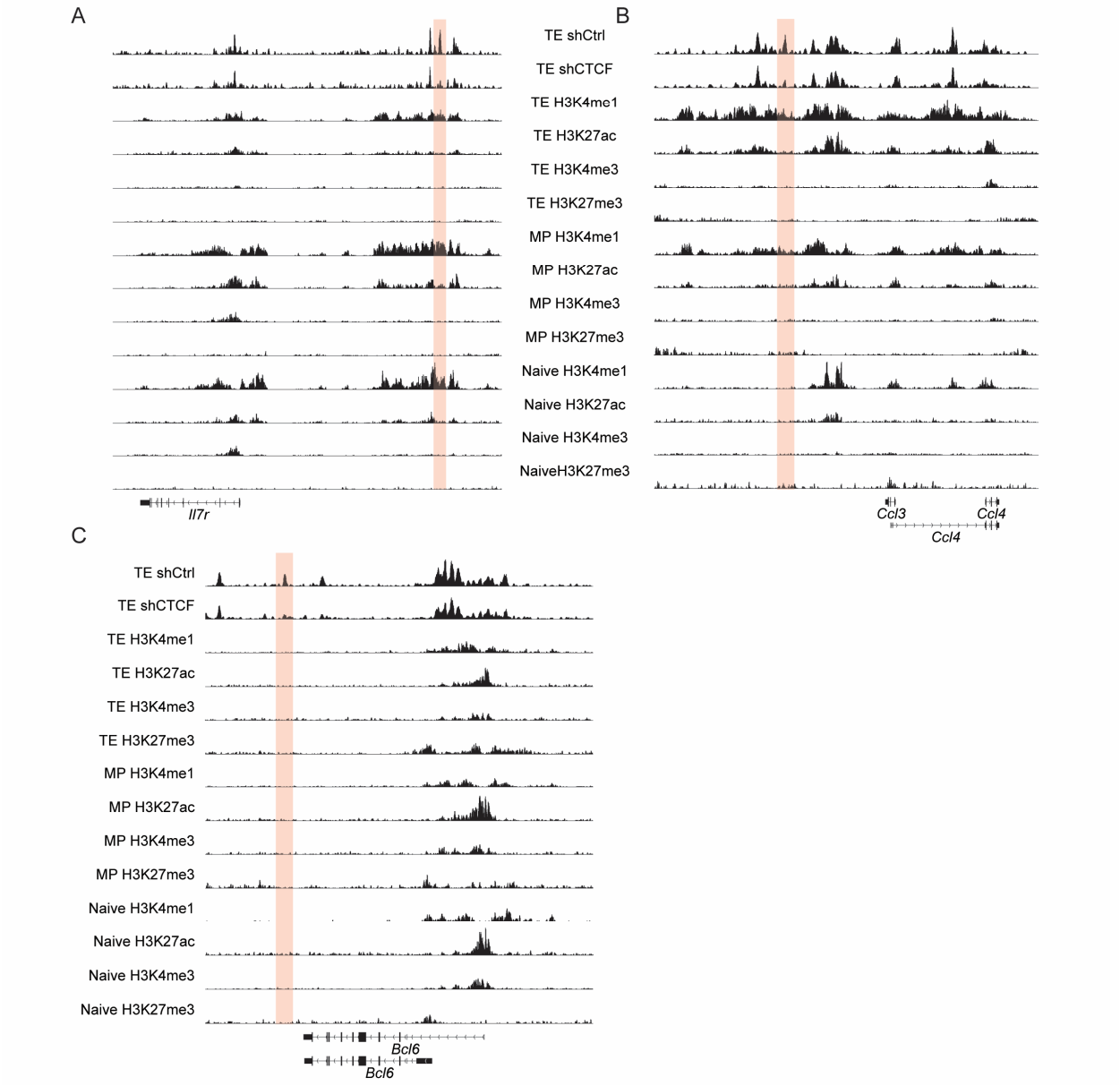

Figure 2.14: Histone marks for CRISPR sites. (A) Signal tracks from previously published ChIP-Seq showing histone marks for CRISPR site near *Il7r*. (B) Signal tracks from previously published ChIP-Seq showing histone marks for CRISPR site near *Ccl3*. (C) Signal tracks from previously published ChIP-Seq showing histone marks for CRISPR site near *Bcl6*.

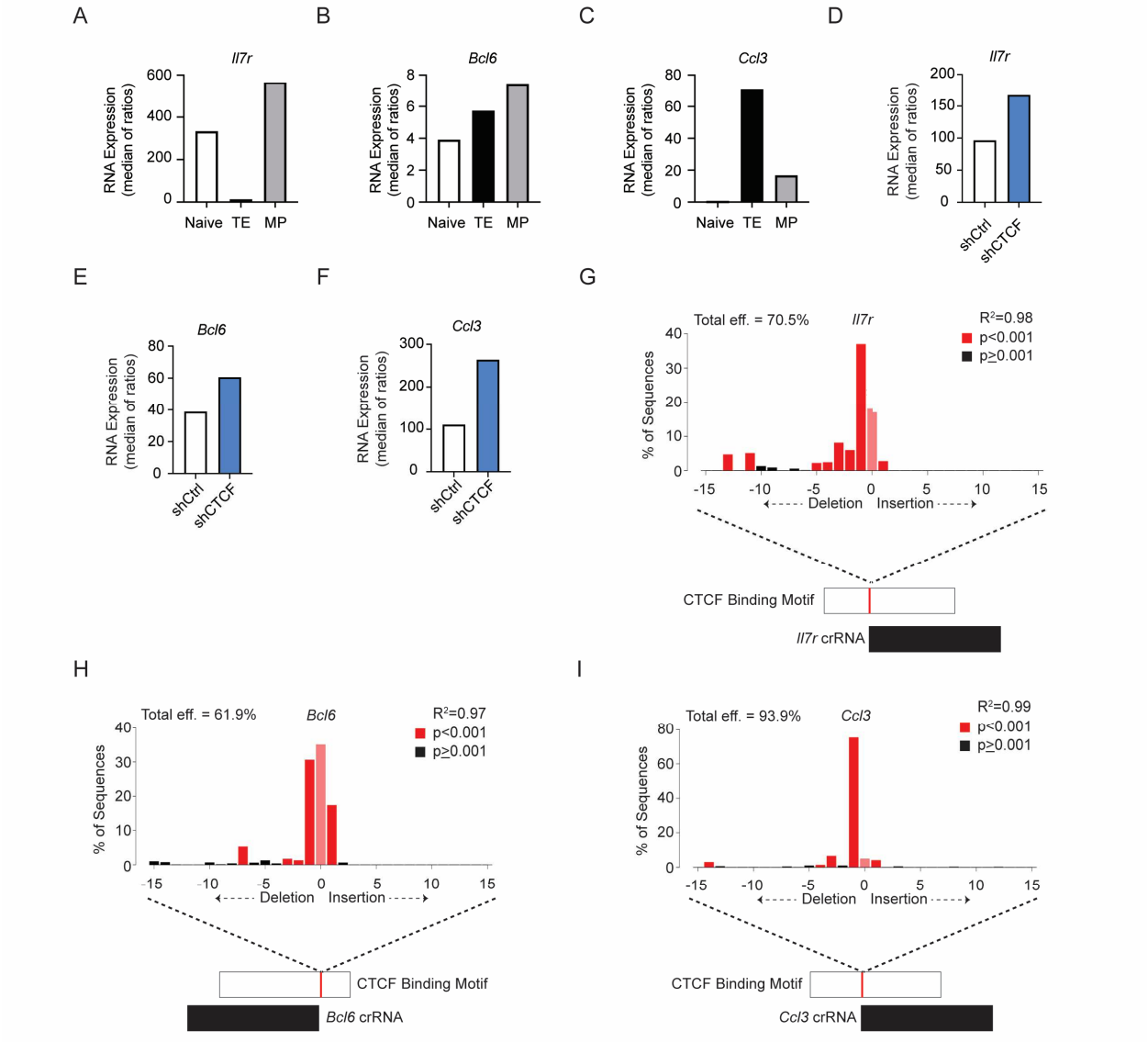

Figure 2.15: Expression of *Il7r*, *Ccl3*, and *Bcl6* with CRISPR/Cas9 editing. (A) RNA expression for *Il7r* expression from RNA-Seq data. (B) RNA expression for *Bcl6* expression from RNA-Seq data. (C) RNA expression of *Ccl3* from RNA-Seq data. (D) RNA expression of *Il7r* in shCtrl and shCTCF RNA-Seq data for TE cells. (E) RNA expression of *Bcl6* in shCtrl and shCTCF RNA-Seq data for TE cells. (F) RNA expression of *Ccl3* in shCtrl and shCTCF RNA-Seq data for TE cells. (G) Characterization of CRISPR-induced genome editing *Il7r* guide and diagram showing cut site in CTCF binding motif labeled in red. (H) Characterization of CRISPR-induced genome editing *Bcl6* guide and diagram showing cut site in CTCF binding motif labeled in red. (I) Characterization of CRISPR-induced genome editing *Ccl3* guide and diagram showing cut site in CTCF binding motif labeled in red.

CHAPTER 3: CONCLUSION

$CD8^+$ T cells protect the body through differentiating into various subsets with specialized function and characteristics in response to pathogenic infections or malignancies. Transcription factor regulators and chromatin remodelers cooperate to regulate the transcriptional program that instructs cell fate decisions. Although previous research has thoroughly identified and characterized key transcription factor regulators of $CD8^+$ T cell differentiation, how genome organization impacts $CD8^+$ T cell differentiation through regulation of transcriptional programs is not well understood. In this dissertation, I addressed this gap in knowledge by using Hi-C to profile the genome organization of $CD8^+$ T cells responding to an infection *in vivo* (Chapter 1) and characterizing how CTCF, a key chromatin organizer, regulates this differentiation process (Chapter 2). We found that effector $CD8^+$ T cell differentiation altered intra-TAD interactions in a subset-specific manner that corresponded with changes at loci encoding for lineage-determining transcription factors, highlighting the close relationship between chromatin organization and transcriptional rewiring. Further, in contrast to naive, MP, and memory cells, TE cells had a unique enrichment of interactions between subset-specific enhancers and promoter, reflective of their terminally-differentiated state, suggesting that interconnected enhancer-promoter regions may be important for TE cell identity. When CTCF function was disrupted through shRNA-mediated knockdown, terminal differentiation was prevented in both an infection and tumor environment, suggesting that terminal differentiation of $CD8^+$ T cells may require the establishment of CTCF-mediated looping. Altogether, our data highlight that changes in genome organization may be contributing to the regulation of $CD8^+$ T cell fate, and a future study characterizing the genome organization in exhausted TIL would further elucidate the relationship between chromatin looping and terminal differentiation in T cells.

A new study characterized chromatin architecture in T cells from developing thymocytes to memory T cells generated in response to a flu infection, revealing that chromatin architecture had extensive changes within discrete functional domains upon $CD8^+$ T cell differentiation, with subset-specific chromatin looping [127]. These subset-specific chromatin interactions were enriched for active and poised regulatory elements as denoted by histone modifications and chromatin accessibility [127]. The study further discovered that Bach2 and Satb1 are both necessary to enforce naive T cell identity through facilitating naive-specific chromatin looping, and the deletion of the end of a chromatin loop near the *Ccl5* locus revealed that the looping at this locus is necessary for the acquisition of transcriptionally permissive epigenetic modifications and upregulation of *Ccl5* expression with effector T cell differentiation [127]. Altogether, this study complements the findings of this dissertation and further reinforces the idea that alterations in chromatin architecture are necessary for $CD8^+$ T cell differentiation through the regulation of epigenetic modifications and transcriptional programs.

$CD8^+$ T cell differentiation is regulated at multiple levels including transcriptional activity, the transcription factor landscape, epigenetic modifications, and chromatin architecture. We proposed that chromatin architecture is interconnected with other levels of regulation. We demonstrated that chromatin interactions between active enhancers and promoters, as identified by histone modifications, were altered with differentiation, while loci encoding for key transcription factors were reorganized upon effector T cell differentiation in a manner reflecting their pattern of expression that align with their regulatory roles. While our findings describe the relationships among the various levels of regulation in $CD8^+$ T cells, future studies such as the previously mentioned study [127] examining the direct impact of disrupting specific chromatin

looping will provide insight into the finer details of chromatin-architecture-mediated regulation of the $CD8^+$ T cell response and may identify new targets to be perturbed for immunotherapy.

Perturbation of CTCF binding is often used to study the role of genome organization as CTCF is a regulator of chromatin interactions [56]. We showed that decreased CTCF expression prevented TE and t-T_{EM} cell differentiation but promoted MP, T_{EM}, and T_{RM} cell differentiation, suggesting a subset-specific function of shRNA-sensitive CTCF binding sites. The profiling of the transcriptome and CTCF binding profile with and without CTCF knockdown revealed that weak-affinity CTCF binding sites regulated transcriptional programs important for T cell differentiation, and perturbation of specific CTCF binding sites demonstrated the role of CTCF as an insulator on neighboring genes. CTCF, however, can also act as an activator of gene expression, and further studies into the different mechanistic roles of CTCF in T cells would clarify how the disruption of weak-affinity binding sites culminates into the prevention of terminal differentiation.

Our study is an example of how studying chromatin interactions and chromatin remodelers can be used to identify novel distal regions that can be targeted to fine-tune the T cell response through subtle changes in gene expression. With recent technological advances reducing the require cell numbers to obtain higher resolution transcriptional, epigenetic, and chromatin interaction data, we can further extend our studies to include rarer $CD8^+$ T cell populations such as T_{RM} and TILs to provide a comprehensive picture of the regulatory networks that coordinate the $CD8^+$ T cell response, which can be harnessed for developing medical therapeutics.

APPENDIX A: MATERIALS AND METHODS

Mice

All mice were bred on the C57BL6/J background and housed in specific pathogen-free conditions in accordance with the Institutional Animal Care and Use Committees of the University of California, San Diego. Both male and female mice were used throughout the study, with sex matched T cell donors and recipients (or female donor cells transferred into male recipients) and between 1.5 and 4 months old. C57BL/6J mice (stock #000664; The Jackson Laboratory), OT-I mice (with transgenic expression of H-2K^{d}-restricted TCR specific for ovalbumin peptide 257-264; stock #003831; The Jackson Laboratory), P14 mice (with transgenic expression of H-2D^{b}-restricted TCR specific for LCMV glycoprotein GP_{33-41}; stock #037394-JAX; The Jackson Laboratory), CD45.1^{+}, and CD45.1.2^{+} congenic mice were bred in house.

Cell culture

For OT-I and P14 CD8^{+} T cell transductions, spleens and lymph nodes were negatively enriched, activated, and spinfected as previously described [82]. Male B16 melanoma cells expressing the LCMV glycoprotein epitope amino acid 33-41 (B16-GP_{33-41}) and female PLAT-E cells were maintained in DMEM containing 5% bovine growth serum, 1% HEPES and 0.1% 2-Mercaptoethanol. Both cell lines have been confirmed to be free of mycoplasma through qPCR. Retroviral particles were generated in PLAT-E cells as previously described [82].

Infection Studies

Activated T cells were transduced with control construct (CD19 shRNA) or CTCF shRNA, mixed at a 1:1 ratio, and adoptively transferred at 1×10^{5} T cells per recipient mouse. Mice were

then infected with 5×10^3 CFU Lm-OVA by intravenous injection or 2×10^5 PFU LCMV-Armstrong by intraperitoneal injection. For secondary infection, mice were re-challenged by intravenous injection of 1×10^6 PFU VSV-OVA.

Tumor Studies

B16-GP_{33-41} cells ($5x10^5$) were transplanted subcutaneously into the right flank of wild-type mice. After tumors became palpable, 7-8 days post transplantation, $2.5x10^6$ P14 cells that were transduced with shCtrl or shCTCF and expanded in vitro with 100 U/ml IL-2 for 2 days, were mixed 1:1 and transferred intravenously. Tumors were monitored daily and mice with ulcerated tumors or tumors exceeding 1500 mm^3 in size were euthanized in accordance with UCSD IACUC. TILs were isolated as previously described [82] one week following adoptive transfer.

Preparation of Single Cell Suspension

Single-cell suspensions were prepared from spleen or lymph node by mechanical disruption with frosted microscope slides. For isolation of lymphocytes from the small intestine IEL compartment, Peyer's patches and luminal contents were removed and the intestine was cut longitudinally and subsequently cut laterally into 0.5-1 cm^2 pieces that were then incubated with 15.4 mg/100 µl dithioerythritol (EMD Millipore) in 10% HBSS/HEPES bicarbonate for 30 minutes at 37˚C while stirring. Tumors were cut into pieces and digested for 30 minutes with 100 U/ml type I collagenase (Worthington) in RPMI 1640, 5% FBS, 2 mM $MgCl_2$, 2 mM $CaCl_2$ at 37 °C while shaking. The tissue was further dissociated over a 70 µm nylon cell strainer (Falcon). For isolation of lymphocytes from the IEL and tumor, single-cell suspensions were purified using a 44/67% Percoll density gradient.

Flow cytometry and cell sorting

Cells were incubated for 30 minutes at 4˚C in PBS supplemented with 2% bovine growth serum and 0.01% sodium azide. For intracellular cytokine staining, splenocytes were re-stimulated with $OVA_{257-264}$ (InvivGen vac-sin) or $GP_{33–41}$ peptide (Anaspec) for 4 hours at 37˚C with Protein Transport Inhibitor Cocktail (eBioscience) added after 1 hour of incubation. CD107a (1D4B, BD Biosciences) antibody was included in the media for the entirety of the stimulation to detect surface expression as a surrogate of degranulation. To better preserve the ametrine reporter signal in transduced populations, samples were fixed and permeabilized using the Cytofix/Cytoperm Fixation/Permeabilization kit (BD). Non-transduced populations were fixed and permeabilized using the Foxp3/Transcription Factor Staining Buffer Set (eBioscience). Stained cells were analyzed using LSRFortessa X-20 or LSRFortessa cytometers (BD) and FlowJo software (TreeStar). Cell sorting was performed on FACSAria or FACSAria Fusion instruments (BD).

shRNA knockdown.

shRNA's targeting CTCF were produced by cloning shRNAmir sequences (CTCF#1: CCAGATGAAGACTGAAGTCAT; CTCF#2: GCAGAGCATTCAGAACAGTGA into our pLMPd-Amt vector [128]. For transfections, $3x10^6$ PLAT-E cells were seeded in a 10 cm dish 1 day before transfection. Each plate was transfected 10 μg of DNA from each pLMPd-Amt clone and 5 μg of pCL-Eco using TransIT-LT1 (Mirus) in Opti-MEM medium. The medium was replaced by T cell medium after 16h and the retroviral supernatant were collected 48 hours later.

For $CD8^+$ T cell activation, naive $CD8^+$ T cells from spleens and lymph nodes were negatively enriched with MACS columns using biotin anti-CD4, anti-Ter119, anti-GR-1, anti-

MHCII, anti-B220, and anti-NK1.1. 2×10^6 OT-I or P14 cells were plated in a well of a 6-well plate that was pre-coated with 100 μg/ml goat anti-hamster IgG (H+L, Thermo Fisher Scientific). The activation medium contained 1 μg/ml anti-CD3 (145-2C11) and 1 μg/ml anti-CD28 (37.51) (eBioscience). Culture medium was replaced after 18h of activation with retroviral supernatant mixed with 50 μM BME and 8 μg/ml polybrene (Millipore) followed by spin-infection (1-hour centrifugation at 2000 RPM, 37˚C). The plate was incubated at 37˚C for 3 hours after spin-infection, and then the retroviral supernatant was replaced by T cell medium and incubated for 24 hours.

RNAi screening approach

As described previously, the targeted shRNA library was generated on the basis of key genes identified from the computational screening approach as well as genes with known roles in regulating circulating memory $CD8^+$ T cells from literature [82, 128]. The library was produced by cloning shERWOOD-designed shRNAsequences, after PCR of synthetic 97-mer oligonucleotides, into our pLMPd-Amt vector. Purified DNA from sequence-verified clones was used to package retroviral particles in PLAT-E cells. The PLAT-E cell line was obtained from Cell Biolabs. For transfections, PLAT-E cells were seeded in the middle 60 wells of a 96-well flat-bottom plate at a density of 4×10^4–6×10^4 cells per well 1 day before transfection. Next, each well was individually transfected with 0.2 μg of DNA from each pLMPd-Amt clone and 0.2 μg of pCL-Eco using TransIT-LT1 (Mirus). Retroviral supernatant was collected 36, 48 and 60 hours after transfection, and retroviral supernatant from each well was used to individually transduce in vitro activated P14 cells in 96-well round-bottom plates.

For $CD8^+$ T cell activation in vitro, naive $CD8^+$ T cells from spleen and lymph nodes were negatively enriched and 2×10^5 P14 cells were plated in the middle 60 wells of 96-well round-bottom plates pre-coated with 100 μg/ml goat anti-hamster IgG (H+L, Thermo Fisher Scientific) and 1 μg/ml anti-CD3 (145-2C11) and 1 μg/ml anti-CD28 (37.51) (both from eBioscience). Culture medium was removed 18 hours after activation and replaced with retroviral supernatant supplemented with 50 μM BME and 8 μg/ml polybrene (Millipore) followed by spinfection (1-hour centrifugation at 805 g, 37°C). Two hours after the spin-infection, the P14 cells were washed 3 times with cold PBS and 90% of each well of cells (individually transduced with distinct retroviral constructs) was collected, pooled and 5×10^5 pooled P14 cells were transferred into recipient mice, which were then infected 1 hour later with 1.5×10^5 PFU of LCMV Armstrong intraperitoneally, resulting in an acute infection. The remaining cells in vitro were cultured for an additional 24 hour and either pooled for 'input' sequencing (6×10^5 P14 cells) or were used to test transduction efficiency of each construct using flow cytometry to detect the percentage of $Ametrine^+$ cells in each well.

T_{CM}, T_{EM}, t-T_{EM} cells were sorted from the spleen (2×10^5–6×10^5 cells total). Genomic DNA was then collected from sorted cells using the FlexiGene kit (Qiagen). The integrated proviral passenger strand shRNA sequences in each cell subset were amplified from 20–100 ng total genomic DNA per reaction, with 23–28 cycles of PCR using Ion Proton-compatible barcoded primers that anneal to the common 5′ mir30 and shRNA loop sequences. Between two and three replicate reactions were performed for each genomic DNA sample and the replicates were pooled after amplification. The pooled reactions were purified using AMPure XP beads, the amplicons in each sample were quantified using a Bioanalyzer, and then pooled in a 1:1 molar ratio for sequencing. In each replicate of the screen, a minimum of 2.5 million reads per sample were

generated and retained, after filtering low-quality reads. Reads assigned to each barcode were aligned to a reference database of all shRNA in the library using BLAST and a custom script to count the top alignment of each read and summarize the number of reads aligned to each shRNA.

For analysis of shRNA representation, the total number of reads in each of the samples was normalized, and the number of reads for each shRNA was scaled proportionally. Subsequently, the normalized number of reads in the T_{EM} or t-T_{EM} cells for a given shRNAmir was divided by the normalized number of reads for the same shRNAmir in the T_{CM} or T_{EM} sample and then $\log_2$ transformed. The mean and s.d. of the ratios of each of the 25 negative-control shRNAmir constructs (targeting Cd19, Cd4, Cd14, Ms4a1, Cd22, Hes1, Klf12, Mafb, Plagl1, Pou2af1 and Smarca1) were used to calculate the Z-score for each shRNAmir construct.

RT-qPCR.

50,000 cells were sorted directly into Trizol, and RNA was extracted by chloroform and isopropanol precipitation. cDNA was synthesized using Superscript II (Life Technologies) following manufacturer's instructions, and quantitative PCR (qPCR) was performed using the Stratagene Brilliant II Syber Green master mix (Agilent Technologies).

Western Blotting.

$CD8^+$ T cells transduced with shCtrl or shCTCF were cultured for 48h with 100 U/ml IL-2. 2×10^6 $Ametrine^+$ cells were sorted, and proteins were extracted in lysis buffer (1% NP-40, 120 mM NaCl, 50 mM Tris-HCl [pH 7.4], and 1 mM EDTA) containing protease inhibitor mixture (Sigma). Then, 10 mg of protein per sample was resolved on NuPage 4-12% Bis-Tris precast gels in MES buffer (Invitrogen), transferred to 0.45 mm PVDF membrane, and then blocked with 5%

BSA in TBS supplemented with 0.1% Tween-20. CTCF (07-729, Millipore) and β-actin (Cell Signaling Technology) primary Abs were incubated overnight at 4˚C followed by HRP-conjugated secondary Abs for 1 hour at room temperature (1:10000, Jackson ImmunoResearch Laboratories). Proteins were visualized with chemiluminescent ECL Prime Western Blotting Detection Reagent (Amersham Biosciences) or ECL Western Blotting Substrate (Pierce) and imaged on a Bio-Rad Laboratories ChemiDoc. ImageJ software was used to quantify protein bands.

RNA Sequencing

1×10^3 transduced KLRG1^{hi} CD127^{lo} CD8$^+$ T cells on day 8 after Lm-OVA infection and 1×10^3 transduced OT-I cells that were cultured in 100 U/mL IL-2 for 2 days were sorted into TCL buffer (QIAGEN) with 1% 2-Mercaptoethanol. Isolation of polyA$^+$ RNA, RNA-Seq library preparation and RNA-seq analysis were performed as described (www.immgen.com/Protocols/11cells.pdf). DESeq2 was used to normalize the data and create differential gene lists using a FC cutoff of 1.5 and a q-value cutoff of 0.05.

For the overlap of subset gene signatures in Figure 1.1I-K, 2.1G-H, 2.8G-I, gene signatures from Milner et al, 2017 was used. The naive gene signature was made of genes upregulated in naive cells compared to TE cells. The TE gene signature included genes upregulated in TE cells versus MP cells. The MP gene signature contained genes upregulated in MP cells and not TE cells.

For human PBL RNA-seq analysis, the normalized gene expression data was downloaded from GSE46833 and obtained from the authors. In Figure 2.6A-B, Volcano plots were generated by GenePattern multiplot studio module. For Figure 2.6C-D, GSEA was performed using Terminal and Progenitor Exhausted gene lists (Bengsch) and CD8$^+$ T cell effector and memory gene lists (Milner et al. 2020)

For the plot in Figure 2.8B, GSEA was performed using gene signatures from Milner et al, 2017. For the transcription factor heatmap in Figure 2.8C, transcription factors were picked based on known roles in regulating $CD8^+$ T cell differentiation. Heatmaps in Figure 2.8D used gene lists from Luckey et al. 2006. Metascape [101] was used to annotate the gene lists for Figure 2.8E-F.

Hi-C and computation analysis

2.5-4x10^6 OT-I cells were sorted per sample. Naive cells were sorted as $CD44^{lo}CD62L^{hi}$. The effector subsets were sorted 7 days post infection with Lm-OVA with TE cells as $CD127^{lo}KLRG1^{hi}$, and MP cells as $CD127^{hi}KLRG1^{lo}$. The cells were fixed in 1.48% formaldehyde for 1 minute at RT and subsequently quenched with 0.125M glycine. Nuclei were isolated and then permeabilized. The nuclei were incubated with MboI-HF enzyme (NEB) overnight at 37˚C. The enzyme was inactivated at 62˚C for 20 minutes, and the overhangs were marked with biotin. Proximal regions were ligated with T4 DNA ligase (NEB), proteins were degraded with proteinase K, and then the crosslinks were reversed by incubating at 68˚C overnight. The DNA was sheared to the size of 300-500bp using a Covaris LE220. The biotinylated DNA were pulled down using Dynabeads MyOne Streptavidin T1 beads (Life technologies). The ends of the DNA were repaired, and biotin was removed from unligated ends. Illumina indexed adaptors were ligated to the DNA samples, and the library was amplified with 4-12 cycles of PCR. The library was size selected with AMPure XP beads (Beckman Coulter) to retain 300-500bp.

Raw Hi-C FASTQ files were aligned to the mouse genome (mm10 build), and binned Hi-C matrices generated using Juicer [129]. Multihiccompare fastlo function was used to normalize the Hi-C matrices and hic_glm was used to determine differential interactions using the QLF test and fdr arguments with a log2FC cutoff of .667, logCPM cutoff of 1, and a p.adj cutoff of 0.05.

HiCExplorer was used to measure correlation, call compartments with H3K27ac ChIP peaks marking the active compartments, and visualize interactions. Circos was also used to visualize differential interactions. Compartment switching was determined by a change in sign of the PC1 value. HOMER analyzeHiC [80] was used to visualize average interactions around CTCF binding site. Interaction enrichment for lists of subset-specific promoters and enhancers obtained from Yu et al. 2017 was measured using HOMER annotateInteractions [80].

ChIP-seq and computational analysis.

Naive cells were sorted as $CD44^{lo}CD62L^{hi}$. The effector cell subsets were sorted 8 days post infection with Lm-OVA with TE cells as $CD127^{lo}KLRG1^{hi}$, and MP cells as $CD127^{hi}KLRG1^{lo}$. 5×10^6 $CD8^+$ T cells were sorted from spleens and lymph nodes, fixed in 1% formaldehyde for 10 min, and subsequently quenched with 0.125 M glycine. Cells were lysed and sonicated to generate 250-500 bp fragments using a Bioruptor. 30 µl of magnetic dynabeads (Life Technologies) were mixed with 5µg CTCF antibody (07-729, Millipore) in 500µl blocking buffer, rotated for at least 4 hours, and then mixed with diluted lysate and rotated overnight at 4˚C. Beads were washed, eluted and reverse-crosslinked at 65˚C overnight and then treated with RNAse for 30 min at 37˚C and Proteinase K at 55˚C for 1 hour. DNA was purified by Zymo DNA Clean & Concentrator kit (Zymo Research). The ChIPed DNA was end-repaired using End-it End-repair kit (Lucigen) and then added an A base to the 3' end of DNA fragments using Klenow (NEB). Then DNA was ligated with adaptors using quick DNA ligase (NEB) at 25˚C for 15 min followed by size selection of 200-400 bp using AMPure XP beads (Beckman Coulter). The adaptor ligated DNA was amplified using NEBNext High-Fidelity 2X PCR master mix (NEB). Then the amplified library was sized selected as 200-400bp using Ampure beads and quantified by Qubit dsDNA HS

assay kit (ThermoFisher). Finally, the library was sequenced using Hiseq 2500 for single-end 50bp sequencing to get around 10 million reads for each sample. ChIP-seq sequencing files were processed using the ENCODE pipeline (https://github.com/ENCODE-DCC/chip-seq-pipeline2).

CUT&RUN and computational analysis

$1x10^6$ OT-I cells were sorted for the naive, TE, and MP cell subsets. $1.5x10^5$ transduced OT-I cells were sorted 7 days post infection with Lm-OVA. Cut&Run was performed as previously described [130]. The library was prepared as previously described [131, 132]. (https://dx.doi.org/10.17504/protocols.io.wvgfe3w). Samples were sequenced on the NovaSeq S4 with a PE100 run. Sequencing file quality was checked with fastqc. Reads were aligned with bowtie2 and normalized to reads that aligned to the e. coli genome as previously described [91]. Peaks were called using MACS [98].

CTCF binding analysis

CTCF peak sets were made using MSPC [133] to call consensus peaks between ChIP-Seq and Cut&Run samples. HOMER [80] was used on these peak sets to call differential peaks with default settings. Bedtools [134] was used to quantify the jaccard index for bed files. HOMER [80] was used to determine the overlap of peak sets.

ATAC-Seq and computational analysis

$5x10^4$ transduced OT-I cells were for the TE cell subset and *in vitro* activated cells were sorted. ATAC-Seq and library prep was performed as previously described [135]. In vivo samples were sequenced on the NovaSeq S4 with a PE100 run. In vitro samples were sequenced on the

HiSeq 4000 with a SE100 run. Fastq files were using the ENCODE pipeline (https://github.com/ENCODE-DCC/atac-seq-pipeline). HOMER [80] was used to identify differential peaks and quantify tag enrichment.

CRISPR Cas9 targeting

One day post activation, T cells were electroporated with complexed tracrRNA (IDT), Cas9 (UC Berkeley), and crRNA (IDT). crRNA targeting Thy1 or CD4 was used alone as a control and was mixed with the conditional crRNA to be used as a marker of electroporated cells. Electroporated cells were cultured in 100 U/ml of IL-2 for 24 or 48 hours. 24 hours after electroporation, control and experimental samples were mixed 1:1 and transferred into recipients. 48 hours post-electroporation, cells were collected for DNA sequencing. DNA modifications were quantified using TIDE [136].

scRNA-Seq Reanalysis

Fastq files were downloaded from GeneOmnibus (GSE131847). Reads were aligned to the mm10 genome using cellranger count. The resulting counts matrix was then processed using Seurat and cells with < 500 reads or a mitochondrial read % greater than 7 were discarded. Data was normalized using sctransform in Seurat with with vars.to.regress = "percent.mt". PCA calculation was performed using RunPCA using the 3000 most variable features from sctransform. The top 30 principal components were used to calculate a UMAP dimensional reduction using the RunUMAP function. Louvain clustering was performed with Seurat's FindClusters based on the top 30 principal components with default parameters. Additionally, data imputation was performed using MAGIC with the sctransform expression values and the

default settings and the exact solver. Cells were assigned to KLRG1 high / low based on a manually chosen cutoff of 0.25 in the MAGIC imputed data. Expression of indicated markers was then plotted using the MAGIC imputed expression values. Statistics were calculated using the FindMarkers function in Seurat using the SCT assay with ident.1 = "KLRG1_low" and ident.2 = "KLRG1_high" for each timepoint separately.

QUANTIFICATION AND STATISTICAL ANALYSIS

Statistical parameters are reported in the Figures and Figure Legends. Asterisks in figures denote statistical significance (*$p < 0.05$, **$p < 0.01$, ***$p < 0.001$, ****$p < 0.0001$), and data is judged to be statistically significant when $p < 0.05$. All sequencing was performed and analyzed independently in at least two biological replicates, and gene expression signatures were compared by Fisher's exact tests. Statistical significance for re-analyzed scRNA-Seq data was calculated using the Wilcoxon Rank Sum test. In all other data analysis, statistical significance was calculated by paired two-tailed Student's t test. Statistical analysis was performed in GraphPad Prism software and R.

REFERENCES

1. Joshi, N.S. and S.M. Kaech, *Effector CD8 T cell development: a balancing act between memory cell potential and terminal differentiation.* J Immunol, 2008. **180**(3): p. 1309-15.

2. Cui, W. and S.M. Kaech, *Generation of effector CD8+ T cells and their conversion to memory T cells.* Immunol Rev, 2010. **236**: p. 151-66.

3. Joshi, N.S., W. Cui, A. Chandele, H.K. Lee, D.R. Urso, J. Hagman, L. Gapin, and S.M. Kaech, *Inflammation directs memory precursor and short-lived effector CD8(+) T cell fates via the graded expression of T-bet transcription factor.* Immunity, 2007. **27**(2): p. 281-95.

4. Kaech, S.M., J.T. Tan, E.J. Wherry, B.T. Konieczny, C.D. Surh, and R. Ahmed, *Selective expression of the interleukin 7 receptor identifies effector CD8 T cells that give rise to long-lived memory cells.* Nat Immunol, 2003. **4**(12): p. 1191-8.

5. Milner, J.J., H. Nguyen, K. Omilusik, M. Reina-Campos, M. Tsai, C. Toma, A. Delpoux, B.S. Boland, S.M. Hedrick, J.T. Chang, and A.W. Goldrath, *Delineation of a molecularly distinct terminally differentiated memory CD8 T cell population.* Proc Natl Acad Sci U S A, 2020. **117**(41): p. 25667-25678.

6. Topham, D.J. and E.C. Reilly, *Tissue-Resident Memory CD8(+) T Cells: From Phenotype to Function.* Front Immunol, 2018. **9**: p. 515.

7. Wherry, E.J., *T cell exhaustion.* Nat Immunol, 2011. **12**(6): p. 492-9.

8. Miller, B.C., D.R. Sen, R. Al Abosy, K. Bi, Y.V. Virkud, M.W. LaFleur, K.B. Yates, A. Lako, K. Felt, G.S. Naik, M. Manos, E. Gjini, J.R. Kuchroo, J.J. Ishizuka, J.L. Collier, G.K. Griffin, S. Maleri, D.E. Comstock, S.A. Weiss, F.D. Brown, A. Panda, M.D. Zimmer, R.T. Manguso, F.S. Hodi, S.J. Rodig, A.H. Sharpe, and W.N. Haining, *Subsets of exhausted CD8(+) T cells differentially mediate tumor control and respond to checkpoint blockade.* Nat Immunol, 2019. **20**(3): p. 326-336.

9. Beltra, J.C., S. Manne, M.S. Abdel-Hakeem, M. Kurachi, J.R. Giles, Z. Chen, V. Casella, S.F. Ngiow, O. Khan, Y.J. Huang, P. Yan, K. Nzingha, W. Xu, R.K. Amaravadi, X. Xu, G.C. Karakousis, T.C. Mitchell, L.M. Schuchter, A.C. Huang, and E.J. Wherry, *Developmental Relationships of Four Exhausted CD8(+) T Cell Subsets Reveals Underlying Transcriptional and Epigenetic Landscape Control Mechanisms.* Immunity, 2020. **52**(5): p. 825-841 e8.

10. Hudson, W.H., J. Gensheimer, M. Hashimoto, A. Wieland, R.M. Valanparambil, P. Li, J.X. Lin, B.T. Konieczny, S.J. Im, G.J. Freeman, W.J. Leonard, H.T. Kissick, and R. Ahmed, *Proliferating Transitory T Cells with an Effector-like Transcriptional Signature Emerge from PD-1(+) Stem-like CD8(+) T Cells during Chronic Infection.* Immunity, 2019. **51**(6): p. 1043-1058 e4.

11. Ford, M.L., B.H. Koehn, M.E. Wagener, W. Jiang, S. Gangappa, T.C. Pearson, and C.P. Larsen, *Antigen-specific precursor frequency impacts T cell proliferation, differentiation, and requirement for costimulation.* J Exp Med, 2007. **204**(2): p. 299-309.

12. Solouki, S., W. Huang, J. Elmore, C. Limper, F. Huang, and A. August, *TCR Signal Strength and Antigen Affinity Regulate CD8(+) Memory T Cells.* J Immunol, 2020. **205**(5): p. 1217-1227.

13. Cox, M.A., L.E. Harrington, and A.J. Zajac, *Cytokines and the inception of CD8 T cell responses.* Trends Immunol, 2011. **32**(4): p. 180-6.

14. Chang, J.T., E.J. Wherry, and A.W. Goldrath, *Molecular regulation of effector and memory T cell differentiation.* Nat Immunol, 2014. **15**(12): p. 1104-15.

15. He, B., S. Xing, C. Chen, P. Gao, L. Teng, Q. Shan, J.A. Gullicksrud, M.D. Martin, S. Yu, J.T. Harty, V.P. Badovinac, K. Tan, and H.H. Xue, *CD8(+) T Cells Utilize Highly Dynamic Enhancer Repertoires and Regulatory Circuitry in Response to Infections.* Immunity, 2016. **45**(6): p. 1341-1354.

16. Kaech, S.M. and W. Cui, *Transcriptional control of effector and memory CD8+ T cell differentiation.* Nat Rev Immunol, 2012. **12**(11): p. 749-61.

17. Xin, A., F. Masson, Y. Liao, S. Preston, T. Guan, R. Gloury, M. Olshansky, J.X. Lin, P. Li, T.P. Speed, G.K. Smyth, M. Ernst, W.J. Leonard, M. Pellegrini, S.M. Kaech, S.L. Nutt, W. Shi, G.T. Belz, and A. Kallies, *A molecular threshold for effector CD8(+) T cell differentiation controlled by transcription factors Blimp-1 and T-bet.* Nat Immunol, 2016. **17**(4): p. 422-32.

18. Omilusik, K.D., M.S. Nadjsombati, L.A. Shaw, B. Yu, J.J. Milner, and A.W. Goldrath, *Sustained Id2 regulation of E proteins is required for terminal differentiation of effector CD8(+) T cells.* J Exp Med, 2018. **215**(3): p. 773-783.

19. Dominguez, C.X., R.A. Amezquita, T. Guan, H.D. Marshall, N.S. Joshi, S.H. Kleinstein, and S.M. Kaech, *The transcription factors ZEB2 and T-bet cooperate to program*

cytotoxic T cell terminal differentiation in response to LCMV viral infection. J Exp Med, 2015. **212**(12): p. 2041-56.

20. Banerjee, A., S.M. Gordon, A.M. Intlekofer, M.A. Paley, E.C. Mooney, T. Lindsten, E.J. Wherry, and S.L. Reiner, *Cutting edge: The transcription factor eomesodermin enables CD8+ T cells to compete for the memory cell niche.* J Immunol, 2010. **185**(9): p. 4988-92.

21. Ichii, H., A. Sakamoto, M. Hatano, S. Okada, H. Toyama, S. Taki, M. Arima, Y. Kuroda, and T. Tokuhisa, *Role for Bcl-6 in the generation and maintenance of memory CD8+ T cells.* Nat Immunol, 2002. **3**(6): p. 558-63.

22. Yang, C.Y., J.A. Best, J. Knell, E. Yang, A.D. Sheridan, A.K. Jesionek, H.S. Li, R.R. Rivera, K.C. Lind, L.M. D'Cruz, S.S. Watowich, C. Murre, and A.W. Goldrath, *The transcriptional regulators Id2 and Id3 control the formation of distinct memory CD8+ T cell subsets.* Nat Immunol, 2011. **12**(12): p. 1221-9.

23. Zhou, X. and H.H. Xue, *Cutting edge: generation of memory precursors and functional memory CD8+ T cells depends on T cell factor-1 and lymphoid enhancer-binding factor-1.* J Immunol, 2012. **189**(6): p. 2722-6.

24. Bordon, Y., *TOX for tired T cells.* Nat Rev Immunol, 2019. **19**(8): p. 476.

25. Man, K., S.S. Gabriel, Y. Liao, R. Gloury, S. Preston, D.C. Henstridge, M. Pellegrini, D. Zehn, F. Berberich-Siebelt, M.A. Febbraio, W. Shi, and A. Kallies, *Transcription Factor IRF4 Promotes CD8(+) T Cell Exhaustion and Limits the Development of Memory-like T Cells during Chronic Infection.* Immunity, 2017. **47**(6): p. 1129-1141 e5.

26. Wang, Y., J. Hu, Y. Li, M. Xiao, H. Wang, Q. Tian, Z. Li, J. Tang, L. Hu, Y. Tan, X. Zhou, R. He, Y. Wu, L. Ye, Z. Yin, Q. Huang, and L. Xu, *The Transcription Factor TCF1 Preserves the Effector Function of Exhausted CD8 T Cells During Chronic Viral Infection.* Front Immunol, 2019. **10**: p. 169.

27. Yao, C., G. Lou, H.W. Sun, Z. Zhu, Y. Sun, Z. Chen, D. Chauss, E.A. Moseman, J. Cheng, M.A. D'Antonio, W. Shi, J. Shi, K. Kometani, T. Kurosaki, E.J. Wherry, B. Afzali, L. Gattinoni, Y. Zhu, D.B. McGavern, J.J. O'Shea, P.L. Schwartzberg, and T. Wu, *BACH2 enforces the transcriptional and epigenetic programs of stem-like CD8(+) T cells.* Nat Immunol, 2021. **22**(3): p. 370-380.

28. Andrey, G. and S. Mundlos, *The three-dimensional genome: regulating gene expression during pluripotency and development.* Development, 2017. **144**(20): p. 3646-3658.

29. Russ, B.E., M. Olshanksy, H.S. Smallwood, J. Li, A.E. Denton, J.E. Prier, A.T. Stock, H.A. Croom, J.G. Cullen, M.L. Nguyen, S. Rowe, M.R. Olson, D.B. Finkelstein, A. Kelso, P.G. Thomas, T.P. Speed, S. Rao, and S.J. Turner, *Distinct epigenetic signatures delineate transcriptional programs during virus-specific CD8(+) T cell differentiation.* Immunity, 2014. **41**(5): p. 853-65.

30. Yu, B., K. Zhang, J.J. Milner, C. Toma, R. Chen, J.P. Scott-Browne, R.M. Pereira, S. Crotty, J.T. Chang, M.E. Pipkin, W. Wang, and A.W. Goldrath, *Epigenetic landscapes reveal transcription factors that regulate CD8(+) T cell differentiation.* Nat Immunol, 2017. **18**(5): p. 573-582.

31. Chen, Y., R. Zander, A. Khatun, D.M. Schauder, and W. Cui, *Transcriptional and Epigenetic Regulation of Effector and Memory CD8 T Cell Differentiation.* Front Immunol, 2018. **9**: p. 2826.

32. Greenberg, M.V.C. and D. Bourc'his, *The diverse roles of DNA methylation in mammalian development and disease.* Nat Rev Mol Cell Biol, 2019. **20**(10): p. 590-607.

33. Youngblood, B., J.S. Hale, H.T. Kissick, E. Ahn, X. Xu, A. Wieland, K. Araki, E.E. West, H.E. Ghoneim, Y. Fan, P. Dogra, C.W. Davis, B.T. Konieczny, R. Antia, X. Cheng, and R. Ahmed, *Effector CD8 T cells dedifferentiate into long-lived memory cells.* Nature, 2017. **552**(7685): p. 404-409.

34. Barnes, C.E., D.M. English, and S.M. Cowley, *Acetylation & Co: an expanding repertoire of histone acylations regulates chromatin and transcription.* Essays Biochem, 2019. **63**(1): p. 97-107.

35. Bannister, A.J. and T. Kouzarides, *Regulation of chromatin by histone modifications.* Cell Res, 2011. **21**(3): p. 381-95.

36. Puri, D., H. Gala, R. Mishra, and J. Dhawan, *High-wire act: the poised genome and cellular memory.* FEBS J, 2015. **282**(9): p. 1675-91.

37. Russ, B.E., M. Olshansky, J. Li, M.L.T. Nguyen, L.J. Gearing, T.H.O. Nguyen, M.R. Olson, H.A. McQuilton, S. Nussing, G. Khoury, D.F.J. Purcell, P.J. Hertzog, S. Rao, and S.J. Turner, *Regulation of H3K4me3 at Transcriptional Enhancers Characterizes*

Acquisition of Virus-Specific CD8(+) T Cell-Lineage-Specific Function. Cell Rep, 2017. **21**(12): p. 3624-3636.

38. Santos-Rosa, H., R. Schneider, A.J. Bannister, J. Sherriff, B.E. Bernstein, N.C. Emre, S.L. Schreiber, J. Mellor, and T. Kouzarides, *Active genes are tri-methylated at K4 of histone H3.* Nature, 2002. **419**(6905): p. 407-11.

39. Sharifi-Zarchi, A., D. Gerovska, K. Adachi, M. Totonchi, H. Pezeshk, R.J. Taft, H.R. Scholer, H. Chitsaz, M. Sadeghi, H. Baharvand, and M.J. Arauzo-Bravo, *DNA methylation regulates discrimination of enhancers from promoters through a H3K4me1-H3K4me3 seesaw mechanism.* BMC Genomics, 2017. **18**(1): p. 964.

40. Magana-Acosta, M. and V. Valadez-Graham, *Chromatin Remodelers in the 3D Nuclear Compartment.* Front Genet, 2020. **11**: p. 600615.

41. Sivakumar, A., J.I. de Las Heras, and E.C. Schirmer, *Spatial Genome Organization: From Development to Disease.* Front Cell Dev Biol, 2019. **7**: p. 18.

42. Hu, G., K. Cui, D. Fang, S. Hirose, X. Wang, D. Wangsa, W. Jin, T. Ried, P. Liu, J. Zhu, E.V. Rothenberg, and K. Zhao, *Transformation of Accessible Chromatin and 3D Nucleome Underlies Lineage Commitment of Early T Cells.* Immunity, 2018. **48**(2): p. 227-242 e8.

43. van Schoonhoven, A., D. Huylebroeck, R.W. Hendriks, and R. Stadhouders, *3D genome organization during lymphocyte development and activation.* Brief Funct Genomics, 2020. **19**(2): p. 71-82.

44. Isoda, T., A.J. Moore, Z. He, V. Chandra, M. Aida, M. Denholtz, J. Piet van Hamburg, K.M. Fisch, A.N. Chang, S.P. Fahl, D.L. Wiest, and C. Murre, *Non-coding Transcription Instructs Chromatin Folding and Compartmentalization to Dictate Enhancer-Promoter Communication and T Cell Fate.* Cell, 2017. **171**(1): p. 103-119 e18.

45. Shih, H.Y. and M.S. Krangel, *Chromatin architecture, CCCTC-binding factor, and V(D)J recombination: managing long-distance relationships at antigen receptor loci.* J Immunol, 2013. **190**(10): p. 4915-21.

46. Sekimata, M., M. Perez-Melgosa, S.A. Miller, A.S. Weinmann, P.J. Sabo, R. Sandstrom, M.O. Dorschner, J.A. Stamatoyannopoulos, and C.B. Wilson, *CCCTC-binding factor and the transcription factor T-bet orchestrate T helper 1 cell-specific structure and function at the interferon-gamma locus.* Immunity, 2009. **31**(4): p. 551-64.

47. Grogan, J.L., M. Mohrs, B. Harmon, D.A. Lacy, J.W. Sedat, and R.M. Locksley, *Early transcription and silencing of cytokine genes underlie polarization of T helper cell subsets.* Immunity, 2001. **14**(3): p. 205-15.

48. Hewitt, S.L., F.A. High, S.L. Reiner, A.G. Fisher, and M. Merkenschlager, *Nuclear repositioning marks the selective exclusion of lineage-inappropriate transcription factor loci during T helper cell differentiation.* Eur J Immunol, 2004. **34**(12): p. 3604-13.

49. Bediaga, N.G., H.D. Coughlan, T.M. Johanson, A.L. Garnham, G. Naselli, J. Schroder, L.G. Fearnley, E. Bandala-Sanchez, R.S. Allan, G.K. Smyth, and L.C. Harrison, *Multi-level remodelling of chromatin underlying activation of human T cells.* Sci Rep, 2021. **11**(1): p. 528.

50. Shan, Q., S.S. Hu, S. Zhu, X. Chen, V.P. Badovinac, W. Peng, C. Zang, and H.H. Xue, *Tcf1 preprograms the mobilization of glycolysis in central memory CD8(+) T cells during recall responses.* Nat Immunol, 2022. **23**(3): p. 386-398.

51. Shan, Q., X. Li, X. Chen, Z. Zeng, S. Zhu, K. Gai, W. Peng, and H.H. Xue, *Tcf1 and Lef1 provide constant supervision to mature CD8(+) T cell identity and function by organizing genomic architecture.* Nat Commun, 2021. **12**(1): p. 5863.

52. Wang, W., A. Chandra, N. Goldman, S. Yoon, E.K. Ferrari, S.C. Nguyen, E.F. Joyce, and G. Vahedi, *TCF-1 promotes chromatin interactions across topologically associating domains in T cell progenitors.* Nat Immunol, 2022.

53. Schwarzer, W., N. Abdennur, A. Goloborodko, A. Pekowska, G. Fudenberg, Y. Loe-Mie, N.A. Fonseca, W. Huber, C.H. Haering, L. Mirny, and F. Spitz, *Two independent modes of chromatin organization revealed by cohesin removal.* Nature, 2017. **551**(7678): p. 51-56.

54. Franke, M., E. De la Calle-Mustienes, A. Neto, M. Almuedo-Castillo, I. Irastorza-Azcarate, R.D. Acemel, J.J. Tena, J.M. Santos-Pereira, and J.L. Gomez-Skarmeta, *CTCF knockout in zebrafish induces alterations in regulatory landscapes and developmental gene expression.* Nat Commun, 2021. **12**(1): p. 5415.

55. Nora, E.P., A. Goloborodko, A.L. Valton, J.H. Gibcus, A. Uebersohn, N. Abdennur, J. Dekker, L.A. Mirny, and B.G. Bruneau, *Targeted Degradation of CTCF Decouples Local Insulation of Chromosome Domains from Genomic Compartmentalization.* Cell, 2017. **169**(5): p. 930-944 e22.

56. Ong, C.T. and V.G. Corces, *CTCF: an architectural protein bridging genome topology and function.* Nat Rev Genet, 2014. **15**(4): p. 234-46.

57. Xu, B., H. Wang, S. Wright, J. Hyle, Y. Zhang, Y. Shao, M. Niu, Y. Fan, W. Rosikiewicz, M.N. Djekidel, J. Peng, R. Lu, and C. Li, *Acute depletion of CTCF rewires genome-wide chromatin accessibility.* Genome Biol, 2021. **22**(1): p. 244.

58. Heger, P., B. Marin, M. Bartkuhn, E. Schierenberg, and T. Wiehe, *The chromatin insulator CTCF and the emergence of metazoan diversity.* Proc Natl Acad Sci U S A, 2012. **109**(43): p. 17507-12.

59. Moore, J.M., N.A. Rabaia, L.E. Smith, S. Fagerlie, K. Gurley, D. Loukinov, C.M. Disteche, S.J. Collins, C.J. Kemp, V.V. Lobanenkov, and G.N. Filippova, *Loss of maternal CTCF is associated with peri-implantation lethality of Ctcf null embryos.* PLoS One, 2012. **7**(4): p. e34915.

60. Bell, A.C., A.G. West, and G. Felsenfeld, *The protein CTCF is required for the enhancer blocking activity of vertebrate insulators.* Cell, 1999. **98**(3): p. 387-96.

61. Zlatanova, J. and P. Caiafa, *CTCF and its protein partners: divide and rule?* J Cell Sci, 2009. **122**(Pt 9): p. 1275-84.

62. Beagan, J.A., M.T. Duong, K.R. Titus, L. Zhou, Z. Cao, J. Ma, C.V. Lachanski, D.R. Gillis, and J.E. Phillips-Cremins, *YY1 and CTCF orchestrate a 3D chromatin looping switch during early neural lineage commitment.* Genome Res, 2017. **27**(7): p. 1139-1152.

63. Hansen, A.S., I. Pustova, C. Cattoglio, R. Tjian, and X. Darzacq, *CTCF and cohesin regulate chromatin loop stability with distinct dynamics.* Elife, 2017. **6**.

64. Chernukhin, I., S. Shamsuddin, S.Y. Kang, R. Bergstrom, Y.W. Kwon, W. Yu, J. Whitehead, R. Mukhopadhyay, F. Docquier, D. Farrar, I. Morrison, M. Vigneron, S.Y. Wu, C.M. Chiang, D. Loukinov, V. Lobanenkov, R. Ohlsson, and E. Klenova, *CTCF interacts with and recruits the largest subunit of RNA polymerase II to CTCF target sites genome-wide.* Mol Cell Biol, 2007. **27**(5): p. 1631-48.

65. Chen, J., Z.X. Yao, J.S. Chen, Y.J. Gi, N.M. Munoz, S. Kundra, H.F. Herlong, Y.S. Jeong, A. Goltsov, K. Ohshiro, N.A. Mistry, J. Zhang, X. Su, S. Choufani, A. Mitra, S. Li, B. Mishra, J. White, A. Rashid, A.Y. Wang, M. Javle, M. Davila, P. Michaely, R. Weksberg, W.L. Hofstetter, M.J. Finegold, J.W. Shay, K. Machida, H. Tsukamoto, and

L. Mishra, *TGF-beta/beta2-spectrin/CTCF-regulated tumor suppression in human stem cell disorder Beckwith-Wiedemann syndrome.* J Clin Invest, 2016. **126**(2): p. 527-42.

66. Takayama, N., A. Murison, S.I. Takayanagi, C. Arlidge, S. Zhou, L. Garcia-Prat, M. Chan-Seng-Yue, S. Zandi, O.I. Gan, H. Boutzen, K.B. Kaufmann, A. Trotman-Grant, E. Schoof, K. Kron, N. Diaz, J.J.Y. Lee, T. Medina, D.D. De Carvalho, M.D. Taylor, J.M. Vaquerizas, S.Z. Xie, J.E. Dick, and M. Lupien, *The Transition from Quiescent to Activated States in Human Hematopoietic Stem Cells Is Governed by Dynamic 3D Genome Reorganization.* Cell Stem Cell, 2021. **28**(3): p. 488-501 e10.

67. Luckey, C.J., D. Bhattacharya, A.W. Goldrath, I.L. Weissman, C. Benoist, and D. Mathis, *Memory T and memory B cells share a transcriptional program of self-renewal with long-term hematopoietic stem cells.* Proc Natl Acad Sci U S A, 2006. **103**(9): p. 3304-9.

68. Stik, G., E. Vidal, M. Barrero, S. Cuartero, M. Vila-Casadesus, J. Mendieta-Esteban, T.V. Tian, J. Choi, C. Berenguer, A. Abad, B. Borsari, F. le Dily, P. Cramer, M.A. Marti-Renom, R. Stadhouders, and T. Graf, *CTCF is dispensable for immune cell transdifferentiation but facilitates an acute inflammatory response.* Nat Genet, 2020. **52**(7): p. 655-661.

69. Heath, H., C. Ribeiro de Almeida, F. Sleutels, G. Dingjan, S. van de Nobelen, I. Jonkers, K.W. Ling, J. Gribnau, R. Renkawitz, F. Grosveld, R.W. Hendriks, and N. Galjart, *CTCF regulates cell cycle progression of alphabeta T cells in the thymus.* EMBO J, 2008. **27**(21): p. 2839-50.

70. Qi, C.F., A. Martensson, M. Mattioli, R. Dalla-Favera, V.V. Lobanenkov, and H.C. Morse, 3rd, *CTCF functions as a critical regulator of cell-cycle arrest and death after ligation of the B cell receptor on immature B cells.* Proc Natl Acad Sci U S A, 2003. **100**(2): p. 633-8.

71. Perez-Garcia, A., E. Marina-Zarate, A.F. Alvarez-Prado, J.M. Ligos, N. Galjart, and A.R. Ramiro, *CTCF orchestrates the germinal centre transcriptional program and prevents premature plasma cell differentiation.* Nat Commun, 2017. **8**: p. 16067.

72. Park, J.H., Y. Choi, M.J. Song, K. Park, J.J. Lee, and H.P. Kim, *Dynamic Long-Range Chromatin Interaction Controls Expression of IL-21 in CD4+ T Cells.* J Immunol, 2016. **196**(10): p. 4378-89.

73. Ribeiro de Almeida, C., H. Heath, S. Krpic, G.M. Dingjan, J.P. van Hamburg, I. Bergen, S. van de Nobelen, F. Sleutels, F. Grosveld, N. Galjart, and R.W. Hendriks, *Critical role*

for the transcription regulator CCCTC-binding factor in the control of Th2 cytokine expression. J Immunol, 2009. **182**(2): p. 999-1010.

74. Chisolm, D.A., D. Savic, A.J. Moore, A. Ballesteros-Tato, B. Leon, D.K. Crossman, C. Murre, R.M. Myers, and A.S. Weinmann, *CCCTC-Binding Factor Translates Interleukin 2- and alpha-Ketoglutarate-Sensitive Metabolic Changes in T Cells into Context-Dependent Gene Programs.* Immunity, 2017. **47**(2): p. 251-267 e7.

75. Belton, J.M., R.P. McCord, J.H. Gibcus, N. Naumova, Y. Zhan, and J. Dekker, *Hi-C: a comprehensive technique to capture the conformation of genomes.* Methods, 2012. **58**(3): p. 268-76.

76. Stansfield, J.C., K.G. Cresswell, and M.G. Dozmorov, *multiHiCcompare: joint normalization and comparative analysis of complex Hi-C experiments.* Bioinformatics, 2019. **35**(17): p. 2916-2923.

77. Ramirez, F., V. Bhardwaj, L. Arrigoni, K.C. Lam, B.A. Gruning, J. Villaveces, B. Habermann, A. Akhtar, and T. Manke, *High-resolution TADs reveal DNA sequences underlying genome organization in flies.* Nat Commun, 2018. **9**(1): p. 189.

78. Wolff, J., V. Bhardwaj, S. Nothjunge, G. Richard, G. Renschler, R. Gilsbach, T. Manke, R. Backofen, F. Ramirez, and B.A. Gruning, *Galaxy HiCExplorer: a web server for reproducible Hi-C data analysis, quality control and visualization.* Nucleic Acids Res, 2018. **46**(W1): p. W11-W16.

79. Wolff, J., L. Rabbani, R. Gilsbach, G. Richard, T. Manke, R. Backofen, and B.A. Gruning, *Galaxy HiCExplorer 3: a web server for reproducible Hi-C, capture Hi-C and single-cell Hi-C data analysis, quality control and visualization.* Nucleic Acids Res, 2020. **48**(W1): p. W177-W184.

80. Heinz, S., C. Benner, N. Spann, E. Bertolino, Y.C. Lin, P. Laslo, J.X. Cheng, C. Murre, H. Singh, and C.K. Glass, *Simple combinations of lineage-determining transcription factors prime cis-regulatory elements required for macrophage and B cell identities.* Mol Cell, 2010. **38**(4): p. 576-89.

81. Pekowska, A., B. Klaus, W. Xiang, J. Severino, N. Daigle, F.A. Klein, M. Oles, R. Casellas, J. Ellenberg, L.M. Steinmetz, P. Bertone, and W. Huber, *Gain of CTCF-Anchored Chromatin Loops Marks the Exit from Naive Pluripotency.* Cell Syst, 2018. **7**(5): p. 482-495 e10.

82. Milner, J.J., C. Toma, B. Yu, K. Zhang, K. Omilusik, A.T. Phan, D. Wang, A.J. Getzler, T. Nguyen, S. Crotty, W. Wang, M.E. Pipkin, and A.W. Goldrath, *Runx3 programs CD8(+) T cell residency in non-lymphoid tissues and tumours.* Nature, 2017. **552**(7684): p. 253-257.

83. Escobar, G., D. Mangani, and A.C. Anderson, *T cell factor 1: A master regulator of the T cell response in disease.* Sci Immunol, 2020. **5**(53).

84. Buitrago, D., M. Labrador, J.P. Arcon, R. Lema, O. Flores, A. Esteve-Codina, J. Blanc, N. Villegas, D. Bellido, M. Gut, P.D. Dans, S.C. Heath, I.G. Gut, I. Brun Heath, and M. Orozco, *Impact of DNA methylation on 3D genome structure.* Nat Commun, 2021. **12**(1): p. 3243.

85. Johanson, T.M., A.T.L. Lun, H.D. Coughlan, T. Tan, G.K. Smyth, S.L. Nutt, and R.S. Allan, *Transcription-factor-mediated supervision of global genome architecture maintains B cell identity.* Nat Immunol, 2018. **19**(11): p. 1257-1264.

86. Lettre, G. and J.D. Rioux, *Autoimmune diseases: insights from genome-wide association studies.* Hum Mol Genet, 2008. **17**(R2): p. R116-21.

87. Sud, A., B. Kinnersley, and R.S. Houlston, *Genome-wide association studies of cancer: current insights and future perspectives.* Nat Rev Cancer, 2017. **17**(11): p. 692-704.

88. Fasolino, M., N. Goldman, W. Wang, B. Cattau, Y. Zhou, J. Petrovic, V.M. Link, A. Cote, A. Chandra, M. Silverman, E.F. Joyce, S.C. Little, H. Consortium, K.H. Kaestner, A. Naji, A. Raj, J. Henao-Mejia, R.B. Faryabi, and G. Vahedi, *Genetic Variation in Type 1 Diabetes Reconfigures the 3D Chromatin Organization of T Cells and Alters Gene Expression.* Immunity, 2020. **52**(2): p. 257-274 e11.

89. Hsieh, T.H., A. Weiner, B. Lajoie, J. Dekker, N. Friedman, and O.J. Rando, *Mapping Nucleosome Resolution Chromosome Folding in Yeast by Micro-C.* Cell, 2015. **162**(1): p. 108-19.

90. Hsieh, T.S., C. Cattoglio, E. Slobodyanyuk, A.S. Hansen, O.J. Rando, R. Tjian, and X. Darzacq, *Resolving the 3D Landscape of Transcription-Linked Mammalian Chromatin Folding.* Mol Cell, 2020. **78**(3): p. 539-553 e8.

91. Meers, M.P., T.D. Bryson, J.G. Henikoff, and S. Henikoff, *Improved CUT&RUN chromatin profiling tools.* Elife, 2019. **8**.

92. Skene, P.J., J.G. Henikoff, and S. Henikoff, *Targeted in situ genome-wide profiling with high efficiency for low cell numbers.* Nat Protoc, 2018. **13**(5): p. 1006-1019.

93. Kurd, N.S., Z. He, T.L. Louis, J.J. Milner, K.D. Omilusik, W. Jin, M.S. Tsai, C.E. Widjaja, J.N. Kanbar, J.G. Olvera, T. Tysl, L.K. Quezada, B.S. Boland, W.J. Huang, C. Murre, A.W. Goldrath, G.W. Yeo, and J.T. Chang, *Early precursors and molecular determinants of tissue-resident memory CD8(+) T lymphocytes revealed by single-cell RNA sequencing.* Sci Immunol, 2020. **5**(47).

94. Milner, J.J., C. Toma, Z. He, N.S. Kurd, Q.P. Nguyen, B. McDonald, L. Quezada, C.E. Widjaja, D.A. Witherden, J.T. Crowl, L.A. Shaw, G.W. Yeo, J.T. Chang, K.D. Omilusik, and A.W. Goldrath, *Heterogenous Populations of Tissue-Resident CD8(+) T Cells Are Generated in Response to Infection and Malignancy.* Immunity, 2020. **52**(5): p. 808-824 e7.

95. Gregor, A., M. Oti, E.N. Kouwenhoven, J. Hoyer, H. Sticht, A.B. Ekici, S. Kjaergaard, A. Rauch, H.G. Stunnenberg, S. Uebe, G. Vasileiou, A. Reis, H. Zhou, and C. Zweier, *De novo mutations in the genome organizer CTCF cause intellectual disability.* Am J Hum Genet, 2013. **93**(1): p. 124-31.

96. Konrad, E.D.H., N. Nardini, A. Caliebe, I. Nagel, D. Young, G. Horvath, S.L. Santoro, C. Shuss, A. Ziegler, D. Bonneau, M. Kempers, R. Pfundt, E. Legius, A. Bouman, K.E. Stuurman, K. Ounap, S. Pajusalu, M.H. Wojcik, G. Vasileiou, G. Le Guyader, H.M. Schnelle, S. Berland, E. Zonneveld-Huijssoon, S. Kersten, A. Gupta, P.R. Blackburn, M.S. Ellingson, M.J. Ferber, R. Dhamija, E.W. Klee, M. McEntagart, K.D. Lichtenbelt, A. Kenney, S.A. Vergano, R. Abou Jamra, K. Platzer, M. Ella Pierpont, D. Khattar, R.J. Hopkin, R.J. Martin, M.C.J. Jongmans, V.Y. Chang, J.A. Martinez-Agosto, O. Kuismin, M.I. Kurki, O. Pietilainen, A. Palotie, T.J. Maarup, D.S. Johnson, K. Venborg Pedersen, L.W. Laulund, S.A. Lynch, M. Blyth, K. Prescott, N. Canham, R. Ibitoye, E.H. Brilstra, M. Shinawi, E. Fassi, D.D.D. Study, H. Sticht, A. Gregor, H. Van Esch, and C. Zweier, *CTCF variants in 39 individuals with a variable neurodevelopmental disorder broaden the mutational and clinical spectrum.* Genet Med, 2019. **21**(12): p. 2723-2733.

97. Li, Q.H., J.B. Brown, H.Y. Huang, and P.J. Bickel, *Measuring Reproducibility of High-Throughput Experiments.* Annals of Applied Statistics, 2011. **5**(3): p. 1752-1779.

98. Zhang, Y., T. Liu, C.A. Meyer, J. Eeckhoute, D.S. Johnson, B.E. Bernstein, C. Nusbaum, R.M. Myers, M. Brown, W. Li, and X.S. Liu, *Model-based analysis of ChIP-Seq (MACS).* Genome Biol, 2008. **9**(9): p. R137.

99. Grant, C.E., T.L. Bailey, and W.S. Noble, *FIMO: scanning for occurrences of a given motif.* Bioinformatics, 2011. **27**(7): p. 1017-8.

100. Essien, K., S. Vigneau, S. Apreleva, L.N. Singh, M.S. Bartolomei, and S. Hannenhalli, *CTCF binding site classes exhibit distinct evolutionary, genomic, epigenomic and transcriptomic features.* Genome Biol, 2009. **10**(11): p. R131.

101. Zhou, Y., B. Zhou, L. Pache, M. Chang, A.H. Khodabakhshi, O. Tanaseichuk, C. Benner, and S.K. Chanda, *Metascape provides a biologist-oriented resource for the analysis of systems-level datasets.* Nat Commun, 2019. **10**(1): p. 1523.

102. Zhao, X., Q. Shan, and H.H. Xue, *TCF1 in T cell immunity: a broadened frontier.* Nat Rev Immunol, 2021.

103. Mackay, L.K., M. Minnich, N.A. Kragten, Y. Liao, B. Nota, C. Seillet, A. Zaid, K. Man, S. Preston, D. Freestone, A. Braun, E. Wynne-Jones, F.M. Behr, R. Stark, D.G. Pellicci, D.I. Godfrey, G.T. Belz, M. Pellegrini, T. Gebhardt, M. Busslinger, W. Shi, F.R. Carbone, R.A. van Lier, A. Kallies, and K.P. van Gisbergen, *Hobit and Blimp1 instruct a universal transcriptional program of tissue residency in lymphocytes.* Science, 2016. **352**(6284): p. 459-63.

104. ENCODE-DCC, *ENCODE ATAC-seq pipeline.* 2018.

105. Burrows, K., F. Antignano, M. Bramhall, A. Chenery, S. Scheer, V. Korinek, T.M. Underhill, and C. Zaph, *The transcriptional repressor HIC1 regulates intestinal immune homeostasis.* Mucosal Immunol, 2017. **10**(6): p. 1518-1528.

106. Crowl, J.T., M. Heeg, A. Ferry, J.J. Milner, K.D. Omilusik, C. Toma, Z. He, C.J. T., and A.W. Goldrath, *Tissue-resident memory CD8+ T cells possess unique transcriptional, epigenetic and functional adaptations to different tissue environments.* Nature Immunology, 2022. **in press**.

107. Kallies, A. and K.L. Good-Jacobson, *Transcription Factor T-bet Orchestrates Lineage Development and Function in the Immune System.* Trends Immunol, 2017. **38**(4): p. 287-297.

108. Mackay, L.K., E. Wynne-Jones, D. Freestone, D.G. Pellicci, L.A. Mielke, D.M. Newman, A. Braun, F. Masson, A. Kallies, G.T. Belz, and F.R. Carbone, *T-box Transcription Factors Combine with the Cytokines TGF-beta and IL-15 to Control Tissue-Resident Memory T Cell Fate.* Immunity, 2015. **43**(6): p. 1101-11.

109. Intlekofer, A.M., N. Takemoto, E.J. Wherry, S.A. Longworth, J.T. Northrup, V.R. Palanivel, A.C. Mullen, C.R. Gasink, S.M. Kaech, J.D. Miller, L. Gapin, K. Ryan, A.P. Russ, T. Lindsten, J.S. Orange, A.W. Goldrath, R. Ahmed, and S.L. Reiner, *Effector and memory CD8+ T cell fate coupled by T-bet and eomesodermin.* Nat Immunol, 2005. **6**(12): p. 1236-44.

110. Li, J., Y. He, J. Hao, L. Ni, and C. Dong, *High Levels of Eomes Promote Exhaustion of Anti-tumor CD8(+) T Cells.* Front Immunol, 2018. **9**: p. 2981.

111. Roychoudhuri, R., D. Clever, P. Li, Y. Wakabayashi, K.M. Quinn, C.A. Klebanoff, Y. Ji, M. Sukumar, R.L. Eil, Z. Yu, R. Spolski, D.C. Palmer, J.H. Pan, S.J. Patel, D.C. Macallan, G. Fabozzi, H.Y. Shih, Y. Kanno, A. Muto, J. Zhu, L. Gattinoni, J.J. O'Shea, K. Okkenhaug, K. Igarashi, W.J. Leonard, and N.P. Restifo, *BACH2 regulates CD8(+) T cell differentiation by controlling access of AP-1 factors to enhancers.* Nat Immunol, 2016. **17**(7): p. 851-860.

112. Martin, M.D. and V.P. Badovinac, *Defining Memory CD8 T Cell.* Front Immunol, 2018. **9**: p. 2692.

113. Narni-Mancinelli, E., L. Campisi, D. Bassand, J. Cazareth, P. Gounon, N. Glaichenhaus, and G. Lauvau, *Memory CD8+ T cells mediate antibacterial immunity via CCL3 activation of TNF/ROI+ phagocytes.* J Exp Med, 2007. **204**(9): p. 2075-87.

114. Seki, A. and S. Rutz, *Optimized RNP transfection for highly efficient CRISPR/Cas9-mediated gene knockout in primary T cells.* J Exp Med, 2018. **215**(3): p. 985-997.

115. Karvelis, T., G. Gasiunas, A. Miksys, R. Barrangou, P. Horvath, and V. Siksnys, *crRNA and tracrRNA guide Cas9-mediated DNA interference in Streptococcus thermophilus.* RNA Biol, 2013. **10**(5): p. 841-51.

116. Kim, S., N.K. Yu, and B.K. Kaang, *CTCF as a multifunctional protein in genome regulation and gene expression.* Exp Mol Med, 2015. **47**: p. e166.

117. Pace, L., C. Goudot, E. Zueva, P. Gueguen, N. Burgdorf, J.J. Waterfall, J.P. Quivy, G. Almouzni, and S. Amigorena, *The epigenetic control of stemness in CD8(+) T cell fate commitment.* Science, 2018. **359**(6372): p. 177-186.

118. Henning, A.N., C.A. Klebanoff, and N.P. Restifo, *Silencing stemness in T cell differentiation.* Science, 2018. **359**(6372): p. 163-164.

119. Ladle, B.H., K.P. Li, M.J. Phillips, A.B. Pucsek, A. Haile, J.D. Powell, E.M. Jaffee, D.A. Hildeman, and C.J. Gamper, *De novo DNA methylation by DNA methyltransferase 3a controls early effector CD8+ T-cell fate decisions following activation.* Proc Natl Acad Sci U S A, 2016. **113**(38): p. 10631-6.

120. Gray, S.M., R.A. Amezquita, T. Guan, S.H. Kleinstein, and S.M. Kaech, *Polycomb Repressive Complex 2-Mediated Chromatin Repression Guides Effector CD8(+) T Cell Terminal Differentiation and Loss of Multipotency.* Immunity, 2017. **46**(4): p. 596-608.

121. Dehghani, H., *Regulation of Chromatin Organization in Cell Stemness: The Emerging Role of Long Non-coding RNAs.* Stem Cell Rev Rep, 2021.

122. Donohoe, M.E., L.F. Zhang, N. Xu, Y. Shi, and J.T. Lee, *Identification of a Ctcf cofactor, Yy1, for the X chromosome binary switch.* Mol Cell, 2007. **25**(1): p. 43-56.

123. Kentepozidou, E., S.J. Aitken, C. Feig, K. Stefflova, X. Ibarra-Soria, D.T. Odom, M. Roller, and P. Flicek, *Clustered CTCF binding is an evolutionary mechanism to maintain topologically associating domains.* Genome Biol, 2020. **21**(1): p. 5.

124. Kalia, V. and S. Sarkar, *Regulation of Effector and Memory CD8 T Cell Differentiation by IL-2-A Balancing Act.* Front Immunol, 2018. **9**: p. 2987.

125. Kalia, V., S. Sarkar, S. Subramaniam, W.N. Haining, K.A. Smith, and R. Ahmed, *Prolonged interleukin-2Ralpha expression on virus-specific CD8+ T cells favors terminal-effector differentiation in vivo.* Immunity, 2010. **32**(1): p. 91-103.

126. Love, M.I., W. Huber, and S. Anders, *Moderated estimation of fold change and dispersion for RNA-seq data with DESeq2.* Genome Biol, 2014. **15**(12): p. 550.

127. Russ, B.E., T. K., S. Quon, B. Yu, J. Li, J.K.C. Lee, M. Olshansky, Z. He, P.F. Harrison, A. Barugahare, M. See, S. Nussing, A.E. Morey, V.A. Udupa, T.J. Bennet, A. Kallies, C. Murre, P. Collas, D.R. Powell, A.W. Goldrath, and S.J. Turner, *Active Maintenance of CD8(+) T cell naivety through regulation of global genome architecture.* In Submission, 2022.

128. Chen, R., S. Belanger, M.A. Frederick, B. Li, R.J. Johnston, N. Xiao, Y.C. Liu, S. Sharma, B. Peters, A. Rao, S. Crotty, and M.E. Pipkin, *In vivo RNA interference screens identify regulators of antiviral CD4(+) and CD8(+) T cell differentiation.* Immunity, 2014. **41**(2): p. 325-38.

129. Durand, N.C., M.S. Shamim, I. Machol, S.S. Rao, M.H. Huntley, E.S. Lander, and E.L. Aiden, *Juicer Provides a One-Click System for Analyzing Loop-Resolution Hi-C Experiments.* Cell Syst, 2016. **3**(1): p. 95-8.

130. Hainer, S.J. and T.G. Fazzio, *High-Resolution Chromatin Profiling Using CUT&RUN.* Curr Protoc Mol Biol, 2019. **126**(1): p. e85.

131. Liu, N., V.V. Hargreaves, Q. Zhu, J.V. Kurland, J. Hong, W. Kim, F. Sher, C. Macias-Trevino, J.M. Rogers, R. Kurita, Y. Nakamura, G.C. Yuan, D.E. Bauer, J. Xu, M.L. Bulyk, and S.H. Orkin, *Direct Promoter Repression by BCL11A Controls the Fetal to Adult Hemoglobin Switch.* Cell, 2018. **173**(2): p. 430-442 e17.

132. Liu, N. *Library Prep for CUT&RUN with NEBNext® Ultra™ II DNA Library Prep Kit for Illumina® (E7645).* . 2019.

133. Jalili, V., M. Matteucci, M. Masseroli, and M.J. Morelli, *Using combined evidence from replicates to evaluate ChIP-seq peaks.* Bioinformatics, 2018. **34**(13): p. 2338.

134. Quinlan, A.R., *BEDTools: The Swiss-Army Tool for Genome Feature Analysis.* Curr Protoc Bioinformatics, 2014. **47**: p. 11 12 1-34.

135. Corces, M.R., A.E. Trevino, E.G. Hamilton, P.G. Greenside, N.A. Sinnott-Armstrong, S. Vesuna, A.T. Satpathy, A.J. Rubin, K.S. Montine, B. Wu, A. Kathiria, S.W. Cho, M.R. Mumbach, A.C. Carter, M. Kasowski, L.A. Orloff, V.I. Risca, A. Kundaje, P.A. Khavari, T.J. Montine, W.J. Greenleaf, and H.Y. Chang, *An improved ATAC-seq protocol reduces background and enables interrogation of frozen tissues.* Nat Methods, 2017. **14**(10): p. 959-962.

136. Brinkman, E.K., T. Chen, M. Amendola, and B. van Steensel, *Easy quantitative assessment of genome editing by sequence trace decomposition.* Nucleic Acids Res, 2014. **42**(22): p. e168.